Development of numerical methods and approaches to simulate colloid transport and stream-aquifer interaction in heterogeneous natural soils

vorgelegt von
M.Sc.
Dan Zhou
geb. in Anhui, China

von der Fakultät VI – Planen Bauen Umwelt
der Technischen Universität Berlin
zur Erlangung des akademischen Grades

Doktor der Naturwissenschaften
- Dr. rer. nat. –

genehmigte Dissertation

Promotionsausschuss:

Vorsitzender: Prof. Dr. Reinhard Hinkelmann
Gutachterin: Prof. Dr. Irina Engelhardt
Gutachter: Prof. Dr. Martin Sauter

Tag der wissenschaftlichen Aussprache: 15. Dezember 2017

Berlin 2018

Summary

Groundwater recharge and contamination are important aspects of groundwater resource management. Groundwater systems are typically constrained by the availability of field observations. Therefore, mathematical models are developed by hydrologists and hydrogeologists to provide a reliable description of the groundwater system for quantitative analysis and uncertainty forecast. However, many current mathematical models are unable to solve emerging issues, such as colloid transport, colloid-facilitated contaminant transport, and stream-aquifer interaction, under varying physicochemical conditions. For example, these issues can be transient flow rate, presence of multiple solutes with competitive sorption, aquifer heterogeneity of porosity, permeability, and spatially and temporally variable streambed hydraulic conductivity.

Therefore, this thesis concerns three specific important topics (colloid transport, colloid-facilitated contaminant transport, and stream-aquifer interaction) to develop the corresponding numerical methods and approaches while answering the following important questions: (1) What are the behaviors and mechanisms of silver nanoparticle (AgNP) transport in soil under variable flow and ionic strength (IS)? (2) What is the impact of manure composition on the transport of three sulfonamides, i.e. sulfadiazine (SDZ), sulfamethoxypyridazine (SMPD), and sulfamoxole (SMOX), in soils? (3) How do transient streambed permeability and aquifer heterogeneity influence stream-aquifer interaction?

Regarding each question, three individual numerical models are developed. (1) For colloid transport, the conventional colloid filtration theory, Derjaguin−Landau−Verwey−Overbeek (DLVO) theory, and the colloid release theory are fully integrated to simulate and analyze the AgNP transport under variable flow and IS. (2) A comprehensive colloid-facilitated contaminant transport model is developed based on the general advection-dispersion equation to simulate the manure-derived colloid facilitated sulfonamides transport. The model incorporates the potential competitive sorption of sulfonamides with immobile manure colloids on soil surface, and sulfonamides with sulfonamides on soil surface and mobile manure colloids. (3) A variably saturated groundwater flow model is developed to simulate the stream-aquifer interaction under alternative losing and gaining conditions. The model integrates the temporally variable streambed permeability that is calculated from the inversion of stream stage and groundwater tables, and the spatially heterogeneous aquifer permeability fields that are implemented using multiple-point geostatistics.

The key findings from each topic are: (1) Flow interruption can dramatically decrease AgNP transport in soil. Evaporation during flow interruption results in an increased electrical conductivity of the soil solution, leading to a totally reduced mobility of AgNP. The reduction of ionic strength after flow interruption slightly enhances AgNP mobility. Soil colloids might facilitate the transport of AgNP given the strongly increased Al and Fe concentrations in the effluent. The model results reveal that the attachment at the air-water interface (AWI) during flow interruption is the key process of AgNP retention under variably saturated conditions. (2) Manure colloids from fattening pigs with low C/N ratio, high $SUVA_{280nm}$ and protein C can facilitate the transport of SMOX, while manure colloids from sows, farrows and weaners have little effects on SMOX transport. In contrast, only retardation is observed for SDZ and SMPD when manure colloids are present. The model results demonstrate that mobile colloids act as carriers for SMOX, while immobile colloids block SMOX from sorbing on the soil. The low affinity of SMOX to immobile colloids promotes SMOX's colloid-facilitated transport. Conversely, the high affinity of SDZ and SMPD to sorb on all types of immobile colloids

retard their transport. Thus, manure properties play a fundamental role in increasing the leaching risk of hydrophobic sulfonamides. (3) Stream-aquifer exchange flux during infiltration periods was constrained by aquifer permeability. During exfiltration, exchange flux is constrained by the reduced streambed permeability. The two dimensional probability distribution of the infiltration path in the aquifer reveals that such pathways and the associated prediction of the extent of the contaminant plume are highly dependent on aquifer heterogeneity.

Zusammenfassung

Grundwasserneubildung und -verunreinigung sind wichtige Themen im Management von Grundwasserressourcen. Die Charakterisierung von Grundwassersystemen ist normalerweise durch fehlende Feldbeobachtungen eingeschränkt. So werden mathematische Modelle von Hydrologen und Hydrogeologen entwickelt, um eine zuverlässige Beschreibung des Grundwassersystems für die quantitative Analyse und die Unsicherheitsprognose zu liefern. Viele derzeitige mathematische Modelle reichen nicht aus um die auftretenden Probleme wie Kolloidtransport, Schadstofftransport mittels Kolloiden und Fluss-Grundwasser-Interaktion, unter unterschiedlich komplexen physikochemischen Bedingungen darzustellen. Herausforderungen können zum Beispiel entstehen durch transiente Flussraten, Vorhandensein von mehreren gelösten Stoffen mit kompetitiver Sorption oder Aquifer-Heterogenität der Porosität, Permeabilität und räumlich und zeitlich veränderliche hydraulische Strömungsleitfähigkeit sein.

Daher werden in dieser Arbeit drei spezielle Themen (Kolloidtransport, Schadstofftransport mittels Kolloiden und Fluss-Grundwasser-Wechselwirkung) zur Entwicklung der entsprechenden numerischen Methoden und Ansätze für breitere Anwendungen behandelt, wobei die folgenden Fragen beantwortet werden: (1) Was sind die Verhalten und Mechanismen des Transports von Silbernanopartikeln (AgNP) im Boden unter variabler Strömung und Ionenstärke? (2) Was ist die Auswirkung der Dungzusammensetzung auf den Sulfonamidtransport (im speziellen Sulfadiazin (SDZ), Sulfamethoxypyridazin (SMPD) und Sulfamoxol (SMOX)) in Böden? (3) Wie beeinflussen transiente Permeabilität und Aquifer-Heterogenität die Fluss-Grundwasser-Interaktion?

Zu jeder Fragestellung werden drei individuelle numerische Modelle entwickelt. (1) Für den Kolloidtransport sind die konventionelle Kolloidfiltrations-theorie, die Derjaguin-Landau-Verwey-Overbeek (DLVO) Theorie und die Kolloidfreisetzungstheorie (colloid release theory) vollständig integriert, um den AgNP-Transport unter variabler Strömung und Ionenstärke zu simulieren und zu analysieren. (2) Ein umfassendes Modell für den Transport von Schadstoffen durch Kolloide wird auf der Basis der allgemeinen Advektions-Dispersions-Gleichung zur Simulation des Sulfonamidtransports durch Kolloide entwickelt, wobei die potentielle kompetitive Sorption von Sulfonamiden mit immobilen Dungkolloiden an der Bodenoberfläche und Sulfonamiden berücksichtigt wird. (3) Ein Grundwasserströmungsmodell, welches die Wechselwirkungen von Oberflächen- und Grundwasser als auch zeitlich variable Flussbettpermeabilität berücksichtigt, wird entwickelt, um die Fluss-Grundwasser-Wechselwirkung unter variierenden Zu- und Abflüssen zu simulieren. Die variable Flussbettpermeablität wird aus der Inversion von Flutwellenantworten und dem räumlich heterogenen Aquifer berechnet, mittels Permeabilitätsfeldern, die mithilfe von Mehrpunkt-Geostatistik implementiert werden.

Die wichtigsten Ergebnisse zu jedem Thema sind: (1) Strömungs-unterbrechung kann den AgNP-Transport im Boden drastisch verringern. Die Verdunstung während der Strömungsunterbrechung führt zu einer erhöhten elektrischen Leitfähigkeit der Bodenlösung, was zu einer vollständig reduzierten Beweglichkeit von AgNP führt. Die Verringerung der Ionenstärke nach einer Strömungsunterbrechung verbessert die AgNP-Mobilität geringfügig. Bodenkolloide könnten angesichts der stark erhöhten Al- und Fe-Konzentrationen im Abwasser den Transport von AgNP erleichtern. Die Modellergebnisse zeigen, dass die Sorption an der Luft-Wasser-Grenzfläche (AWI) während der Strömungsunterbrechung der Schlüsselprozess der AgNP-Retention unter variabel gesättigten Bedingungen ist. (2)

Dungkolloide von Mastschweinen mit niedrigem C/N-Verhältnis, hohem SUVA280nm und Protein C können den Transport von SMOX erleichtern, während Dungkolloide von Sauen und Ferkeln wenig Einfluss auf den SMOX-Transport haben. Im Gegensatz dazu werden für SDZ und SMPD nur Verzögerungen im Transport beobachtet, wenn Dungkolloide vorhanden sind. Die Modellergebnisse zeigen, dass mobile Kolloide als Träger für SMOX fungieren, während unbewegliche Kolloide SMOX daran hindern, auf dem Boden zu sorbieren. Die geringe Affinität von SMOX zu unbeweglichen Kolloiden fördert den Kolloidtransport von SMOX. Umgekehrt verzögert die hohe Affinität von SDZ und SMPD an allen Arten von unbeweglichen Kolloiden zu sorbieren ihren Transport. Somit spielen die Gülleeigenschaften eine fundamentale Rolle bei der Erhöhung des Auswaschungsrisikos von hydrophoben Sulfonamiden. (3) Fluss-Grundwasser-Austauschraten während der Infiltrationsperioden wurden durch die Aquiferpermeabilität eingeschränkt. Während der Exfiltration wird der Austausch durch die reduzierte Flussbettpermeabilität eingeschränkt. Die 2-dimensionale Wahrscheinlichkeitsverteilung des Infiltrationsweges im Aquifer zeigt, dass solche Pfade und die damit verbundene Vorhersage der Ausbreitung der Schadstofffahne stark von der Aquiferheterogenität abhängen.

Acknowledgements

First of all, I would like to express my greatest gratitude to my supervisor Prof. Dr. Irina Engelhardt who gave me such a glorious opportunity to conduct doctoral research in Germany in the past four years. Your patience, unique insight, constructive advice, and foresight awareness helped me overcome many difficulties during research and keep pushing me forward. My doctoral work was carried out sequentially in Forschungszentrum Jülich, TU Freiberg, and TU Berlin, a wonderful PhD career in Germany.

During the stay at the Agrosphere Institute (IBG-3) of Forschungszentrum Jülich, great thanks to Prof. Dr. Harry Vereecken for discussion and advice on presentation, half-year reports, and manuscripts. Thanks to Prof. Dr. Erwin Klumpp and Joanna Makselon for our great cooperation. Thanks to Dr. Anne E. Berns, Jannis Groh, Dr. Wolfgang Kurtz, Qi Tang, Dr. Wolfgang Tappe, and Dr. Miaoyue Zhang for solving my scientific questions, and Horst Hardelauf and Thomas Schuster for the cluster and PC support. Also many thanks to Anne Klosterhalfen, Dr. Gaochao Cai, Di Wu, Zhan Gao, Dr. Xujun Han, Dazhi Li, Dr. Shurong Liu, Gaby Pillert, Dr. Inge Wiekenkamp, Hongjuan Zhang, and Dr. Minghua Zhou for their help and company in Jülich.

The stay in TU Freiberg is temporary but meaningful by acquainting with many friends. Thanks to Isabelle Weber, Dr. Volkmar Dunger, Dr. Katrin Breede, Dr. Nikolaus Klamerth, and Ms. Arite Ingrid Berg for their great help either in life or science. Also best wishes to Dr. Jingxin Qi, Dr. Pu Liu, Dr. Lifu Chang, Dr. Li Fan, Dr. Jingyu Zhao, Dr. Wengang Dang, Dr. Shan Zhong, Dr. Jun Li, Dr. Bing Dai, Guangzhe Zhang, Yuan Liu, Yanyan Du, Miao Zhang, Miao Wang, Yufeng Zhao, and Xiaoqi Gao, who have been obtained or are still struggling for their degree in TU Freiberg, and who offered me great help and company.

The stay in TU Berlin is short but nice. It is glad to get acquaintance with Olga Greulich, Dr. Mirko Schankat, Dr. Francesca De Gaspari, Morgan Tranter, Dustin Knabe, Laslo Städtler. Thanks for their help and support to me.

My great appreciation is to Prof. Dr. Thiele-Bruhn Sören and Martina Gesine Arenz-Leufen at the University of Trier for our great cooperation. Thanks to Dr. Diederik Jacques at the Belgian Nuclear Research Centre for guiding me the use of Hydrus. Thanks to Prof. Dr. Ye Zhang at University of Wyoming for your precious advice of geostatistical modeling and help in manuscript revision. Thanks to Dr. Peter Lichtner at OFM Research, who offers me a great help for the use of PFLOTRAN and manuscript revision.

I gratefully acknowledge Prof. Dr. Reinhard Hinkelmann for being the chairman of the doctoral committee and Prof. Dr. Irina Engelhardt and Prof. Dr. Martin Sauter for reviewing this dissertation.

Finally, I would like to greatly appreciate China Scholarship Council (CSC) for the financial support, and my family for their unconditional love and support for my study abroad.

Table of Contents

Abbreviations ..... **I**

1 Introduction **1**

2 Experimental and numerical investigations of silver nanoparticle transport under variable flow and ionic strength in soil **12**

3 Impact of manure-related DOM on sulfonamide transport in arable soils **37**

4 Numerical modeling of stream-aquifer interaction: quantifying the impact of transient streambed permeability and aquifer heterogeneity **62**

5 Synthesis and Outlook **89**

Statement of contributions **98**

Bibliography **99**

Abbreviations

AgNP	Silver Nanoparticle
ARGs	Antibiotic Resistance Genes
AWI	Air Water Interface
BMBF	German Federal Ministry Of Education And Research
Br	Bromide
BTCs	Breakthrough Curves
CEC	Cation Exchange Capacity
CFSTr	Colloid-Facilitated Solute Transport
CFT	Colloid Filtration Theory
CMAE	Cumulative Mean Absolute Error
CRM	Colloid Release Model
CSC	China Scholarship Council
D_2O	Deuterium Oxide
DHPS	Dihydropteroate Synthetase
DLS	Dynamic Light Scattering
DLVO	Derjaguin−Landau−Verwey−Overbeek
DM	Dry Matter
DN	Dissolved Nitrogen
DOC	Dissolved Organic Carbon
DOM	Dissolved Organic Matter
DOM_F	DOM From Fattening Pigs
DOM_SF	DOM From Sows + Farrows
DOM_W	DOM From Weaners
EC	Electrical Conductivity
EDL	Electrical Double Layer
F	Fattening Pigs

FI	Flow Interruption
FNR	Fonds National De La Recherche
HP1	Hydrus1D-Phreeqc
HPLC	High-Performance Liquid Chromatography
HSISIM	Hierarchical Sequential Indicator Simulation
IBG	Institute Of Bio- And Geosciences
ICP-MS	Inductively Coupled Plasma Mass Spectrometry
IS	Ionic Strength
MAE	Mean Absolute Error
MPS	Multiple-Point Geostatistics
NRMSE	Normalized Root Mean Square Error
NW	Northwest
OC	Organic Carbon
POW	Parameter Optimization Window
RPs	Retention Profiles
SAs	Sulfonamides
SDZ	Sulfadiazine
SE	Southeast
SF	Sows and Farrows
SGS	Sequential Gaussian Simulation
SISIM	Sequential Indicator Simulation
SMOX	Sulfamoxole
SMPD	Sulfamethoxypyridazine
SNESIM	Single Normal Equation Simulation
SUVA	Specific Ultraviolet Absorbance
SWI	Soil Water Interface
TEM	Transmission Electron Microscopy
TI	Training Image

URG	Upper Rhine Graben
VGM	van Genuchten-Mualem
W	Weaners
XDLVO	Extended Derjaguin−Landau−Verwey−Overbeek

1 Introduction

1.1 Background 2

1.1.1 Environmental contamination 2

1.1.2 Colloids and silver nanoparticles 2

1.1.3 Silver nanoparticle transport 3

1.1.4 Colloid-facilitated transport 4

1.1.5 Colloid filtration theory 5

1.1.6 Stream-aquifer interaction 7

1.1.7 Aquifer heterogeneity 8

1.2 Thesis objective and structure 9

1.2.1 What are the behaviors and mechanisms of AgNP transport in soils under variable flow and ionic strength? 9

1.2.2 What is the impact of manure composition on sulfonamide transport in soils? 10

1.2.3 How do transient streambed permeability and aquifer heterogeneity influence stream-aquifer interaction? 11

1.1 Background

1.1.1 Environmental contamination

Environmental contamination is one of the urgent issues in the twenty-first century, which may result from natural and anthropogenic activities (Kvesitadze et al., 2006). Natural contamination may be due to elemental processes, for example the emission of poisonous gas during volcanic eruption and excretion of toxic compounds by flood or earthquakes (Kvesitadze et al., 2006). In contrast to natural processes, human beings produce and discharge more contaminants to our environment. As a negative effect of urbanization, the growth of industry leads to a dramatic increase of chemical production and a subsequent groundwater pollution by emerging contaminants, for example, silver nanoparticles (Colman et al., 2014), antibiotic resistance genes (Pruden et al., 2006), endocrine disrupting chemicals, and pharmaceuticals and personal care products (Barceló, D. and Petrovic, 2007; Esplugas et al., 2007; McClellan and Halden, 2010). In agriculture, agriculture-related contaminants, such as veterinary antibiotics (Brown, 1962), pesticides and fungicides (Wang et al., 2004), are also largely released into the subsurface and pose serious threat to the environment. The toxicity of those contaminants either from urban or agricultural pathway makes them hazardous when they enter into the food chain. Thus, understanding the fate and transport of those contaminants in the subsurface under variable hydrological and hydrochemical conditions is necessary to evaluate and remediate groundwater contamination.

1.1.2 Colloids and silver nanoparticles

Colloids are mixtures of a continuous phase with dispersed particles inside (Figure 1.1). The dispersed particles are called dispersoid with a linear dimension between 1 nanometer and 10 micrometers, and the continuous phase is called dispersion medium (Berg, 2010). There are many colloid examples in our daily life, for example, indian ink, milk, blood serum, clays, and humus (Jirgensons and Straumanis, 2013). Colloids have various properties, such as Tyndall effect, electrophoresis, and thixotropy. Due to their diverse and excellent properties, colloids have been widely used in health care products, chemical and lighting industries.

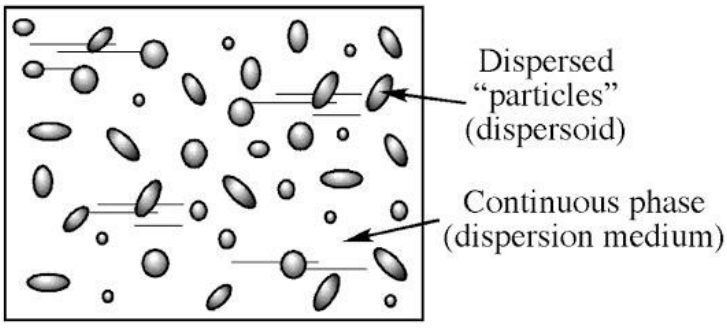

Figure 1.1: The definition of colloid in a structureless continuum (Berg, 2010).

In biological and medical sciences, the traditional antibacterial agents usually have selectivity in killing or suppressing microbial growth, and many of them have induced the microbial resistance (Halbus et al., 2017). In contrast, the artificially synthesized nanoparticles exhibit strong and universal antibacterial, antifungal, and antiviral capacities, and can be designed to target the microbes those with resistance. Their unique properties, e.g. size, catalytic, electric, photoactive, optical, and thermal features, have prompted nanoparticles being the novel antiseptic and antibiotic agents (Brayner et al., 2010; Liu et al., 2009; Zhang et al., 2010). The nanoparticles with an antimicrobial function are reported to range from metal elements, e.g. Cu and Ag, to metal oxides, e.g. ZnO, CuO, MgO, TiO_2, GeO_2; and metal hydroxides, e.g. $Mg(OH)_2$ (Halbus et al., 2017).

Silver nanoparticle (AgNP) is one of the most promising and extensively used nanoparticles in many industries. In health care field, metallic silver has been used to sterilize the water as early as 1000 B.C. (Castellano et al., 2007). The silver antimicrobial property is inert when it is metallic state and will get activated by ionized state under moisture condition. The ionized silver changes the bacterial cell wall and nuclear membrane by binding to proteins' specific functional group like thiol and leads to cell death (Li et al., 2010). It can also bind to DNA and RNA to denature and inhibit the cell growth (Lansdown, 2002; Castellano et al., 2007). The antimicrobial activities of the modern AgNPs are highly enhanced due to their increased specific surface area. The large surface area of AgNPs enables themselves to have a higher percentage to interact with bacterial cells (Morones et al., 2005; Pal et al., 2007). Nowadays, many products have contained AgNPs in our daily life, such as paint, wound dressings, cosmetics, packaging, and medical devices (Rai et al., 2009; Li et al. 2010). However, due to the extensive use, high concentrations of AgNPs have been detected in sediments, soils, and sludge-treated soils which originate from industry and wastewater treatment plant discharge, health care, and household products (Benn and Westerhoff, 2008; Benn et al., 2010). The contamination of AgNPs may break the ecological balance by extending their antimicrobial effects on environmental microorganisms and can be aggravated by their transport mobility in the porous media.

1.1.3 Silver nanoparticle transport

The mobility of AgNPs in soil determines its concentration and contaminated area in space and time. Studies have shown that the mobility of AgNPs in soil is influenced by the physicochemical properties of the system, such as the properties of AgNP, soil grain, and the aqueous phase (Lin et al., 2011; Song et al., 2011; Thio et al., 2011). Surface modification of AgNPs and the existing of stabilizers and organic matters like humic acid are able to enhance the mobility of AgNPs by increasing the repulsions between AgNPs and AgNPs, and AgNPs and soil surface (El Badawy et al., 2013; Liang et al., 2013b; Lin et al., 2012; Thio et al., 2011; Wang et al., 2015). Large soil grain size can improve AgNP mobility due to the small specific surface area with less retention sites and vice versa (Liang et al., 2013b). High input concentration of AgNP can enhance AgNP transport by quickly saturating the retention sites

on the soil surface (Liang et al., 2013b). The mobility of AgNP also increases with an increased flow velocity and a decreased ionic strength and monovalent ion concentrations (Liang et al., 2013a; Liang et al., 2013b). Moreover, researchers demonstrate that soil surface heterogeneity and soil texture also have influences on AgNP transport in soil (Liang et al., 2013b; Lin et al., 2011; Sagee et al., 2012).

Another factor that determines the transport and retention of AgNP in soil is the water content. Studies on bacteria or other colloids transport in unsaturated sand columns show that the decrease of water content led to decreased effluent concentrations and greater retention of colloids (Gargiulo et al., 2008; Torkzaban et al., 2008). The resultant stagnant regions that occurred at solid-water-air interface led to a greater colloid retention due to their low flow velocity (Torkzaban et al., 2008). Low water content also results in smaller pores, which increase the retention of colloids by a stronger straining force. However, few researches have been conducted on the impact of varying water content on AgNP transport in a transient flow.

1.1.4 Colloid-facilitated transport

In subsurface, mobile colloids may act as carriers for contaminants resulting in an enhanced transport of contaminants. This phenomenon is called colloid-facilitated transport. Honeyman (1999) and Kretzschmar et al. (1999) gave the prerequisites for colloid-facilitated transport: (1) there are mobile colloids in the subsurface; (2) contaminants are able to strongly sorb or attach to the mobile colloids. This phenomenon can have either positive or negative consequences with regard to the strong binding of contaminants to colloids (Flury and Qiu, 2008). On the positive side, contaminants may be removed by leaching or washing; while on the negative side, colloid-facilitated transport of contaminants may aggravate the groundwater contamination. This phenomenon has been observed for many chemical substances. Zhu et al. (2014) found that the colloidal organic matter from soils and the organic matter coated minerals may act as the transport carriers for heavy metal Hg. Chen et al. (2005) demonstrated the colloid-facilitated transport of the radionuclide cesium by the soil colloids at the Hanford Reservation in southcentral Washington State. The pesticide prochloraz was found to cotransport with mobile soil colloids (de Jonge et al., 1998). More substances such as Pu (Kersting et al., 1999), atrazine (Sprague et al., 2000), and phosphorus (de Jonge et al., 2004) were reported to have facilitated transport by colloids one after another.

Veterinary antibiotics are globally used in disease treating and health protection of animals, especially in animal husbandry. However, the extensive use of veterinary antibiotics so far has caused severe threat to public and environmental health. Antibiotics cannot be assimilated or metabolized completely in vivo and approximate 30-90% of them are excreted into environment by animal droppings on the pastures or the application of manures which are contaminated by antibiotics for the crops (Burkholder et al., 2007; Heberer, 2002; Bound and Voulvoulis, 2004). An investigation for the residue levels of antibiotics in chicken manures showed that the maximum residue concentration of the selected antibiotics can reach to as

high as 1420.76 mg/kg for enrofloxacin in chicken manures (Zhao et al., 2010). Once the antibiotics are exposed to soil environment, they can be transported to ditches, streams, and rivers by runoff and drain flow (Burkhardt et al., 2005; Stoob et al., 2007; Topp et al., 2008), and groundwater system by leaching (Blackwell et al., 2007), risking the contamination of drinking water (ter Laak et al., 2006). Additionally, it is worth mentioning that some of the antibiotics are still bioactive after entering the environment (Zhou et al., 2006) and promote the occurrence of antibiotic resistance genes (ARGs) in various environmental components such as soil, sediments, wastewater, and drinking water in different countries (Knapp et al., 2010).

Studies have demonstrated that animal manure may impact the mobility of antibiotics in soils and some of them can be carriers to facilitate the transport of certain antibiotics. Burkhardt and Stamm (2007) reported three sulfonamides (sulfadimidine, sulfadiazine, and sulfathiazole) that may sorb to pig manure and thus favor their mobility in soils. Unold et al. (2009) observed the retardation effect of pig manure on the transport of sulfadiazine, while Zou and Zheng (2013) demonstrated the pig manure facilitated transport of the antibiotic florfenicol in saturated soil. The manure-colloid facilitated transport of veterinary antibiotics is highly dependent on the antibiotic species. However, few researches have systematically investigated the influences of manure sources and compositions and the potential interactions among multiple antibiotics and soil grains, such as competitive sorption, on antibiotic transport in soils.

1.1.5 Colloid filtration theory

The transport and deposition of colloids in porous media are commonly described by the conventional colloid filtration theory (CFT) developed by Yao et al. (1971). CFT describes the fate and transport of colloid at 3 scales: (1) interface scale: quantifying the interfacial energy of colloid at the solid-water interface (SWI), the air-water interface (AWI), and colloid-colloid interface (Derjaguin and Landau, 1993; Elimelech and O'Melia, 1990; Hogg et al., 1966); (2) collector scale: calculating the water flow bypass a collector or an air bubble (Rajagopalan and Tien, 1976; Yao et al., 1971); (3) pore scale: straining and size exclusion at grain-grain contacts or constriction and retention at solid-water-air triple contact points. The simulation of colloid transport in porous media based on CFT is derived from the general advection-dispersion equation in a 3D form by accounting for the retentions at SWI and AWI (Flury and Qiu, 2008; Šimůnek et al., 2006):

$$\frac{\partial \theta_w C}{\partial t} + \rho \frac{\partial S_{SWI}}{\partial t} + \frac{\partial A_{aw} S_{AWI}}{\partial t} = \nabla \cdot (\theta_w D \nabla C) - \nabla \cdot (qC) - R \quad (1.1)$$

where θ_w [L^3 L^{-3}] is volumetric water content, C [M L^{-3}] is colloid concentration in the solution, ρ [M L^{-3}] is bulk density, D [L^2 T^{-1}] is dispersion coefficient, q [L T^{-1}] is volumetric water flux. S_{SWI} [M M^{-1}] and S_{AWI} [M L^{-2}] is colloid concentrations attached at the soil-water and air-water interface, respectively. A_{aw} [L^2 L^{-3}] is area of AWI per unit volume. R [M L^{-3}

T^{-1}] represents chemical and/or biological reactions of the aqueous colloids. A relative brief explanation for each term is described as followings:

$$\rho \frac{\partial S_{SWI}}{\partial t} = \theta_w k_{str} C + \theta_w \psi_{SWI} f_{SWI} k_{att}^{SWI} C - \rho k_{det}^{SWI} S_{SWI} - R_{SWI} \quad (1.2)$$

$$k_{str} = 269.7 \left(\frac{a_p}{a_c}\right)^{1.42} \quad (1.3)$$

$$k_{att}^{SWI} = \frac{3(1-\theta_w)}{2a_c} \eta_0 \alpha v \quad (1.4)$$

where k_{str} [T^{-1}] is first-order straining coefficient, ψ_{SWI} [-] is blocking function, k_{att}^{SWI} [T^{-1}] and k_{det}^{SWI} [T^{-1}] is colloid attachment and detachment coefficient at the SWI, respectively. a_p [L] and a_c [L] is median colloid and soil grain diameter, respectively. f_{SWI} [-] is fraction of the soil-water interfacial area that is available for attachment. R_{SWI} [M L^{-3} T^{-1}] represents chemical and/or biological reactions of colloids attached at the SWI. η_0 [-] is single collector contact efficiency. α [-] is attachment efficiency. v [L T^{-1}] is pore water flow velocity.

$$\frac{\partial A_{aw} S_{AWI}}{\partial t} = \theta_w \psi_{AWI} f_{AWI} k_{att}^{AWI} C - A_{aw} k_{det}^{AWI} S_{AWI} - R_{AWI} \quad (1.5)$$

where k_{att}^{AWI} [T^{-1}] and k_{det}^{AWI} [T^{-1}] is colloid attachment and detachment coefficient at the AWI, respectively. ψ_{AWI} [-] is blocking function. f_{AWI} [-] is fraction of the air-water interfacial area that is available for attachment. R_{AWI} [M L^{-3} T^{-1}] represents chemical and/or biological reactions of colloids attached at the AWI.

The CFT theory has been widely used in many colloid transport models to investigate the different fate and transport of colloids under various physicochemical conditions. Bradford et al. (2012) simulated the transport of *E. coli* D21g under various ionic strengths with a CFT model. Liang et al. (2013b) investigated the influence of ionic strength, sand grain size, water velocity, and input concentration on the transport of AgNP with CFT models. Besides, Torkzaban et al. (2015) developed a CFT-based colloid release model to investigate the influence of ionic strength and flow rate on the colloid release and clogging effect with an analytical approach. More colloidal substances, such as polydisperse kaolinite clay (Lin et al., 2008), nano-iron (Hydutsky et al., 2007), and nanoscale C_{60} (Wang et al., 2008) were studied using CFT.

Although the wide use of CFT, the implicit assumptions in CFT limit its application. For example, the attachment at SWI is linked to flow velocity and can be expanded to link to ionic strength by coupling Derjaguin−Landau−Verwey−Overbeek theory (DLVO) (Gregory, 1981; Hogg et al., 1966), while the attachment at AWI and the detachment at SWI and AWI do not take flow velocity and ionic strength into account. Thus, the model inversed values of attachment coefficient at AWI, the detachment coefficients at SWI and AWI are only valid in a given experimental condition of flow velocity or solution ionic strength. Therefore, the calibrated model is unable to simulate the colloid transport under a different flow velocity or ionic strength by using the calibrated attachment coefficient at AWI and the detachment coefficients at SWI and AWI. These assumptions limit the application of CFT when the flow rate or ionic strength is transient, which is usually the case in the field with periodic precipitation and evaporation, dynamic groundwater flow, and infiltration of surface water

with varying ionic strength. Hence, a deeper development of CFT is necessary to consider the variable physicochemical situations.

1.1.6 Stream-aquifer interaction

Streams and groundwater compose the major parts of the water cycle. Water exchange in stream and aquifer interaction occurs in hyporheic and riparian zones. It provides our ecosystem valuable physical (e.g. water and solutes transport), chemical (e.g. chemical reactions), and biological processes (e.g. biodegradation). For example, discharging groundwater and bi-directionally exchanged surface water constitute the hyporheic water (Daniluk et al., 2013). Denitrifying environment in the riparian and hyporheic zones can impact nitrate concentration during surface water-groundwater interaction (Lasagna et al., 2016). The biocenoses inhabited in riparian and hyporheic zones can highly influence the biochemical environment, e.g. dissolved organic matter, redox potential, and nitrogen speciation (Bertrand et al., 2014). Thus, scientists have conducted lots of research on stream-aquifer interactions by multiple disciplines, such as hydrology and hydrogeology (Fleckenstein et al., 2006; Frei et al., 2009; Langhoff et al., 2006), biology (Mueller et al., 2013; Newcomer et al., 2016), ecology (Boulton et al., 2010), sedimentology (Evans and Wilcox, 2014; Rosenberry and Pitlick, 2009), and chemistry (Rassam et al., 2008) in various perspectives, as well as developing new methodologies (Gianni et al., 2016; Pozdniakov et al., 2016).

Studies have shown that streambed is one of the key factors that control the stream-aquifer interaction (Sophocleous, 2002; Winter et al., 1998). It constitutes an interface with physical, chemical, and biological environments between stream and groundwater, and controls the exchange water flux and the fate and transport of solutes during stream-aquifer interaction. A lot of studies have uncovered various physical, chemical, and biological processes within streambed. For example, the preferential entrainment of particles with finer sizes during flood events can reduce the sediment thickness resulting in the increase of streambed hydraulic conductivity and streamflow loss under losing condition (Simpson and Meixner, 2012). Increase of stream flow velocity, such as in storm events, will release high concentration of nitrate to the stream due to the lower residence time of nitrate in the reactive sediments within streambed (Gu et al., 2007). Biomass growth induced streambed bioclogging can reduce seepage for losing-connected and losing-disconnected rivers (Newcomer et al., 2016). More perspectives of streambed are increasingly being studied in the context of river restoration (Rollet et al., 2014), streambed morphology and habitats (Grabowski et al., 2014; Neumann and Curtis, 2016), and contaminant transport (Mustafa et al., 2016).

Currently, significant efforts have been made towards the development of integrated surface and subsurface flow model by incorporating the complexities regarding physical, chemical, and biological processes. Ala-aho et al. (2015) developed a fully integrated hydrological model to estimate the temporal and spatial distribution of water flux at the

surface water-groundwater interface. Engelhardt et al. (2013) simulated the transport and biochemical transformation processes of iomeprol during stream-groundwater interaction with a process-based reactive transport model. Liggett et al. (2014) demonstrated the high sensitivity of solute transport to the representation of the surface-subsurface interface by the tracer-based integrated surface-subsurface code. A detailed review of the various integrated surface-subsurface hydrological models was given by Paniconi and Putti (2015). However, despite these efforts on improving the numerical models, current modeling work is still far away from integrating the full complexities of surface water-groundwater interactions (Brunner et al., 2017). The current simulation of streambed is usually modeled as a static and homogeneous entity in physical and hydraulic parameters (e.g. thickness, permeability, and porosity) (Partington et al., 2017). The processes of sediment erosion, transport, and deposition are usually treated as a black box. Moreover, limited observation data used in the simplified surface water-groundwater model may induce potential uncertainty which can remain covered in the modeling process (Brunner et al., 2017). The proper complexity level of process, scale, and heterogeneity is another unsolved issue during the model conceptualization (Brunner et al., 2017).

1.1.7 Aquifer heterogeneity

In earth science, heterogeneity can be defined as the complexity or variability of a specific system property in a particular volume of space and/or time (Fitch et al, 2015). The spatially heterogeneous distribution of the subsurface properties, such as porosity, permeability, and facies, imposes a significant influence on groundwater flow and solute transport (Michael et al, 2010). Thus, the development of methods to characterize and simulate the aquifer heterogeneity has been a research focus of hydrogeologists and petroleum engineers in the past decades. Various methods have been developed, among them, geostatistical and stochastic tools are more favored. Geostatistical tools characterize and quantify the spatial heterogeneity of subsurface properties, e.g. porosity and hydraulic conductivity, using probabilistic models to generate parameter realizations. Multiple realizations of a parameter distribution can be used to reflect the uncertainty of a parameter in the model output within the statistical framework. Sequential indicator simulation (SISIM) is the most popular cell-based geostatistical method to interpret subsurface structure (Pyrcz and Deutsch, 2014), which is based on the indicator variograms to describe the spatial structure with a limited number of parameters using the kriging algorithm (Emery and Parra, 2013). A hierarchical sequential indicator simulation (HSISIM) was proposed by Zappa et al. (2006) and an alternative refined HSISIM version was subsequently developed by Comunian et al. (2016) aiming to simplify the simulation workflow based on the subdivision of the stochastic simulation according to a binary tree. However, the convenient parametric approaches sacrifice the precise representation of heterogeneity (Schlüter and Vogel, 2011), since variograms are simply calculated based on two point data correlations and unable to characterize realistic heterogeneity in complex geological environments, such as curvilinear features (e.g. sinuous

fluvial, deepwater channels, and dispersive patterns in distributary lobes) and ordering relationships (e.g. natural transitions in channel axis to off-axis to margin and from upper shore face to lower shore face and to marine facies) (Huysmans and Dassargues, 2009; Pyrcz and Deutsch, 2014). Multiple-point geostatistics (MPS) was then developed to overcome the limitations of traditional geostatistical approaches and has been shown to be a powerful tool (Guardiano and Srivastava, 1993; Zhou et al., 2012). The key step of MPS is to use a training image (TI) as a prior description of the subsurface physical reality. TI is a conceptual explicit representation of the expected spatial distribution of hydraulic properties or facies types (Huysmans and Dassargues, 2009), and can be derived from remote sensing images, outcrop analogues, or conceptual drawing by geologists (Bayer et al., 2011; He et al., 2014). The empirical multivariate distributions then can be inferred from TI for stochastic modeling. The construction of TI is one of the most critical and difficult steps in MPS, which should be representative of the geological heterogeneity and large enough so that the essential features can be characterized by statistics defined on a limited point configuration (Hu and Chugunova, 2008). Thus, compared with SISIM, MPS sacrifices convenience but obtains more precision.

1.2 Thesis objective and structure

The main objective of this thesis is to develop numerical methods and approaches to solve the hot issues with regard to colloid transport, colloid-facilitated contaminant transport, and stream-aquifer interaction for groundwater resource management.

As highlighted in the background section, the soil contamination by AgNP and veterinary antibiotics and stream-aquifer interaction all influence our ecosystem and human health directly or indirectly. These processes are continuously being focused by researchers due to their far-reaching influences on environment and human beings, and unknown behaviors and implicit mechanisms that need to be solved. This thesis selects AgNP transport, manure-colloid facilitated sulfonamide transport and stream-aquifer interaction at a riparian zone of Schwarzbach in Germany as 3 specific topics to develop and provide numerical solutions for future investigations on colloid and colloid-facilitate solute reactive transport and surface water-groundwater interaction. To address the development of numerical methods and approaches, these 3 specific topics are presented as 3 different questions, which are answered in chapter 2, 3, and 4, respectively. The motivation for each question and the chapter structure are described as followings:

1.2.1 What are the behaviors and mechanisms of AgNP transport in soils under variable flow and ionic strength?

Since the contamination of AgNPs in soils and their potential risk of breaking ecological balance have been realized, scientists have conducted lots of research on AgNP mobility under various physicochemical conditions. For example, the influence of soil properties (e.g.

grain size, organic matter content, surface heterogeneity), AgNP size, and system chemical conditions on the AgNP mobility have been well understood as illustrated in Section 1.1.2. However, few studies have been conducted on the impact of variably saturated conditions on the AgNP transport as a result of the periodic precipitation events, surface runoff, groundwater recharge, and evaporation, nevertheless the transient ionic strength due to variable saturation or external solution, which was commonly defined as a static parameter in previous studies. Moreover, the conventional colloid transport model using CFT is not exhausted to describe the transport of colloids under transient hydrological (e.g. flow rate) and transient hydrochemistry (e.g. ionic strength) conditions. Especially, CFT ignoring the impact of transient flow rate and ionic strength on colloid detachment by inappropriately integrating into a solo parameter (detachment coefficient) is not feasible. A novel colloid transport model by incorporating the transient hydrological and hydrochemistry at either soil-water or air-water interface is needed.

Chapter 2 investigates AgNP transport under variable flow and ionic strength in soil using laboratory column experiments and numerical simulations. Three scenarios of AgNP transport under different physicochemical conditions are presented: (1) AgNP transport under continuous flow and constant ionic strength; (2) AgNP transport under varying flow rate and constant ionic strength; (C) AgNP transport under varying flow rate and varying ionic strength. A new colloid transport model is developed by coupling colloid filtration theory, Derjaguin−Landau−Verwey−Overbeek (DLVO) theory and a colloid release theory to simulate AgNP transport behaviors under different scenarios and analyze the implicit mechanisms.

1.2.2 What is the impact of manure composition on sulfonamide transport in soils?

The fertilization of antibiotic-contaminated manures may not only introduce veterinary antibiotics to the field, but also large amount of manure-derived dissolved organic matter (DOM), which has been demonstrated to facilitate contaminant transport in soils (Li and Zhou, 2010; Morales et al., 2011; Zou and Zheng, 2013). The interactions between DOM and veterinary antibiotics depend on their characteristics that determine the stability of their co-transport complex. Although the facilitated antibiotic transport by manure colloids has been investigated, few studies have been conducted to investigate the key factors that determine the facilitated transport from either antibiotic chemical structure (e.g. functional groups) or the manure source and composition, nevertheless to consider the interactions, for example, the competitive sorption of immobile colloids and antibiotics for solid phase, and antibiotics for mobile and immobile colloids using a numerical investigation.

Chapter 3 investigates the transport of three sulfonamides, sulfadiazine (SDZ), sulfamethoxypyridazine (SMPD), and sulfamoxole (SMOX) in saturated soil columns with and without manure colloids from sows and farrows, weaners, and fattening pigs. These three sulfonamides possess similar molecular structure but differ in the R substituents which enable

them with different hydrophobic properties. Sows and farrows, weaners, and fattening pigs represent different life stages and feeding regimes, whose manure-derived colloids show different contents in, for example, organic carbon, pH, Protein C, and dissolved nitrogen. The potential colloid transport, sulfonamides transport, and colloid-facilitated sulfonamide transport as well as the competitive sorption of antibiotics on mobile and immobile colloids, antibiotics with immobile colloids on soil surface are interpreted by a newly developed numerical model, which is calibrated by the breakthrough curves of colloids and sulfonamides. The impact of manure colloid composition and antibiotic molecular structure on the cotransport of sulfonamides with colloids are systematically analyzed.

1.2.3 How do transient streambed permeability and aquifer heterogeneity influence stream-aquifer interaction?

The stream-aquifer interaction is an important process in riparian zones. This interaction is often influenced by human activities such as irrigation, groundwater pumping or surface water division. Understanding the stream-aquifer system is very important for regional groundwater resource management. Early studies have pointed out that streambed is one of the key factors controlling the stream-aquifer interaction (Sophocleous, 2002; Winter et al., 1998). However, due to the difficulties in measuring and estimating the streambed hydraulic conductivity as it is dynamic and subject to river stage and discharge, the key parameter (hydraulic conductivity) in many researches is still assumed to be static and homogeneous. The adjacent aquifer is another factor that may control the groundwater migration. Many approaches have been developed to characterize aquifer properties, such as facies, porosity, and hydraulic conductivity distributions either in homogeneous or heterogeneous assumption. However, few studies have been conducted to characterize the stream-aquifer system by integrating the transient streambed property (e.g. permeability) and the aquifer heterogeneity (e.g. permeability) with a numerical model, and demonstrate the dominant factor that controlls the stream-aquifer interaction under periodic precipitations and varying stream gaining and losing conditions.

Chapter 4 develops a 2D stream- aquifer interaction model by incorporating the transient streambed permeability and the heterogeneous aquifer permeability to investigate their influence on the interaction. The temporal transient streambed permeability is estimated by a latest analytical method which is simply based on stream stage and the adjacent groundwater table records. The multiple point geostatistics is adopted to estimate the aquifer heterogeneous permeability in a stochastic sense. The state-of-the-art groundwater modelling code PFLOTRAN is used to setup the stream-aquifer interaction model by incorporating the transient streambed permeability and aquifer permeability dataset. The role of streambed and aquifer in stream-aquifer interaction under varying losing and gaining condition is analysed. A further stream water infiltration path is revealed by a Monte Carlo based groundwater age simulation.

2 Experimental and numerical investigations of silver nanoparticle transport under variable flow and ionic strength in soil*

Authors: Joanna Makselon, Dan Zhou, Irina Engelhardt, Diederik Jacques, Erwin Klumpp

Abstract **13**

2.1 Introduction **14**

2.2 Materials and Methods **15**

2.3 Results and Discussion **19**

2.4 Supporting Information **26**

2.5 Acknowledgements **32**

2.6 References **32**

* Reprinted (adapted) with permission from

Makselon, J., Zhou, D., Engelhardt, I., Jacques, D., Klumpp, E., 2017. Experimental and numerical investigations of silver nanoparticle transport under variable flow and ionic strength in soil. Environmental Science & Technology, 51(4), 2096-2104. https://doi.org/10.1021/acs.est.6b04882.

Abstract

Unsaturated column experiments were conducted with an undisturbed loamy sand soil to investigate the influence of flow interruption (FI) and ionic strength (IS) on the transport and retention of surfactant-stabilized silver nanoparticles (AgNP) and the results were compared to those obtained under continuous flow conditions. AgNP concentrations for breakthrough curves (BTCs) and retention profiles (RPs) were analyzed by ICP-MS. Experimental results were simulated by the numerical code HP1 (Hydrus1D-PhreeqC) with the DLVO theory, extended colloid filtration theory and colloid release model. BTCs of AgNP showed a dramatic drop after FI compared to continuous flow conditions. Evaporation increased due to FI, resulting in increased electrical conductivity of the soil solution, which led to a totally reduced mobility of AgNP. A reduction of IS after FI enhanced AgNP mobility slightly. Here the strongly increased Al and Fe concentration in the effluent suggested that soil colloids facilitated the release of AgNP (cotransport). The numerical model reproduced the measured AgNP BTCs and indicated that attachment to the air-water interface (AWI) occurring during FI was the key process for AgNP retention.

Graphical Abstract

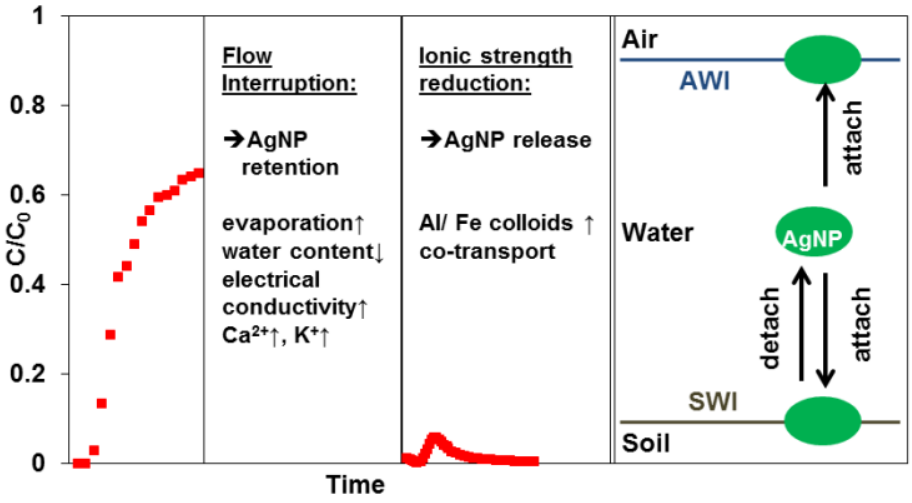

2.1 Introduction

Silver nanoparticles (AgNP) are one of the most widely used engineered nanoparticles due to their excellent physical-chemical properties and antimicrobial activity. AgNP can reach the subsurface via discharge from industry and waste water treatment plants. Recent exposure modeling approaches have shown that AgNP concentrations in sediments, soils and sludge-treated soils are much higher than in surface waters (Gottschalk et al., 2015; Sun et al., 2014). Extreme weather conditions can influence the fate of AgNP. There are only a few studies about AgNP mobility in soils (Braun et al., 2015; Cornelis et al., 2013; Liang et al., 2013b; Sagee et al., 2012; Wang et al., 2015). It was reported that AgNP mobility in soils depends on chemical and physical soil properties such as mineralogical composition (Cornelis et al., 2013; Wang et al., 2015), organic matter content (Cornelis et al., 2012; Sagee et al., 2012; Wang et al., 2015), soil texture (Sagee et al., 2012), and soil surface heterogeneity (Lin et al., 2011). Batch experiments suggested that there is a high long-term risk of AgNP mobilization when applied to agricultural soils characterized by low clay contents and weakly acidic conditions (pH 5-7) (Hoppe et al., 2014). Furthermore, AgNP transport and retention are very sensitive to physicochemical parameters. The mobility of AgNP increases with increasing input concentration, flow velocity, grain size, and decreasing ionic strength (Braun et al., 2015; Liang et al., 2013b), but is inhibited by bivalent cations (e.g., calcium) due to the formation of cation bridging (Liang et al., 2013b). Other factors controlling AgNP transport are NP stabilization mechanisms and the presence of stabilizing agents (El Badawy et al., 2013), as they enhance AgNP mobility in porous media (Liang et al., 2013a; Tian et al., 2010). Furthermore, transformation processes of AgNP depending on environmental conditions such as solution chemistry may result in dissolution (Li et al., 2012), oxidation (Lui and Hurt, 2010), sulfidation (Lowry et al., 2012), homo- (El Badawy et al., 2010) and heteroaggregation (Zhou et al., 2012), and thus influence the fate of AgNP in the environment.

Another important parameter for the transport and retention of NP in soil is water content. Transport studies with bacteria or colloids in unsaturated porous media show an increase in retention with decreasing water content (Gargiulo et al., 2008; Torkzaban et al., 2008). In unsaturated porous media, stagnant regions of flow can occur at the solid-water-air-interface (Patzek and Kristensen, 2001; Patzek and Silin, 2001). The extent of these stagnant regions increase with decreasing water content and enhance the retention of colloids (Torkzaban et al., 2008). Under unsaturated conditions mobile colloids need to be transported through smaller pores, which can also lead to a higher retention of colloids due to straining (Gargiulo et al., 2007; Torkzaban et al., 2008). Low water content can promote retention of colloids in thin water films that are smaller than the colloid diameter (Wan and Tokunaga, 1997). However, there are even fewer studies about AgNP transport under variable saturation conditions accounting for the impact of air-water interface on AgNP transport (Kumahor et al., 2015). Therefore, further knowledge of key processes that affect the transport and retention of AgNP in soils and under different hydrological conditions are urgently needed for an enhanced risk assessment in the future. In the natural environment, different hydrological conditions prevail with rain events and dry periods which are expected to affect the transport of AgNP as they

directly influence the hydraulic and geochemical patterns within the soil and aquifer. Therefore, the present research focuses on AgNP transport experiments with flow interruption, which simulates rain and dry weather conditions followed by changes in ionic strength to mimic natural environmental conditions.

In numerical modeling studies, the colloid filtration theory (CFT) is commonly used to describe the fate and transport of colloids such as microbes (Bradford et al., 2012; Seetha et al., 2014), nanoparticles (Jaisi et al., 2008; Liang et al., 2013b; Liang et al., 2013a), and clay minerals (Syngouna and Chrysikopoulos, 2013) in porous media. Shang et al. (2013) conducted flow interruption column experiments with variable stop-flow durations in saturated quartz sand with engineered silicate colloids (200-450 nm) to evaluate the validity of various kinetic models. They found that particle transport models which include attachment and straining processes provide a good description of colloid transport under continuous and interrupted flow conditions. Current models usually use an extended CFT that accounts for blocking, straining and single collector efficiency (Bradford et al., 2006; Bradford et al., 2003; Flury and Qiu, 2008). However, the extended CFT is still not able to describe the influence of transient hydrochemistry (e.g., ionic strength) as the calculation of the attachment coefficient does not consider the impact of hydrochemistry. In addition, a constant value of the detachment coefficient in CFT cannot account for transient hydrological and hydrochemical conditions (Bradford et al., 2012). Thus, in this study a colloid release model (CRM) (Torkzaban et al., 2015) and the Derjaguin-Landau-Verwey-Overbeek (DLVO) theory were coupled with the CFT so that the influence of transient hydrology and hydrochemistry can both be accounted for in the numerical simulation. The CRM describes colloid release by using different detachment coefficients and fractions of unreleased colloids to account for the alteration in soil chemistry or flow rate (Torkzaban et al., 2015). The DLVO theory describes the total interaction energy (sum of van der Waals attraction and double layer forces) as a function of the separation distance between the colloid and the collector (Gregory, 1981; Hogg et al., 1966). In addition to the CFT, the DLVO theory considers the impact of variable temperature, ionic strength, surface charge, and permittivity on colloid transport. As yet no investigations are available on AgNP transport considering variable saturated, transient hydrological (e.g., flow rate) and hydrochemical (e.g., ionic strength) conditions that couple laboratory experiments with comprehensive numerical analyses.

Therefore, the objectives of this study were (i) to investigate the influence of interrupted irrigation (flow interruption (FI)) and thus abrupt changes in flow velocity, (ii) variable water saturation, and (iii) variable ionic strength (IS) on AgNP transport in soil, and (iv) to extend numerical modeling concepts of AgNP transport using an extended version of the CFT theory.

2.2 Materials and Methods

AgNP and Solution Chemistry. AgNP (Ag, 10.16 % w/w) were purchased from AgPURE, rent a scientist GmbH, Germany. The AgNP were spherical in shape with a

diameter in the size range of 15-20 nm determined by transmission electron microscopy (TEM) (Liang et al., 2013a). The AgNP were modified using a mixture of two stabilizers, 4 % w/w each of polyoxyethylene glycerol trioleate and polyoxyethylene (20) sorbitan monolaurate (Tween 20). The amount of free surfactants in the stock suspension was around 5 % (Liang et al., 2013a). Both of these surfactants are nonionic and form steric repulsion barriers between AgNP that help to stabilize the suspension and minimize aggregation. The release of silver ions from the particles was less than 1 % after 3 days (Liang et al., 2013a). For each transport experiment the AgNP suspension was prepared by diluting the stock suspension in 1 mM KNO_3 to achieve concentrations of 10 mg L^{-1} AgNP and the suspension was then sonicated for 15 min in a sonication bath. Measurements of the hydrodynamic diameter taken by dynamic light scattering (DLS) over a period of 24 h indicated a constant hydrodynamic diameter of 58.5 ± 1.1 nm and ensured that the prepared AgNP suspension was stable. The zeta potential of AgNP measured by a Nano-Zetasizer apparatus (Malvern ZetaSizer 4) was -16 mV in 0.2 mM KNO_3. Further zeta potentials in 1, 5, 10 mM KNO_3 were taken from the literature (Liang et al., 2013b) as -15 mV, -10 mV, -5 mV and a linear equation relating zeta potential and ionic strength was used to account for the variation of zeta potential under different ionic strengths (SI Table S2.1).

Soil. Undisturbed soil columns (8 cm inner diameter, 10 cm length) were taken from the upper 30 cm of an agricultural field (Kaldenkirchen, North Rhine-Westphalia, Germany) after the field had been plowed. The soil was classified as loamy sand with 4.9 % clay (<0.002 mm), 26.7 % silt (0.002−0.063 mm), and 68.5 % sand (0.063−2.000 mm) (Unold et al., 2009). The clay fraction contained the clay minerals illite, montmorillonite and kaolinite (Liang et al., 2013b). The median soil grain diameter was determined by sieve analysis as 160 µm. The content of total organic matter was 1.07 % (Unold et al., 2009), the iron content was 0.8 % (Kasteel et al., 2010), the pH was 5.9 (Unold et al., 2009), the cation exchange capacity and specific surface area were in the range at 7.8 $cmol_c/kg$ (Förster et al., 2008) and 1.7 m^2/g (Liang et al., 2013b), respectively. The soil zeta potentials were –37.2 mV and –35,5 mV at 0.2 mM and 1 mM IS, respectively, which were more negative than that of the AgNP (Liang et al., 2013b). The zeta potential at 0.2 mM was estimated from the data of Liang et al. (2013b) (SI Table S2.1). For the preparation of the electrolyte solutions, KNO_3 was dissolved in pure water (18.2 Ω) to an ionic strength of 1 and 0.2 mM, respectively. The KNO_3 solution was used as a background solution for the transport experiments and also as an electrolyte solution for the AgNP suspension and tracer solution.

Transport Experiments. First, the column was irrigated with 1 mM KNO_3 until a constant flow velocity of 0.02 cm/min was achieved. Then the tracer and AgNP transport experiments were conducted simultaneously using a suspension consisting of 0.5 M deuterium oxide (D_2O) as a conservative tracer and a AgNP concentration of 10 mg L^{-1} in 1 mM KNO_3 by injecting a pulse (around 2.5–2.7 pore volumes, 500 mL) at the top of the column.

AgNP transport experiments were carried out in three scenarios (Table 2.1): (A) immediately after AgNP irrigation the soil column was irrigated with 1 mM KNO_3; (B) after

AgNP irrigation the flow was interrupted for 2.7 days followed by irrigation with 1 mM KNO_3, and (C) after AgNP irrigation the flow was interrupted for 2.7 days followed by irrigation with KNO_3 with a lower ionic strength of 0.2 mM. All column experiments were conducted with software-controlled systems to ensure a constant irrigation and a homogeneous water saturation distribution at the beginning of the experiment (Unold et al., 2009). Effluent samples were collected at the bottom of the column with a fraction sampler and the electrical conductivity (EC) was recorded. During FI the column was open at the top. The soil column was weighed before and after flow interruption as well as at the end of the experiment to obtain the water saturation and water loss due to flow interruption, respectively. At the end of the transport experiments, the soil was carefully excavated in 1 cm layers, freeze dried and homogenized. From each soil layer three aliquots of 0.5 g were taken and used for microwave digestion with 65 % HNO_3. Effluent samples were treated with 30 % HNO_3 to digest the particles. Effluent and soil concentrations of AgNP were determined based on Ag concentrations that were measured by inductively coupled plasma mass spectrometry (ICP-MS, Agilent 7500ce). Samples were diluted as needed before analysis by ICP-MS and rhodium was used as an internal standard. Measurements were repeated three times and Ag concentrations were directly related to the amount of AgNP in the sample. In addition the Al, Fe, Ca and K concentrations were determined in the effluent samples. The effluent concentration of D_2O was quantified by high-performance liquid chromatography (HPLC, High-Technologies Corporation, Japan) with a refractive index detector (RI, L-2490). D_2O concentrations were evaluated by using a calibration curve between the peak area of the RI signal and standard solutions. Details of the experimental procedure are given in the Supporting Information.

Numerical Model Setup. The HP1 code was used to simulate variable saturated flow, conservative transport, and reactive transport of silver nanoparticles (Jacques et al., 2008a; Jacques et al., 2008b). HP1 couples Hydrus-1D (Simunek et al., 2005) with the geochemical code PhreeqC (Parkhurst and Appelo, 1999) and can simulate a broad range of biogeochemical reactions in variable saturated media. The 0.1 m soil column was discretized into 101 nodes. In order to simulate the flow, the upper and lower boundary conditions were designated as atmospheric boundary condition with surface layer and a variable pressure head, respectively. To simulate conservative transport, a concentration flux boundary was set up at the top of the column to mimic the injection of 0.5 M D_2O for 8 h at a constant flow velocity of 0.02 cm min^{-1}, while a zero concentration gradient boundary was used for the bottom of the column. For the simulation of reactive transport, a time-variable boundary condition was defined at the top of the column in three time steps; I.: AgNP irrigation + evaporation, II.: no irrigation + evaporation and III.: electrolyte solution irrigation + evaporation.

Reactive Transport Simulations. Simulation of the AgNP transport was based on the general advection-dispersion equation in one-dimensional form that accounts for colloid filtration at the soil-water and air-water interfaces (Bradford et al., 2003; Simunek et al., 2006):

$$\frac{\partial \theta_w C}{\partial t} + \rho \frac{\partial S_{SWI}}{\partial t} + \rho \frac{\partial S_{AWI}}{\partial t} = \frac{\partial}{\partial x}\left(\theta_w D \frac{\partial C}{\partial x}\right) - \frac{\partial qC}{\partial x} \quad (2.1)$$

where θ_w [L L^{-1}] is the volumetric water content, C [mol L^{-1}] is the AgNP concentration in the solution, ρ [kg L^{-1}] is the bulk density of soil, D [m^2 s^{-1}] the dispersion coefficient, q [m s^{-1}] the volumetric water flux, and x [m] the distance from the column inlet. S_{SWI} [mol kg^{-1}] and S_{AWI} [mol kg^{-1}] are the AgNP concentrations attached at the soil-water and air-water interface, respectively. A first-order kinetic equation was employed to account for colloid transport at the soil-water interface (SWI). The equation considers attachment, detachment and straining (Bradford et al., 2003; Flury and Qiu, 2008; Foppen and Schijven, 2006; Torkzaban et al., 2015), and is implemented with:

$$\rho \frac{\partial S_{SWI}}{\partial t} = \theta_w k_{str} C + \theta_w \psi k_{att}^{SWI} C - \rho k_{det}^{SWI} \left(S_{SWI} - f_i S_{SWI}^i\right) H_o(S_{SWI} - f_i S_{SWI}^i) \quad (2.2)$$

$$k_{str} = 269.7 \left(\frac{a_p}{a_c}\right)^{1.42} \quad (2.3)$$

$$k_{det}^{SWI} = M_{det}^{SWI} A_{SWI} \quad (2.4)$$

$$A_{SWI} = 6 \left(\frac{1-\theta_w}{a_c}\right) \quad (2.5)$$

$$k_{att}^{SWI} = \frac{3(1-\theta_w)}{2a_c} \eta_0 \alpha v \quad (2.6)$$

$$\psi = 1 - \frac{S_{SWI}}{S_{max}} \quad (2.7)$$

where k_{str} [s^{-1}] is the first-order straining coefficient, k_{att}^{SWI} [s^{-1}] is the colloid attachment coefficient, a_p [m] is the median colloid radius, a_c [m] is the median soil grain radius, k_{det}^{SWI} [s^{-1}] is the colloid detachment coefficient, f_i is the fraction of retained colloids that is not released by the flow rate (i =1) or chemical (i =2) alteration, S_{SWI}^i is the retained colloid before the flow rate (i =1) or chemical (i =2) alteration, and $H_o(S_{SWI} - f_i S_{SWI}^i)$ is the Heaviside function that is equal to 1 when $S_{SWI} > f_i S_{SWI}^i$ and 0 when $S_{SWI} \leqq f_i S_{SWI}^i$. During steady-state conditions, before flow interruption, f_i is equal to 0, M_{det}^{SWI} [m s^{-1}] is the mass transfer rate coefficient for detachment at SWI, A_{SWI} [m^{-1}] is the specific SWI area, θ_w [-] is the volumetric water content, v [m s^{-1}] is the pore water flow velocity, η_0 [-] is the single collector contact efficiency (Foppen and Schijven, 2006), α is the attachment efficiency, ψ [-] is a dimensionless function to account for blocking, S_{max} [mol kg^{-1}] is the maximum sorption places of the soil for AgNP. A description of the attachment efficiency calculation is given in the SI.

The attachment to the air-water interface (AWI) was assumed to be irreversible and simulated using a first-order kinetic equation (Flury and Qiu, 2008; Simunek et al., 2006):

$$\rho \frac{\partial S_{AWI}}{\partial t} = \theta_w k_{att}^{AWI} C \quad (2.8)$$

$$k_{att}^{AWI} = M_{att}^{AWI} A_{AWI} \quad (2.9)$$

$$A_{AWI} = \frac{\rho_f g \theta_w}{\alpha \sigma} \left[(S_e^{-1})^{\frac{n}{n-1}} - 1 \right]^{\frac{1}{n}} \quad (2.10)$$

$$S_e = \frac{\theta_w - \theta_r}{\theta_s - \theta_r} \quad (2.11)$$

where k_{att}^{AWI} [s^{-1}] is the colloid attachment coefficient, at AWI. M_{att}^{AWI} [m s^{-1}] is the mass transfer rate coefficients for attachment at AWI. A_{AWI} [m^{-1}] is the specific AWI area, θ_s [-] is the saturated water content, θ_r [-] is the residual water content, ρ_f [g m^{-3}] is the fluid density, g [m s^{-2}] is the gravitational constant, σ [g s^{-2}] is the surface tension of water, S_e[-] is the effective saturation, and α [m^{-1}] and n [-] are the Van Genuchten water retention function parameters. Description of the model calibration, summary of input variables for the model and fitted AgNP transport parameters are shown in the SI.

2.3 Results and Discussion

Effect of Continuous Flow on AgNP transport in an Unsaturated Natural Loamy Sand Soil. BTCs are plotted as normalized effluent concentrations (C/C_0) versus eluted pore volumes (Figure 2.1a), and RPs are plotted as normalized solid phase concentrations (S/C_0) with distance from the column inlet (Figure 2.1b). Mass balance information for the BTCs, RPs and total column is provided in Table 2.1 with a good total mass balance (91-98 %). During the course of the transport experiments the pH of the effluent ranged between 6 and 7 for experiments A, B and C (SI Figure S2.1).

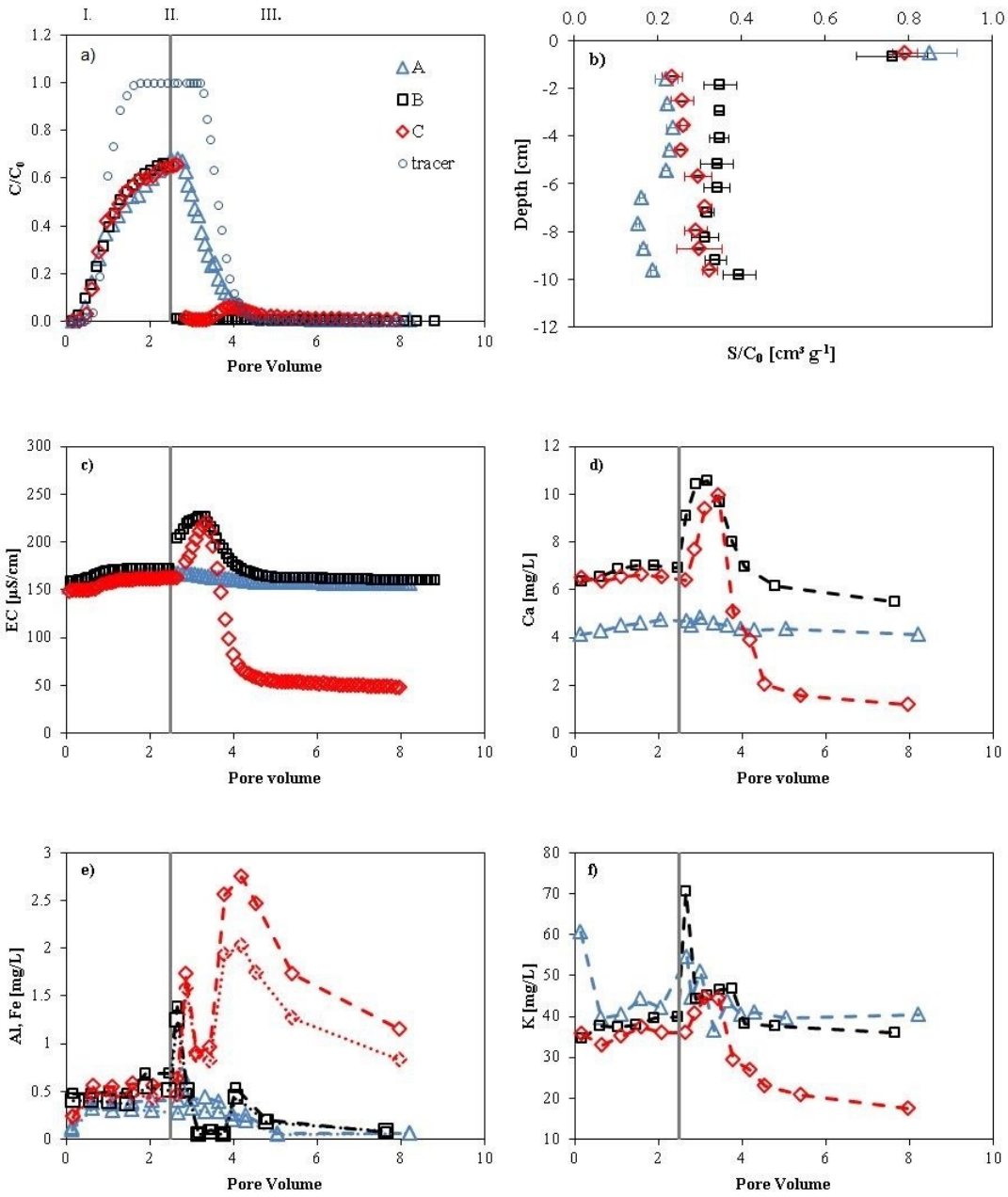

Figure 2.1: Influence of interrupted flow and variable ionic strength on the transport and retention of stabilized AgNP. Breakthrough curves (a) and retention profiles (b) of the AgNP transport experiments A, B and C in unsaturated undisturbed soil columns. Electrical conductivity (EC) (c) and Ca (d), Al (dashed line) (e), Fe (dotted line) (e) and K (f) concentration in the effluent detected during transport experiments A, B and C. Δ Blue Triangle A) = continuous flow and 1 mM ionic strength (IS), □ Black Square B) = flow interruption (FI) and 1 mM ionic strength, and ◊ Red Diamond C) = FI and 1 mM IS before and 0.2 mM after FI. I: Irrigation with AgNP and tracer, II: FI, and III: Irrigation with electrolyte solution. ○ Blue Circle: Tracer.

All AgNP BTCs showed retention in breakthrough compared to the tracer and a similar curve shape during AgNP injection with an increase in effluent concentration up to 0.64 – 0.67 C/C_0 displaying a very good reproducibility of the breakthrough experiments (Figure

2.1a). Direct irrigation with 1 mM KNO_3 after AgNP irrigation showed a continuous decrease in AgNP effluent concentration around 2 PV (experiment A, Figure 2.1a). The breakthrough of AgNP and mass recoveries of effluent and soil were consistent with the results of Liang et al. (2013b) EC and Al, Fe, Ca and K concentration did not change significantly during the whole transport experiment (Figure 2.1c-f). It should be noted here that the presence of Ca^{2+} due to bridging complexation between soil grains and functionalized NP can contribute to AgNP retention (Liang et al., 2013b; Torkzaban et al., 2012). The shape of AgNP BTCs and the tracer was similar during the initial first pore volume but became distinctive as PV increased. This indicates an initially high mobility of AgNP and a time-dependent filling of retention sites (Bradford et al., 2003). The early breakthrough of AgNP in soil can be explained by AgNP size or charge exclusion effects as reported by Sagee et al.(2012) and Braun et al. (2015) It should be noted here that Braun et al. (2015) used the same AgNP-soil system. All RPs showed a hyperexponential shape with a similar high AgNP concentration in the first soil layer (Figure 2.1b).

Table 2.1: Experimental conditions and mass recovery for unsaturated soil column transport with stabilized AgNP in undisturbed loamy sand.

Exp.	flow	IS [mmol/L]		S_w [%]			Recovery [%]			
		before FI	*after FI*	*before FI*	*after FI*	*end*	$M_{I.}$	$M_{III.}$	M_{soil}	M_{total}
A	CF	1	1			81.2	39.4	19.1	39.0	97.5
B	FI	1	1	84.3	68.2	74.5	39.2	3.6	55.5	98.3
C	FI	1	0.2	79.3	61.2	72.2	40.1	6.0	45.1	91.2

CF: continuous flow, FI: flow interruption, IS: ionic strength, S_w: water saturation, end: end of experiment, $M_{I.}$ / $M_{III.}$ / M_{soil} / M_{total}: percentage Ag mass recovered from effluent during AgNP irrigation / during irrigation with electrolyte solution / from soil / and total, respectively.

The model result reproduced measured BTC data well, shown here in a normalized root mean square error (NRMSE) of 0.073 (SI Table S2.2) for experiment A, (SI Figure S2.2). The key process that affects AgNP transport under unsaturated conditions is kinetic attachment both at the SWI and AWI for continuous flow conditions. In experiment A, due to a constant flow rate and ionic strength, the attachment efficiency and attachment coefficient at the SWI remained constant at 0.295 and 31.35 h^{-1}, respectively. The attachment coefficient at AWI was also constant at 0.137 h^{-1} as the water content did not change (eq 2.9-2.11). Values of the attachment coefficient at SWI were about 200-fold larger than the attachment coefficient at AWI. For the same conditions as in experiment A, Liang et al. (2013b) calculated a retention coefficient of 40.02 h^{-1} without a distinction between SWI and AWI. However, the modeled RPs showed that the AgNP concentration attached at SWI was less than that at the AWI (SI Figure S2.3). This is due to the small value of S_{max} giving the available attachment sites at

the SWI (SI Table S2.2), and the assumption of reversible attachment at SWI and irreversible attachment at AWI, respectively. Our results are consistent with previous studies indicating that the SWI has a limited impact for colloid retention even under favorable chemical conditions due to its small S_{max} (Bradford and Torkzaban, 2015). Even though the attachment coefficient at AWI was much smaller than that at SWI, the irreversible attachment at AWI made a comparable contribution to AgNP retention versus the reversible attachment at SWI. Thus, the attachment at both SWI and AWI plays a dominant role in AgNP transport.

Effect of Flow Interruption and Subsequent Ionic Strength Reduction on AgNP Transport. Flow interruption led to dramatically reduced transport and strong AgNP retention in the soil. Furthermore, due to a 3-day flow interruption two significant physicochemical changes were observed. First, water loss took place due to evaporation leading to decreased water saturation (experiment B: from 84.3 % to 68.2 %, experiment C: from 79.3 % to 61.2 %). The water loss (16-18 % of the total soil volume) was most significant in the upper soil layers (Figure 2.2g). Second, an increase of the electrical conductivity (for around 1.5 PV after flow interruption) occurred in experiments B and C (Figure 2.1c), which will be discussed later. It should be noted here that these physicochemical changes could lead to transformation processes such as homo- and heteroaggregation as described in the introduction and may thus influence the transport and retention behavior of AgNP studied (El Badawy et al., 2010; Li et al., 2012; Lowry et al., 2012; Lui and Hurt, 2010; Zhou et al., 2012). These possible processes are unclear and need further investigation.

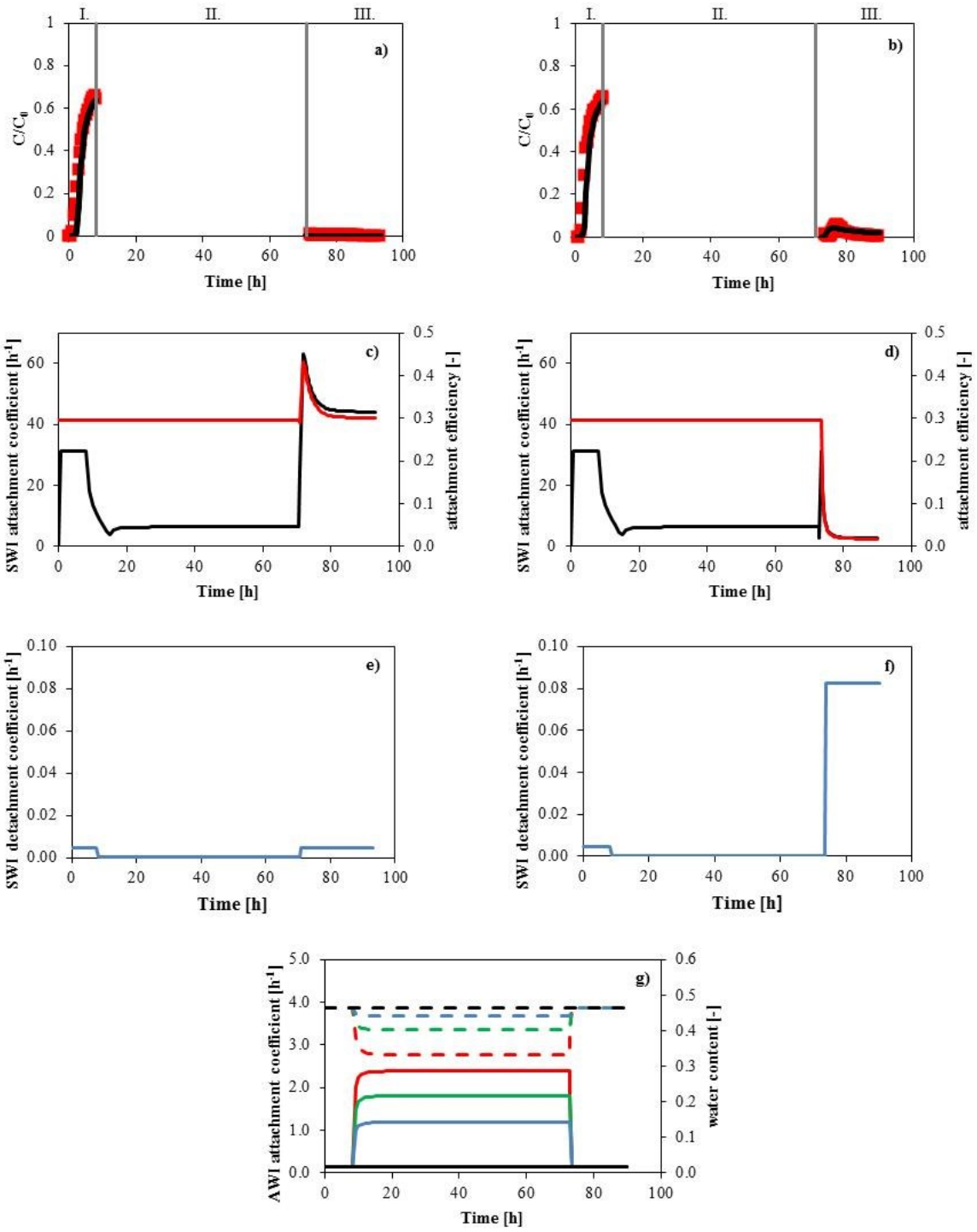

Figure 2.2: Measured (red symbols) versus simulated (black lines) BTCs of AgNP for experiments B (2a) and C (2b). Attachment efficiency (red), attachment coefficient (black) and detachment coefficient at SWI (blue) vary with time observed at the column bottom for experiments B (2c, 2e) and C (2d, 2f). Attachment coefficient at AWI (solid line) and water content (dashed line) vary with time at different column depths for experiments B and C (2g). The red, green, blue and black lines represent column depth of 2, 5, 7 and 10 cm, respectively.

In experiments B and C, the AgNP BTC showed a clear drop directly after flow interruption with a decrease from C/C_0=0.64 (experiment B) and C/C_0=0.66 (experiment C) to C/C_0=0.01, and thus complete retention of the AgNP occurred (Figure 2.1a). The model result

reproduced the measured data well, as shown in an NRMSE of 0.059 (SI Table S2.2) for experiment B (Figure 2.2a). The numerical analysis of experiment B showed that the attachment to the AWI occurring during flow interruption was the key process for AgNP retention. When flow interruption started, flow velocity gradually decreased to zero. Finally, k_{att}^{SWI} decreased 5-fold and k_{det}^{SWI} 11-fold compared to AgNP injection (Figure 2.2c-f). Moreover, only 30 % (1- $f_1^{I,II}$) (SI Table S2.2) of attached AgNP at SWI could be released due to the decrease of the flow rate from step I to step II. This behavior could be explained by the dependence of α on the flow velocity in the CFT (eq 2.6). On the other hand, during flow interruption, attachment at the AWI increased (Figure 2.2g). This was attributed to the extension of the A_{AWI} from 2.08×10^4 to 3.98×10^5 m^{-1} in the upper soil layers due to evaporation caused by flow interruption and by the assumed existence of stagnant zones. Zones with low or stagnant flow velocity formed by grain-grain contacts or developed at the solid-water-air interface can offer a perfect sticking location for NP (Bradford and Torkzaban, 2008; Patzek and Kristensen, 2001; Patzek and Silin, 2001). NP which attached only weakly to a collector surface could easily enter and remain in such areas with low or stagnant flow (Johnson et al., 2007; Li et al., 2010; Torkzaban et al., 2008). Therefore, the decreased water content due to evaporation caused by FI resulted in an increased AgNP retention probably due to more stagnation zones at the solid-water-air interface. Due to the impact of evaporation and subsequent irrigation on the water content distribution and the inverse relation between the specific area (AWI and SWI) and water content (eqs 2.5 and 2.10), the attachment coefficient at the AWI increased (Figure 2.2g) and the detachment coefficient at the SWI decreased (Figure 2.2e-f) during FI, especially at the top layers (eqs 2.9 and 2.4). This resulted in a large accumulation of AgNP at the AWI in experiments B and C, and the attached AgNP at the AWI increased from bottom to top layer (SI Figure S2.3). The retention profile of B showed a much higher AgNP concentration in the soil between 2 and 10 cm compared to continuous flow conditions (Figure 2.1b), which is attributed to evaporation in the upper soil layers (Figure 2.2g) and resulted in higher attachment at the AWI. The key process during flow interruption was the attachment at the AWI. After flow was restarted (III.), flow velocity and water content increased again resulting in an increase of attachment at the SWI (Figure 2.2c-d) and a decrease of attachment at the AWI (Figure 2.2g). Twenty % (1- $f_1^{II,III}$) of attached AgNP at the SWI could be released after flow interruption as given by the model results for experiment B (SI Table S2.2). Due to the large difference between k_{att}^{SWI} and k_{det}^{SWI} (attachment coefficient at the SWI around 10 000 times higher than detachment coefficient) and the irreversible attachment at AWI, only very few AgNP were released when the flow was restarted, which is shown in the experimental results of 3.6 % for AgNP mass (experiment B) recovered from effluent (Table 2.1).

FI resulted in an increase of the electrical conductivity after flow was restarted (III.) (Figure 2.1c) indicating an increase of the ionic strength in the soil water phase. First, this IS increase could result from the evaporation which concentrated the soil solution and second, it could be due to the Ca^{2+} and K^{2+} liberated from the soil matrix under static conditions (Figure 2.1d and 2.1f). The enhanced IS led to an enhanced attachment and reduced AgNP transport

in experiments B and C (Figure 2.1a) due to the compressed electrical double layer (EDL). After flow was restarted (III.) the excess amount of Ca^{2+} and K^+ was washed out at around 2.5-3.7 PV (Figure 2.1d and 2.1f.). This did not directly lead to observable changes in the BTCs until 3.5 PV (Figure 2.1a). A subsequent IS reduction from 1 mM to 0.2 mM (experiment C) after FI showed a decrease of the EC and Ca and K concentration at 3.5 PV (Figure 2.1c, d and 2.1f). Also here the excess Ca^{2+} and K^+ were first washed out and then the IS reduction resulted in a small AgNP effluent peak (C/C_0=0.06) at around 3.5-4.5 PV (Figure 2.1a). The impact of IS reduction on AgNP mobility is consistent with the study by Liang et al. (2013b), where decreasing KNO_3 (10, 5, 1 mM) concentration increased the AgNP transport in soil. It should be noted here that the coating of the soil surface by organic matter can influence AgNP heteroaggregation and thus AgNP mobility. However, because of the relatively low organic matter content of 1.07 % we assume that this effect was only secondary. The release of AgNP correlated highly with the Al and Fe concentration in the effluent (Figure 2.1c). The similar course and PV interval suggest a release of AgNP associated with soil colloids (cotransport) which was not taken into account in the model. The potential for soil colloids to facilitate the release of AgNP (cotransport) is consistent with the study by Liang et al. (2013b) where remobilization experiments showed that the AgNP release from soil columns by IS reduction was linked to the release of soil colloids. It can be assumed that both AgNP release from the soil grain surface and the soil colloids that acted as carriers for AgNP contributed to the small elution peak. The effect of IS on AgNP transport could be explained by the DLVO theory, which does not consider the aggregation of surfactant stabilized particles (Hotze et al., 2010). It should be noted that the calculation with the extended DLVO theory (XDLVO) was not able to reproduce the observed pattern of the BTCs. The XDLVO model predicted unfavorable conditions for AgNP retention and aggregation due to the steric repulsion formed by the adsorbed surfactant layer (Liang et al., 2013a). Consequently, the impact of monovalent cations on the compression of EDL at the NP and the collector calculated by DLVO might be an overestimate. Moreover, the role of surfactants on NP transport in soil needs further investigation. Based on DLVO equations (SI eqs 2.3 and 2.5), the van der Waals potential is independent of IS while the electrostatic potential depends on IS. A lower IS resulted in an upward shift of the total interaction energy curve and thus increased the maximum energy barrier between AgNP and soil surface from 3.79 kT to 5.09 kT (SI Figure S2.4). The overall increase of the total interaction energy was attributed to the increase of electrostatic potential due to an extension of the EDL of AgNP and soil grains. The upward shift of the total interaction energy curve also increased the secondary minimum depth from -4.47×10^{-4} to -6.27×10^{-5} kT, thus decreasing the deposition probability at the secondary minimum depth (SI Figure S2.3). The numerical model was able to replicate the pattern of the impact of IS on the AgNP BTC shown in an NRMSE of 0.076 (SI Table S2.2) for experiment C without considering the cotransport effect (Figure 2.2b). As a result of IS reduction, the attachment efficiency at SWI decreased from 0.3 to 0.02 (Figure 2.2d), which was calculated by the DLVO theory. Due to the relationship between attachment efficiency and attachment coefficient (eq 2.6), the attachment coefficient at SWI also decreased from 31.35 h^{-1} to 2.7 h^{-1}. Compared with experiment B, the detachment coefficient

at SWI increased distinctly when the flow was restarted in experiment C (Figure 2.2e and f). 97 % (1- $f_2^{II,III}$) of attached AgNP at SWI could be released due to the IS reduction given by the model results (SI Table S2.2). However, the decreased attachment and increased detachment at SWI only slightly increased AgNP mobility (Figure 2.1a, 2.2b, d, and f). Indeed only 6 % AgNP mass (experiment C) was recovered from the effluent (Table 2.1). This was attributed to the irreversible attachment at AWI, which counteracted the release of AgNP at SWI, and the relatively small value of the mass transfer rate of AgNP at SWI (eq 2.2), which resulted in a slow release of AgNP from SWI. The retention profile of experiment C showed similar AgNP concentration at the soil depth between 5 cm and 10 cm to that of the RP of experiment B due to FI. However, AgNP concentration at the soil depth between 2 cm and 5 cm was lower than in experiment B, which could be attributed to an influence of the irrigation with a lower IS (0.2 mM) leading to less retention in the soil.

Environmental Implications. Unsaturated soil column experiments with stabilized AgNP in undisturbed loamy sand soil showed that flow interruption led to lower AgNP transport and higher retention. The numerical model according to the CFT-DLVO-CRM theory fitted well with the measured AgNP BTCs under transient hydrological and hydrogeochemical conditions. Flow interruption in an open unsaturated system resulted in a decrease of flow rate and a loss of water content, both of which can significantly enhance AgNP retention. The reduction of IS in soil solution simulating a rain event increased AgNP mobility by increasing the electrical double layer of AgNP, soil colloids and soil grains. In the vadose zone, unsaturated soil conditions usually prevail. The transient hydraulic gradient caused by rain and evaporation events results in a transient flow. Such events also cause the variation of IS in soil water. Thus transient soil water flow with transient IS changes AgNP mobility all the time. A fully process-based numerical model on the field scale incorporating the transient hydrology and hydrochemistry is urgently needed to evaluate and predict the potential risk of subsurface and groundwater contamination by AgNP.

2.4 Supporting Information

Introduction

Appendix A. Supplementary Information. The Supplementary Information provides a brief description and discussion of: (i) procedures for collecting undisturbed soil samples, (ii) running the column experiments, (iii) description of model calibration and summary of the input variables for the model (Table S2.1), (iv) fitted AgNP transport parameters (Table S2.2), (v) pH of effluent samples for experiments A, B and C (Figure S2.1), (vi) measured and simulated BTCs of tracer and AgNP for experiment A (Figure S2.2), (vii) simulated RPs of AgNP at SWI and AWI for experiments A, B and C (Figure S2.3), and (viii) total DLVO interaction energy curve at 1 mM IS and 0.2 mM IS (Figure S2.4).

Collecting Undisturbed Soil Samples. Polyvinyl chloride columns (8 cm inner diameter and 10 cm in length) were filled with undisturbed soil from the upper 30 cm of the field. The

undisturbed soil samples were collected using a metal adaptor with a sharp front attached to the bottom of the column to minimize any disturbance of the soil structure. A water balance was then used to vertically insert the column stepwise into the plowed soil. Between the insertion steps, the surrounding soil was removed, so that at the end the filled column could be easily removed from the sampling field. Before use, the undisturbed soil columns were stored at 4 °C.

Transport Experiments. The bottom of the column was fitted with an acrylic glass plate with 2 mm openings covered by a polyester membrane with 21 μm pores to support uniform flow. The pore volume in the soil column was 228 cm³, 223 cm³ and 239 cm³ for experiments A, B and C, respectively. Before running the transport experiment, the soil column was slowly saturated from the bottom with 1 mM KNO_3 for one week. All column experiments were run with a software-controlled system to achieve unit gradient, steady-state flow conditions in the columns, and to ensure homogeneous water saturation and flow conditions(Unold et al., 2009). In brief, the background solution, tracer and AgNP in one storage bottle were simultaneously pumped through a sprinkling head placed on the top of the column using a peristaltic pump. A constant irrigation rate was controlled and measured by recording the weight of storage bottle for the irrigation solution with a balance linked to a computer. The suction at the bottom of the column was controlled by an air pump and pressure regulation. The matrix potential inside the column was measured using two tensiometers installed 2.5 and 7.5 cm below the column surface. The soil-water tension at the lower column boundary was -7 mbar for experiment A. For experiments B and C, the soil-water tension changed from -7 mbar to -9 mbar after FI. Effluent samples (15 mL for each sample) controlled by an electric circuit with two water level sensors were collected over the course of the experiment using a fraction collector. Important parameters such as electrical conductivity (related to electrolyte concentration), irrigation rate, weight from the balance, and time were recorded automatically for each sample. The columns were irrigated with at least 18 pore volumes of 1mM KNO_3 at 0.2 cm/min until unit gradient (constant matrix potential) and steady state flow and electrical conductivity (baseline conductivity) conditions were achieved. The anions such as chloride were washed out and replaced by nitrate in this equilibrium process to avoid precipitation of silver chloride, which can affect AgNP stability and the subsequent Ag concentration measurements.(Sagee et al., 2012) After this conditioning procedure, the transport experiment was performed as described in the main article. A summary of the experimental conditions is provided in Table S2.1.

Calculations for Attachment Efficiency. The attachment efficiency α [-] is calculated with the Maxwell approach and the DLVO theory (Gregory, 1981; Hogg et al., 1966; Shen et al., 2007):

$$\alpha = \alpha_{pri} + \alpha_{sec} = 1 - \int_{\sqrt{\phi_{sec}}}^{\sqrt{\Delta\phi}} \frac{4}{\pi^{1/2}} x^2 \exp(-x^2)\, dx \quad \text{(S2.1)}$$

$$\phi_t = \phi_{vdw} + \phi_{el} \quad \text{(S2.2)}$$

$$\phi_{vdw} = -\frac{A_{123} a_c a_p}{6y(a_c + a_p)} \left[1 + \frac{14y}{\lambda}\right]^{-1} \quad \text{(S2.3)}$$

$$A_{123} = \left(\sqrt{A_{11}} - \sqrt{A_{33}}\right)\left(\sqrt{A_{22}} - \sqrt{A_{33}}\right) \quad \text{(S2.4)}$$

$$\phi_{el} = \pi\varepsilon_0\varepsilon_r \frac{a_c a_p}{a_c + a_p}\left\{2\psi_p\psi_c \ln\left[\frac{1+\exp(-\kappa y)}{1-\exp(-\kappa y)}\right] + \left(\psi_p^2 + \psi_c^2\right)\ln[1 - \exp(-2\kappa y)]\right\} \quad \text{(S2.5)}$$

$$\kappa = \sqrt{\frac{2N_A e^2 I}{\varepsilon_0\varepsilon_r k_B T}} \quad \text{(S2.6)}$$

where α_{pri} [-] and α_{sec} [-] are the attachment efficiencies at primary and secondary minimum depths, respectively, $\Delta\phi$ is the sum of ϕ_{max} and ϕ_{sec}, ϕ_{max} is the maximum energy barrier and ϕ_{sec} is the secondary minimum, ϕ_t [J] is the total energy barrier, ϕ_{vdw} [J] and ϕ_{el} [J] are the attractive van der Waals potential and repulsive electrostatic potential, respectively. A_{123} [J] is the combined Hamaker constant of the system, A_{11} is the Hamaker constant for AgNP, A_{22} is the Hamaker constant for the collector surface, A_{33} is the Hamaker constant for water, λ is the characteristic wavelength of the interaction [nm], y [nm] is the distance between the colloid and soil grain, ε_0 [C V^{-1} m^{-1}] is the permittivity in the vacuum and ε_r [-] is the relative dielectric permittivity. ψ_p [V] and ψ_c [V] are the zeta potentials of AgNP and the soil grain, respectively. κ [m] is the Debye length, k_B [J K^{-1}] is the Boltzmann constant, T [K] is the temperature, N_A [mol^{-1}] is Avogadro's number, e [C] is the elementary charge, and I is the ionic strength [mol L^{-1}].

Model Calibration. Values of the AgNP diameter (a_p), soil grain diameter (a_c), bulk density (ρ), and volumetric water flux (q) were obtained from laboratory measurements (Table S1). The dispersion coefficient (D) was estimated by the automated calibration of the volumetric water flux (q) and the BTC of D_2O using the inverse model of Hydrus-1D. The AgNP transport parameters (M_{det}^{SWI},f_i,S_{max} and M_{att}^{AWI}) were estimated using PEST (Doherty, 2016). To reduce the uncertainty of the parameter estimation process, the Tikhonov regularization method implemented in PEST is used. Through this method, a parameter field of minimum error variance can be obtained when the regularization constraints are properly formulated. Using the Tikhonov regularization method, PEST minimizes a total objective function:

$$\Phi = \Phi_m + \mu^2\Phi_r \quad \text{(S2.7)}$$

Φ is the target measurement objective function, provided by the user. Φ_m is the measurement objective function, the sum of the squared weighted differences between field measurements and their model-generated counterparts. Φ_r is the regularization objective function, the sum of squared weighted differences between parameters and their preferred conditions (equal to their initial values in this study). μ is the regularization weight factor, which is updated by PEST in every iteration of the inversion process such that a target level of model-to-measurement fit is achieved. Based on the Marquardt-Levenberg method, PEST minimizes the regularization objective function while keeping the measurement objective function smaller than its user-supplied target measurement objective function (Doherty, 2016). The target measurement objective functions in this study were obtained by using a range of parameter values to achieve an acceptable fit between model outputs and field measurements (Fienen et al., 2009). We first estimated M_{det}^{SWI} , S_{max} and M_{att}^{AWI} based on the AgNP BTC

from experiment A. Values obtained for S_{max} and M_{att}^{AWI} were directly transferred to the inversion of experiments B and C and kept fixed during the parameter estimation. f_1 and f_2 were estimated based on the calibration of experiments B and C, respectively. M_{det}^{SWI} was not directly transferred from experiment A but recalibrated in experiments B and C to account for the impact of flow rate and IS, respectively, on the mass transfer rate coefficient during detachment from the SWI according to Torkzaban (Torkzaban et al., 2015).

Table S2.1: Summary of the input variables for the model.

Input variables	Values A, B, C [a]	Unit	Literature/ measured/ estimated/ constant
AgNP radius, a_p	10[b]	nm	measured
Median soil grain radius, a_c	80[c]	µm	
Ionic strength, I	0.001, 0.001/0.001, 0.001/0.0002[d]	mol L^{-1}	
Zeta potential of AgNP, ψ_p	1.1269* I -0.0161[e]	V	(Liang et al., 2013b) / measured
Zeta potential of soil grain, ψ_c	-0.375* I - 0.0371[e]	V	(Liang et al., 2013b) / estimated
Temperature, T	293.15	K	measured
Porosity, n	0.468, 0.465, 0.469	–	
Hamaker constant, A	2.37×10^{-21}	J	(Liang et al., 2013b)
Characteristic wavelength, λ	100	nm	(Zhang et al., 2013)
Boltzmann constant, k_B	1.38×10^{-23}	$J K^{-1}$	constant
Permittivity in vacuum, ε_0	8.85×10^{-12}	$C V^{-1} m^{-1}$	
Relative permittivity, ε_r	78.5	–	
Elementary charge, e	1.60×10^{-19}	C	
Avogadro's number, N_A	6.02×10^{23}	mol^{-1}	
Gravitational constant, g	9.8	$m s^{-2}$	
Fluid density, ρ_f	0.988	$g m^{-3}$	(Zhang et al., 2013)

[a] Input variables for scenario A, B, C, respectively.
[b] AgNP diameter determined by TEM.
[c] Median soil grain diameter determined by sieve analysis.
[d] Ionic strength before and after flow interruption.
[e] Analytical relation between zeta potential and ionic strength.

Table S2.2: Fitted AgNP transport parameters.

Parameters	A	B			C		
		I.	II.	III.	I.	II.	III.
S_{max} [mol kg^{-1}]	2.51×10^{-5}	2.51×10^{-5}	2.51×10^{-5}	2.51×10^{-5}	2.51×10^{-5}	2.51×10^{-5}	2.51×10^{-5}
M_{det}^{SWI} [m h^{-1}]	60.99	60.99	5.00	60.99	60.99	5.00	1137.89
M_{att}^{AWI}[m h^{-1}]	1.83×10^{-9}	1.83×10^{-9}	1.83×10^{-9}	1.83×10^{-9}	1.83×10^{-9}	1.83×10^{-9}	1.83×10^{-9}
f_i [-]	0	0	0.7[a]	0.8[b]	0	0.7[a]	3×10^{-2}[c]
NRMSE [d]	0.073		0.059			0.076	

[a] Fraction of retained colloids at SWI that is not released by the decrease of flow rate ($f_1^{I,II}$).
[b] Fraction of retained colloids at SWI that is not released by the increase of flow rate ($f_1^{II,III}$).
[c] Fraction of retained colloids at SWI that is not released by the decrease of IS ($f_2^{II,III}$).
[d] Normalized root mean square error between measured BTCs and corresponding model results
I.: Irrigation with AgNP and tracer, II.: flow interruption, III.: irrigation with electrolyte solution

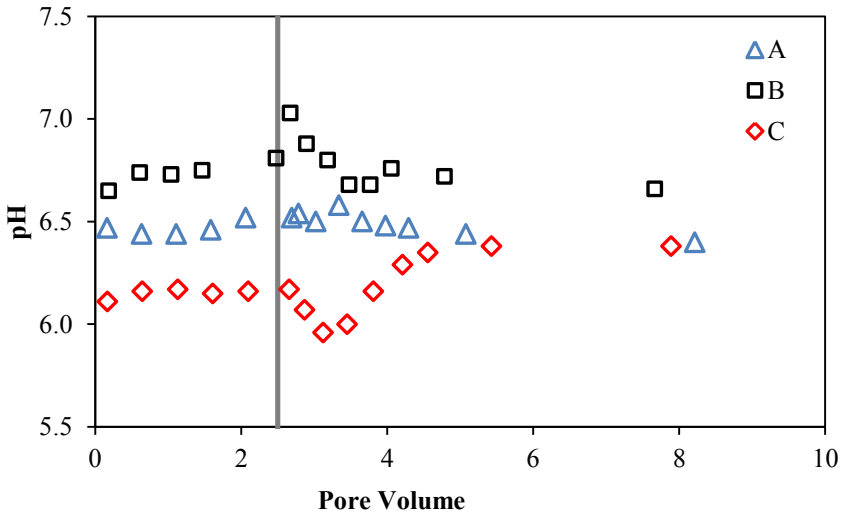

Figure S2.1: pH of effluents samples for experiments A, B and C.

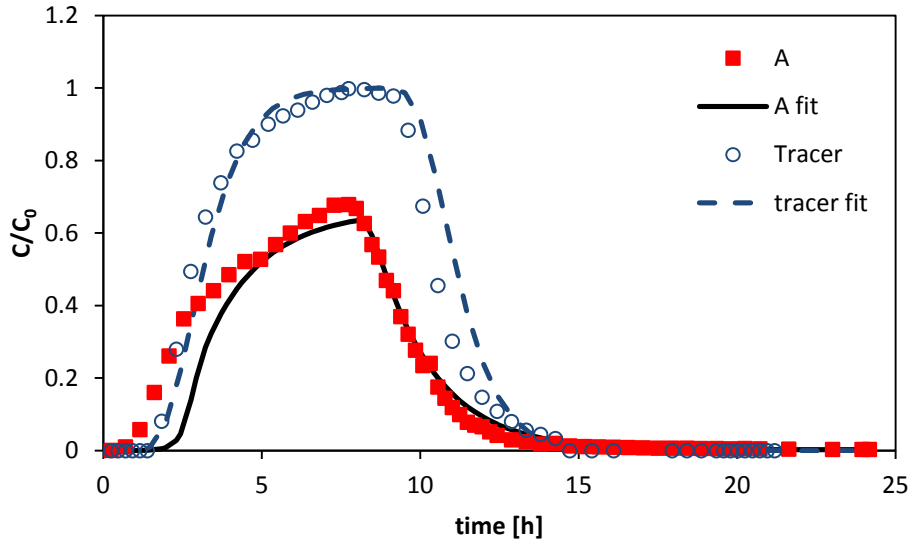

Figure S2.2: Measured and simulated BTCs of AgNP and tracer for experiment A.

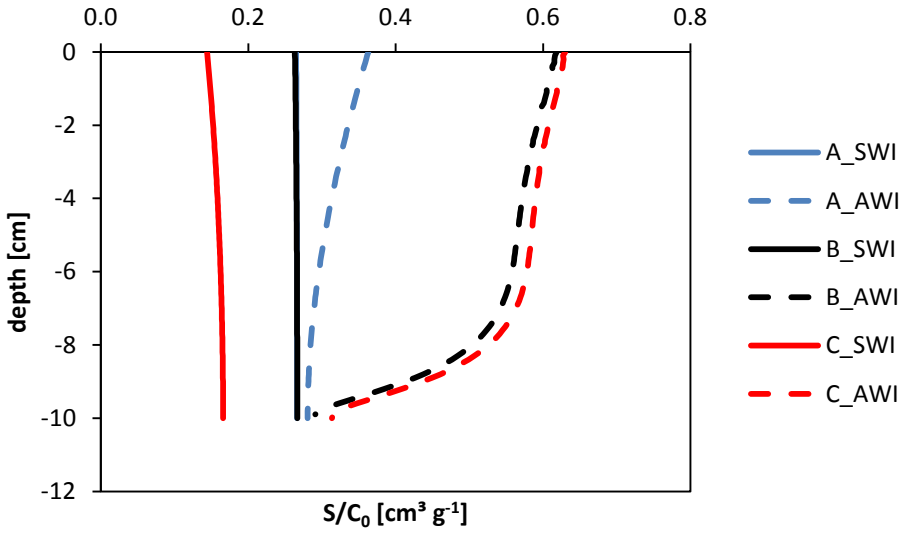

Figure S2.3: Simulated RPs of AgNP at SWI and AWI for experiments A, B and C. The attached AgNP at SWI overlapped for experiments A and B due to their similar values.

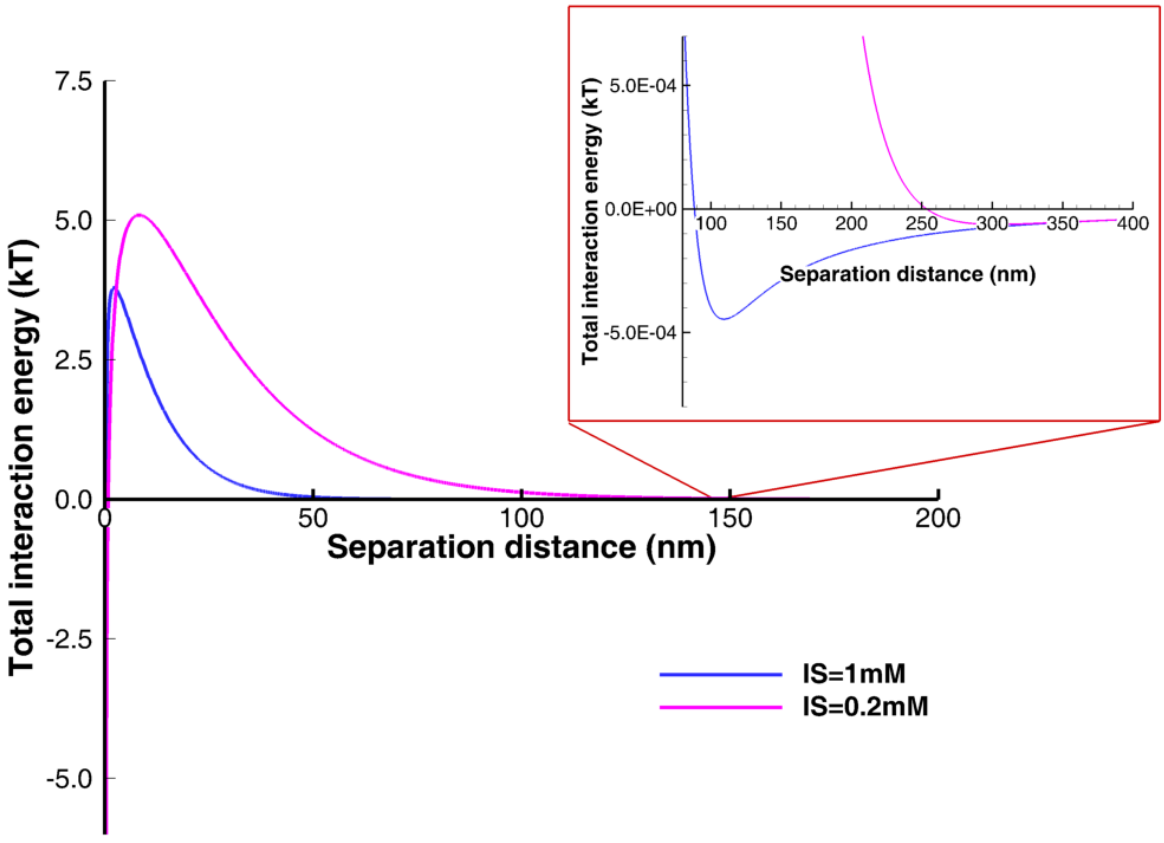

Figure S2.4: The total DLVO interaction energy curve at 1 mM IS and 0.2 mM IS.

2.5 Acknowledgements

Joanna Makselon's work was funded by the Nanomobil project supported by German Federal Ministry of Education and Research (BMBF). Dan Zhou's work was funded by the Chinese Scholarship Council (CSC). We gratefully acknowledge Stephan Köppchen and Astrid Küppers for the analytical measurements.

2.6 References

Bradford, S. A., Simunek, J., Bettahar, M., Van Genuchten, M. T., Yates, S. R., 2006. Significance of straining in colloid deposition: Evidence and implications. Water Resources Research, 42(12), W12S15.

Bradford, S. A., Simunek, J., Bettahar, M., Van Genuchten, M. T., Yates, S. R., 2003. Modeling colloid attachment, straining, and exclusion in sautrated porous media. Environmental Science & Technology, 37(10), 2242-2250.

Bradford, S. A., Torkzaban, S., 2008. Colloid transport and retention in unsaturated porous media: A review of interface-, collector-, and pore-scale processes and models. Vadose Zone Journal, 7(2), 667-681.

Bradford, S. A., Torkzaban, S., 2015. Determining parameters and mechanisms of colloid retention and release in porous media. Langmuir, 31(44), 12096-12105.

Bradford, S. A., Torkzaban, S., Kim, H., Simunek, J., 2012. Modeling colloid and microorganism transport and release with transients in solution ionic strength. Water Resources Research, 48(9), W09509.

Braun, A., Klumpp, E., Azzam, R., Neukum, C., 2015. Transport and deposition of stabilized engineered silver nanoparticles in water saturated loamy sand and silty loam. Science of the Total Environment, 535, 102-112.

Cornelis, G., Pang, L., Doolette, C., Kirby, J. K., McLaughlin, M. J., 2013. Transport of silver nanoparticles in saturated columns of natural soils. Science of the Total Environment, 463-464, 120-130.

Cornelis, G., DooletteMadeleine Thomas, C., McLaughlin, M. J., Kirby, J. K., Beak, D. G., Chittleborough, D., 2012. Retention and dissolution of engineered silver nanoparticles in natural soils. Soil Science Society of America Journal, 76, 891-902.

Doherty, J., 2016. PEST: Model-Independent parameter estimation user manual part I: PEST, SENSAN and Global Optimisers. Watermark Numerical Computing, Brisbane, Australia, 6th ed.

El Badawy, A. M., Hassan, A. A., Scheckel, K. G., Suidan, M. T., Tolaymat, T. M., 2013. Key factors controlling the transport of silver nanoparticles in porous media. Environmental Science & Technology, 47(9), 4039-4045.

Badawy, A. M. E., Luxton, T. P., Silva, R. G., Scheckel, K. G., Suidan, M. T., Tolaymat, T. M., 2010. Impact of environmental conditions (pH, ionic strength, and electrolyte type) on

the surface charge and aggregation of silver nanoparticles suspensions. Environmental Science & Technology, 44(4), 1260-1266.

Fienen, M. N., Muffels, C. T., Hunt, R. J., 2009. On constraining pilot point calibration with regularization in PEST. Groundwater, 47(6), 835-844.

Flury, M., Qiu, H., 2008. Modeling colloid-facilitated contaminant transport in the vadose zone. Vadose Zone Journal, 7(2), 682-697.

Foppen, J. W., Schijven, J. F., 2006. Evaluation of data from the literature on the transport and survival of Escherichia coli and thermotolerant coliforms in aquifers under saturated conditions. Water Research, 40(3), 401-426.

Förster, M., Laabs, V., Lamshöft, M., Pütz, T., Amelung, W., 2008. Analysis of aged sulfadiazine residues in soils using microwave extraction and liquid chromatography tandem mass spectrometry. Analytical and Bioanalytical Chemistry, 391(3), 1029-1038.

Gargiulo, G., Bradford, S., Šimůnek, J., Ustohal, P., Vereecken, H., Klumpp, E., 2007. Bacteria transport and deposition under unsaturated conditions: The role of the matrix grain size and the bacteria surface protein. Journal of Contaminant Hydrology, 92(3-4), 255-273.

Gargiulo, G., Bradford, S., Šimůnek, J., Ustohal, P., Vereecken, H., Klumpp, E., 2008. Bacteria transport and deposition under unsaturated flow conditions: The role of water content and bacteria surface hydrophobicity. Vadose Zone Journal, 7(2), 406-419.

Gottschalk, F., Lassen, C., Kjoelholt, J., Christensen, F., Nowack, B., 2015. Modeling flows and concentrations of nine engineered nanomaterials in the Danish environment. International Journal of Environmental Research and Public Health, 12(5), 5581-5602.

Gregory, J., 1981. Approximate expressions for retarded van der Waals interaction. Journal of Colloid and Interface Science, 83(1),138-145.

Hogg, R., Healy, T. W., Fuerstenau, D. W., 1966. Mutual coagulation of colloidal dispersions. Transactions of the Faraday Society, 62, 1638-1651.

Hoppe, M., Mikutta, R., Utermann, J., Duijnisveld, W., Guggenberger, G., 2014. Retention of sterically and electrosterically stabilized silver nanoparticles in soils. Environmental Science & Technology, 48(21), 12628-12635.

Hotze, E. M., Phenrat, T., Lowry, G. V., 2010. Nanoparticle Aggregation: Challenges to Understanding Transport and Reactivity in the Environment. Journal of Environment Quality, 39(6), 1909-1924.

Jacques, D., Simunek, J., Mallants, D., van Genuchten, M. T., 2008a. Modeling coupled hydrologic and chemical processes: Long-term uranium transport following phosphorus fertilization. Vadose Zone Journal, 7(2), 698-711.

Jacques, D., Simunek, J., Mallants, D., van Genuchten, M. T., 2008b. Modelling coupled water flow, solute transport and geochemical reactions affecting heavy metal migration in a podzol soil. Geoderma, 145(3-4), 449-461.

Jaisi, D. P., Saleh, N. B., Blake, R. E., Elimelech, M., 2008. Transport of single-walled carbon nanotubes in porous media: Filtration mechanisms and reversibility. Environmental Science & Technology, 42(22), 8317-8323.

Johnson, W. P., Li, X., Yal, G., 2007. Colloid retention in porous media: Mechanistic confirmation of wedging and retention in zones of flow stagnation. Environmental Science & Technology, 41(4), 1279-1287.

Kasteel, R., Mboh, C. M., Unold, M., Groeneweg, J., Vanderborght, J., Vereecken, H., 2010. Transformation and sorption of the veterinary antibiotic sulfadiazine in two soils: A short-term batch study. Environmental Science & Technology, 44(12), 4651-4657.

Kumahor, S. K., Hron, P., Metreveli, G., Schaumann, G. E., Vogel, H. J., 2015. Transport of citrate-coated silver nanoparticles in unsaturated sand. Science of the Total Environment, 535, 113-121.

Li, X., Lenhart, J. J., Walker, H. W., 2012. Aggregation kinetics and dissolution of coated silver nanoparticles. Langmuir, 28(2), 1095-104.

Li, X., Li, Z., Zhang, D., 2010. Role of low flow and backward flow zones on colloid transport in pore structures derived from real porous media. Environmental Science & Technology, 44(13), 4936-4942.

Liang, Y., Bradford, S. A., Simunek, J., Heggen, M., Vereecken, H., Klumpp, E., 2013b. Retention and remobilization of stabilized silver nanoparticles in an undisturbed loamy sand soil. Environmental Science & Technology, 47(21), 12229-12237.

Liang, Y., Bradford, S.A., Simunek, J., Vereecken, H., Klumpp, E., 2013a. Sensitivity of the transport and retention of stabilized silver nanoparticles to physicochemical factors. Water Research, 47(7), 2572-2582.

Lin, S., Cheng, Y., Bobcombe, Y., L. Jones, K., Liu, J., Wiesner, M. R., 2011. Deposition of silver nanoparticles in geochemically heterogeneous porous media: Predicting affinity from surface composition analysis. Environmental Science & Technology, 45(12), 5209-5215.

Lowry, G. V., Espinasse, B. P., Badireddy, A. R., Richardson, C. J., Reinsch, B. C., Bryant, L. D., Bone, A. J., Deonarine, A., Chae, S., Therezien, M., Colman, B. P., 2012. Long-term transformation and fate of manufactured Ag nanoparticles in a simulated large scale freshwater emergent wetland. Environmental Science & Technology, 46(13), 7027-7036.

Lui, J., Hurt, R. H., 2010. Ion release kinetics and particle persistence in aqueous nano-silver colloids. Environmental Science & Technology, 44(6), 2169-2175.

Parkhurst, D. L., Appelo, C. A. J., 1999. User's guide to PHREEQC (Version 2) - A computer program for speciation, batch-reaction, one-dimensional transport, and inverse geochemical calculations. Water-Resources Investigations Reports, 99-4259, 1-312.

Patzek, T. W., Kristensen, J. G., 2001. Shape factor correlations of hydraulic conductance in noncircular capillaries: II. Two-phase creeping flow. Journal of colloid and interface science, 236(2), 305-317.

Patzek, T. W., Silin, D. B., 2001. Shape factor and hydraulic conductance in noncircular capillaries: I. One-phase creeping flow. Journal of colloid and interface science, 236(2), 295-304.

Sagee, O., Dror, I., Berkowitz, B., 2012. Transport of silver nanoparticles (AgNPs) in soil. Chemosphere, 88(5), 670-675.

Seetha, N., Mohan Kumar, M. S., Majid Hassanizadeh, S., Raoof, A., 2014. Virus-sized colloid transport in a single pore: Model development and sensitivity analysis. Journal of Contaminant Hydrology, 164, 163-180.

Shang, J., Liu, C., Wang, Z., 2013. Transport and retention of engineered nanoporous particles in porous media: Effects of concentration and flow dynamics. Colloids and Surfaces A: Physicochemical and Engineering Aspects, 417, 89-98.

Shen, C., Li, B., Huang, Y., Jin, Y., 2007. Kinetics of coupled primary- and secondary-minimum deposition of colloids under unfaverable chemical conditions. Environmental Science & Technology, 41(20), 6976-6982.

Simunek, J., He, C., Pang, L., Bradford, S.A., 2006. Colloid-facilitated solute transport in variably saturated porous media. Vadose Zone Journal, 5(3), 1035-1047.

Simunek, J., Van Genuchten, M. T., Sejna, M., 2005. The HYDRUS-1D software package for simulating the one-dimensional movement of water, heat, and multiple solutes in variably-saturated media - Version 3.0, HYDRUS software series 1. Department of Environmental Sciences, University of California Riverside, Riverside, CA, 1-240.

Sun, T. Y., Gottschalk, F., Hungerbühler, K., Nowack, B., 2014. Comprehensive probabilistic modelling of environmental emissions of engineered nanomaterials. Environmental Pollution, 185, 69-76.

Syngouna, V. I., Chrysikopoulos, C. V., 2013. Cotransport of clay colloids and viruses in water saturated porous media. Colloids and Surfaces A: Physicochemical and Engineering Aspects, 416, 56-65.

Tian, Y., Gao, B., Silvera-Batista, C., Ziegler, K. J., 2010. Transport of engineered nanoparticles in saturated porous media. Journal of Nanoparticle Research, 12(7), 2371-2380.

Torkzaban, S., Bradford, S. A., van Genuchten, M. T., Walker, S. L., 2008. Colloid transport in unsaturated porous media: the role of water content and ionic strength on particle straining. Journal of Contaminant Hydrology, 96(1-4), 113-127.

Torkzaban, S., Bradford, S. A., Vanderzalm, J. L., Patterson, B. M., Harris, B., Prommer, H., 2015. Colloid release and clogging in porous media: Effects of solution ionic strength and flow velocity. Journal of Contaminant Hydrology, 181, 161-171.

Torkzaban, S., Wan, J., Tokunaga, T. K., Bradford, S. A., 2012. Impacts of bridging complexation on the transport of surface-modified nanoparticles in saturated sand. Journal of Contaminant Hydrology, 136-137, 86-95.

Unold, M., Kasteel, R., Groeneweg, J., Vereecken, H., 2009. Transport and transformation of sulfadiazine in soil columns packed with a silty loam and a loamy sand. Journal of Contaminant Hydrology, 103(1-2), 38-47.

Wan, J., Tokunaga, T. K., 1997. Film straining of colloids in unsaturated porous media: Conceptual model and experimental testing. Environmental Science & Technology, 31, 2413-2420.

Wang, D., Jaisi, D. P., Yan, J., Jin, Y., Zhou, D., 2015. Transport and retention of polyvinylpyrrolidone-coated silver nanoparticles in natural soils. Vadose Zone Journal, 14(7).

Zhang, H., Nordin, N. A., Olson, M. S., 2013. Evaluating the effects of variable water chemistry on bacterial transport during infiltration. Journal of Contaminant Hydrology, 150, 54-64.

Zhou, D., Abdel-Fattah, A.I. and Keller, A.A., 2012. Clay particles destabilize engineered nanoparticles in aqueous environments. Environmental Science & Technology, 46(14), 7520-7526.

3 Impact of manure-related DOM on sulfonamide transport in arable soils*

Authors: Dan Zhou, Sören Thiele-Bruhn, Martina Gesine Arenz-Leufen, Diederik Jacques, Peter Lichtner, Irina Engelhardt

Abstract **38**

3.1 Introduction **39**

3.2 Materials and methods **40**

3.3 Results and discussion **47**

3.4 Conclusions **57**

Acknowledgements **58**

References **58**

* Published as

Zhou, D., Thiele-Bruhn, S., Arenz-Leufen, M. G., Jacques, D., Lichtner, P., Engelhardt, I., 2016. Impact of manure-related DOM on sulfonamide transport in arable soils. Journal of Contaminant Hydrology, 192, 118-128. https://doi.org/10.1016/j.jconhyd.2016.07.005.

Abstract

Field application of livestock manure introduces colloids and veterinary antibiotics, e.g. sulfonamides (SAs), into farmland. The presence of manure colloids may potentially intensify the SAs-pollution to soils and groundwater by colloid-facilitated transport. Transport of three SAs, sulfadiazine (SDZ), sulfamethoxypyridazine (SMPD), and sulfamoxole (SMOX), was investigated in saturated soil columns with and without manure colloids from sows and farrows, weaners, and fattening pigs. Experimental results showed that colloid-facilitated transport of SMOX was significant in the presence of manure colloids from fattening pigs with low C/N ratio, high $SUVA_{280nm}$ and protein C, while manure colloids from sows and farrows and weaners had little effect on SMOX transport. In contrast, only retardation was observed for SDZ and SMPD when manure colloids were present. Breakthrough curves (BTCs) of colloids and SAs were replicated well by a newly developed numerical model that considers colloid-filtration theory, competitive kinetic sorption, and co-transport processes. Model results demonstrate that mobile colloids act as carriers for SMOX, while immobile colloids block SMOX from sorbing onto the soil. The low affinity of SMOX to sorb on immobile colloids prevents aggregation and also promotes SMOX's colloid-facilitated transport. Conversely, the high affinity of SDZ and SMPD to sorb on all types of immobile colloids retarded their transport. Thus, manure properties play a fundamental role in increasing the leaching risk of hydrophobic sulfonamides.

Keywords: Sulfonamides, Manure, Hydrus-1D, Colloid-facilitated transport

3.1 Introduction

Sulfonamides (SAs) are widely used in animal husbandry. They can restrain growth and multiplication of bacteria by competitively inhibiting the enzyme dihydropteroate synthetase (DHPS) which is involved in folate synthesis (Brown, 1962). The large consumption of thousands of tons of these antibiotics in livestock husbandry every year, and their subsequent excretion and persistence in soil make SAs an environmental issue (Haller et al., 2002; Kemper, 2008). SAs and their transformation products can reach soils via agricultural manure application or livestock droppings from where they can infiltrate to greater soil depths and might be able to migrate into the groundwater (Halling-Sørensen et al., 1998). Application of antibiotic-contaminated animal manure introduces not only veterinary antibiotics to soils, but also large amounts of dissolved organic matter (DOM) (Naden et al., 2010). In the subsurface, suspended mobile colloids can act as carriers for other solutes and particles resulting in an enhanced transport of contaminants. This colloid-facilitated transport has been observed for numerous chemical substances, such as heavy metals (Zhu et al., 2014b), radionuclides (Chen et al., 2005), pesticides (de Jonge et al., 1998), and pharmaceuticals (Sprague et al., 2000). Colloid-facilitated transport has been recognized to play a significant role for contaminant transport processes in natural soils and groundwater. However, our understanding and research on facilitated transport of veterinary antibiotics, e.g. SAs, by manure-derived colloids is still limited.

Fate and transport of colloids in porous media are commonly described by the colloid filtration theory (CFT) that was developed by Yao et al. (1971). This theory has been widely applied in many colloid transport models investigating the fate of microbes (Bradford et al., 2012; Seetha et al., 2014), nanoparticles (Jaisi et al., 2008; Liang et al., 2013), and clay mineral colloids (Syngouna and Chrysikopoulos, 2013). Usually, the sorption sites on the solid surface are limited, especially when high amounts of colloids are present (Flury and Qiu, 2008). In this case, colloids will not only compete with themselves for sorption sites, but also with other contaminants, e.g. SAs. This kind of competitive sorption can be described by the competitive Langmuir kinetic equation (Murali and Aylmore, 1983). Moreover, some contaminants with low aqueous solubility have a strong affinity to sorb not only to the solid phase but also to colloidal particles. The transport of contaminants can then be either enhanced when they sorb to mobile colloids or reduced when the contaminant attach to immobile colloids (Flury and Qiu, 2008). Therefore, ignoring the influence of colloids, which are not only produced by the soil but also externally added by animal manure, on contaminant transport can cause serious underestimation or overestimation of their migration pattern, distance and leaching risk.

Previous studies have showed that the presence of animal manure affects the mobility of antibiotics in soils, but the observed effects vary significantly with respect to the different experimental setups (Burkhardt and Stamm, 2007; Unold et al., 2009; Zou and Zheng, 2013). A systematic investigation of the influence of the manure chemical composition, type, and variability on the transport of hydrophobic and hydrophilic organic contaminants, e.g.

different SAs, in soils that link experimental and numerical analysis is still missing. Currently, various computer codes are available to simulate colloid-facilitated solute transport. These include the Hydrus C-Ride module (Šimůnek et al., 2012) which presets various options covering colloid and Colloid-Facilitated Solute Transport (CFSTr) in variably-saturated porous media, and MATLAB (Zou and Zheng, 2013) which provides a numerical computing environment that users can customize. This includes customization of the solute transport model with colloid-facilitated transport incorporating the necessary specific reactions between colloids and contaminants. However, numerical models that simulate the complete suite of reactive processes between colloids, solid matrix, and multi-species contaminants, including such geochemical processes as competitive sorption between multispecies contaminants for soil, mobile and immobile colloids, degradation, and colloid filtration are currently not available.

In order to systematically understand the environmental fate and transport of veterinary antibiotics in the presence of animal manure, the goal of this study is to: (1) identify the physical and chemical behavior of multiple veterinary SAs, sulfadiazine (SDZ), sulfamethoxypyridazine (SMPD), and sulfamoxole (SMOX) with and without manure-related colloids; (2) explore how the origin of the manure (manures from sows and farrows, weaners, and fattening pigs) and its quantity affect antibiotic mobility; (3) analyze colloid-affected antibiotic transport mechanisms by fully coupled and process-based reactive transport simulations.

3.2 Materials and methods

3.2.1 Chemicals, soil and manure

In the experiments performed in this study, three SAs were tested, i.e. sulfadiazine (SDZ, $C_{10}H_{10}N_4O_2S$, CAS-Nr. 68-35-9), sulfamethoxypyridazine (SMPD, $C_{11}H_{12}N_4O_3S$, CAS-Nr. 80-35-3), and sulfamoxole (SMOX, $C_{11}H_{13}N_3O_2S$, CAS-Nr. 729-99-7). Standard compounds were of > 99 % purity and purchased from Dr. Ehrenstorfer GmbH (Augsburg, Germany). Antibiotic stock solutions of 1 g L^{-1} were prepared in HPLC grade MeOH (Merck, Belgium). For soil spiking, a mixture was prepared in a solution with v/v ratio of 1:100 methanol and MilliQ H_2O.

Disturbed soil samples from a Cambisol were collected from the topsoil (0–10 cm) from an arable field at the Steinseler Plateau, Luxembourg. The air-dried soil was sieved to ≤2 mm and stored in the dark at room temperature before use. The loamy sand soil consisted of 75% sand, 15% silt, and 10% clay. The cation exchange capacity (CEC) was 2.0 cmol kg^{-1} and the organic carbon content (OC) was 7.59 g kg^{-1}. Soil pH of 4.3 was increased by the addition of manure DOM to values between 4.8 and 5.5.

Pig manure was sampled from three pig production units, i.e. sows and farrows (SF), weaners (W), and fattening pigs (F) from a pig farm in Luxembourg, representing different

life stages and feeding regimes. Grab samples were taken with a 10 L bucket at the outlet of the pig stables. On the same day, the manure samples were processed in the lab by centrifugation (1200 g, 45 min) and by two subsequent filtration steps to obtain DOM. In the first filtration step, the supernatant was filtered with a 0.63 µm GF/F glass fiber filter (Whatman, Germany). The resulting substrate was filtered in the second step with a 0.45 µm cellulose-acetate filter membrane (Sartorius, Germany). The obtained DOMs are the major components of colloids in the pig manure filtrate (Zou and Zheng, 2013).

3.2.2 Analytical methods

The dry matter (DM) content [%] was determined gravimetrically after drying for 12 h at 105 °C. The pH and electrical conductivity (EC) [mS cm^{-1}] were determined with a pH electrode (SenTix 21, WTW, Germany) and conductivity meter (Cond 340i, WTW, Germany), respectively. The dissolved organic carbon (DOC) and dissolved nitrogen (DN) were determined by analyzing the organic carbon and total nitrogen concentrations in pig manure DOM using a TOC-VCPN (Total organic carbon analyzer, Shimadzu, Japan) and the Kjeldahl method, respectively. DOC and DN concentrations were corrected to the dry weight of the pig manure and were expressed in mg kg^{-1} dry manure. The specific UV absorbance at a wavelength of 280 nm ($SUVA_{280nm}$) was used to estimate the dissolved aromatic organic carbon content that is formed by tyrosine and tryptophan in the pig manure DOM. UV absorbance measurements were performed on a UV-1650PC UV/VIS spectrophotometer (Shimadzu, Japan) with MilliQ H_2O as blank. A quartz glass cell with 1.0 cm path length was used. The $SUVA_{280nm}$ [l mg^{-1} m^{-1}] was calculated from the relation

$$SUVA_{280nm} = \frac{\lambda_{280} * 100}{C_{DOM}} \tag{3.1}$$

with λ_{280} being the extinction at the wavelength 280 nm, and C_{DOM} being the DOC concentration of the pig manure DOM sample. The protein concentration (protein C) of the DOM was also determined by the Lowry method to quantify the total concentration of proteins in solution which are likely to sorb on solid surfaces (Rabe et al., 2011).

3.2.3 Column experiments

The soil was repacked in Teflon columns with porous Teflon plates installed at the inlet and outlet (10 cm height and 4.7 cm diameter) (EcoTech, Bonn, Germany), adjusting to a bulk density of 1.5 g cm^{-3}, and porosity equals to 0.34. All 13 columns were saturated with 0.01 M $CaCl_2$ with a bottom-up steady state flow of 0.285 cm h^{-1} for 72 h. Then 20 mL of the spiked solution was injected as a pulse while maintaining continuous flow. The spiked solution contained 50 mg of bromide (Br^-) as conservative tracer and an antibiotic mixture with 250 µg SDZ, 250 µg SMOX, and 250 µg SMPD, and/or pig manure DOM from the different pig units. The spiked amount of DOM (expressed as DOC) ranged between 8 and 115 mg (Table 3.1). They were disproportionate with each other due to the extremely heterogeneous

distribution of DOM in manure solution made it impossible to acquire a desired DOC-concentration by dilution. After spiking, the outflow of the column was collected over 96 hours by an automated fraction collector (Köhler Technische Produkte, Neulussheim, Germany) taking one sample every 2 h. The same experimental procedure was also applied to a column that was continuously flushed by 0.01 M $CaCl_2$ without manure and SAs addition for 72 hours to verify the soil-released colloids.

Table 3.1: Solute concentrations in each soil column experimental scenario.

Scenario		Br^- [mol L^{-1}]	SDZ [mol L^{-1}]	SMPD [mol L^{-1}]	SMOX [mol L^{-1}]	DOC [mol L^{-1}]
Loamy sand	AB	0.126	2.02×10^{-4}	1.80×10^{-4}	1.89×10^{-4}	—
	F23mg	0.126	—	—	—	0.3872
	F10mg+AB	0.126	2.02×10^{-4}	1.80×10^{-4}	1.89×10^{-4}	0.1684
	F18mg+AB	0.126	2.02×10^{-4}	1.80×10^{-4}	1.89×10^{-4}	0.3030
	F38mg+AB	0.126	2.02×10^{-4}	1.80×10^{-4}	1.89×10^{-4}	0.6394
	SF40mg	0.126	—	—	—	0.6734
	SF17mg+AB	0.126	2.02×10^{-4}	1.80×10^{-4}	1.89×10^{-4}	0.2862
	SF25mg+AB	0.126	2.02×10^{-4}	1.80×10^{-4}	1.89×10^{-4}	0.4209
	SF34mg+AB	0.126	2.02×10^{-4}	1.80×10^{-4}	1.89×10^{-4}	0.5724
	W24mg	0.126	—	—	—	0.4040
	W8mg+AB	0.126	2.02×10^{-4}	1.80×10^{-4}	1.89×10^{-4}	0.1347
	W54mg+AB	0.126	2.02×10^{-4}	1.80×10^{-4}	1.89×10^{-4}	0.9091
	W115mg+AB	0.126	2.02×10^{-4}	1.80×10^{-4}	1.89×10^{-4}	1.9360

AB: mixture of three sulfonamides.

FXXmg: Colloid derived from fattening pig with XX the amount in mg, etc.

FXXmg+AB: The mixture of three SAs with XXmg colloid from fattening pig.

3.2.4 Numerical model set-up

The code HP1 was used to simulate one-dimensional flow, conservative transport of a tracer, and reactive transport of antibiotics and colloids (Jacques et al., 2008). HP1 couples Hydrus-1D with the geochemical code PhreeqC and can simulate not only water flow and solute transport, but also a broad range of biogeochemical reactions in variably saturated media (Parkhurst and Appelo, 1999; Šimůnek et al., 2008).

The 10 cm high soil column was discretized into 101 nodes. The total simulation time was 96 hours. For the simulation of flow the upper and lower boundary conditions were assigned constant pressure heads. The initial water content was set to 0.34 which equals the measured porosity of the soil. For conservative transport, a concentration flux boundary was assigned as the upper boundary condition where 0.126 mol L^{-1} Br^- was injected for 1 hour, while a zero gradient boundary was used for the lower boundary condition. The same boundary conditions

were applied for reactive transport of SAs, DOM, and SAs and DOM mixtures with the concentrations summarized in Table 3.1.

3.2.5 General advective-dispersive transport

The transport of the colloids (DOM) and the three SAs was simulated based on the modified form of the general advection-dispersion equation in one spatial dimension accounting for colloid filtration and describing the potential colloid-matrix interaction as well as the interaction of SAs with the soil and colloids (Bradford et al., 2003; Šimůnek et al., 2006). These equations are given by:

$$\frac{\partial \theta_w C_{DOM}}{\partial t} + \rho_b \frac{\partial S_{DOM}^{str}}{\partial t} + \rho_b \frac{\partial S_{DOM}^{att}}{\partial t} = \frac{\partial}{\partial z}\left(\theta_w D \frac{\partial C_{DOM}}{\partial z}\right) - \frac{\partial q C_{DOM}}{\partial z} - R \tag{3.2}$$

$$\frac{\partial \theta_w C_i}{\partial t} + \rho_b \frac{\partial S_i}{\partial t} + \frac{\partial \theta_w C_{DOM} S_i^m M_{DOM}}{\partial t} + \rho_b \frac{\partial S_{DOM} S_i^{im} M_{DOM}}{\partial t} = \frac{\partial}{\partial z}\left(\theta_w D \frac{\partial C_i}{\partial z}\right) - \frac{\partial q C_i}{\partial z}$$
$$+ \frac{\partial}{\partial z}\left(\theta_w D \frac{\partial C_{DOM} S_i^m M_{DOM}}{\partial z}\right) - \frac{\partial q C_{DOM} S_i^m M_{DOM}}{\partial z} \tag{3.3}$$

where θ_w [L L^{-1}] is the volumetric water content, C_{DOM} [mol L^{-1}] is the colloid concentration in the solution, ρ_b [kg L^{-1}] is the bulk density of soil, D [m^2 s^{-1}] is the dispersion coefficient, q [m s^{-1}] is the volumetric water flux (generally different for aqueous species and colloids), and z [m] is the distance from the column inlet. S_{DOM}^{str} [mol kg^{-1}] is the concentration of strained colloids by soil, S_{DOM}^{att} [mol kg^{-1}] is the concentration of attached colloids on the soil surface. R describes the rate of decay of DOM [mol L^{-1} s^{-1}] given by

$$R = \theta_w k_{dec} C_{DOM} \tag{3.4}$$

C_i [mol L^{-1}] is the concentration of SAs (i.e. SDZ, SMOX, and SMPD, respectively), S_i [mol kg^{-1}] is the concentration of attached SAs on the soil surface, S_i^m [mol kg^{-1}] is the concentration of attached SAs on the mobile DOM, S_i^{im} [mol kg^{-1}] is the concentration of attached SAs on the immobile DOM. S_{DOM} is the sum of the concentrations of strained and attached colloids on the soil surface [mol kg^{-1}], and M_{DOM} [kg mol^{-1}] is the molar mass of DOM. k_{dec} [s^{-1}] is the solute colloid decay rate coefficient.

3.2.6 Colloid transport of DOM

First-order kinetic expressions are employed to account for colloid transport of DOM. The reactive transport equations for DOM consider attachment, detachment, decay and straining (Bradford et al., 2003; Flury and Qiu, 2008; Foppen and Schijven, 2006), and are given as

$$\rho_b \frac{\partial S_{DOM}^{str}}{\partial t} = \theta_w \, k_{str} C_{DOM} \tag{3.5}$$

$$\rho_b \frac{\partial S_{DOM}^{att}}{\partial t} = \theta_w \psi_s f_s k_{att} C_{DOM} - \rho_b k_{det} S_{DOM} \tag{3.6}$$

where the various coefficients are defined by

$$k_{str} = 0.68\left(\frac{d_p}{d_{50}}\right)^{1.5} v\varepsilon a_{str} f \tag{3.7}$$

$$k_{att} = \frac{\eta v \varepsilon f}{4} \tag{3.8}$$

$$\psi_s = 1 - S_{DOM}/S_{max} \tag{3.9}$$

$$\eta = \eta_0\left[\lambda\alpha_f + (1-\lambda)\alpha_u\right] \tag{3.10}$$

$$f = \frac{6(1-\varepsilon)}{\varepsilon d_{50}} \tag{3.11}$$

where k_{str} [s^{-1}] is the first-order straining coefficient, ψ_s [-] is the blocking function, S_{max} [mol kg^{-1}] are the maximum number of sorption sites on the soil surface for a particular DOM type. f_s [-] is the fraction of available soil surface area for attachment and was assumed to be 0.5. k_{att} [s^{-1}] is the colloid attachment coefficient. v [m s^{-1}] is the pore water flow velocity calculated by the model and ε [-] is the effective porosity measured for each column, f [m^{-1}] is the specific surface area, η [-] is the collector efficiency, η_0 [-] is the single collector contact efficiency (Foppen and Schijven, 2006), k_{det} [s^{-1}] is the colloid detachment coefficient. d_p [m] is the median colloid diameter and d_{50} [m] is the median porous medium grain diameter, with the measured value 1.85×10^{-4} m. α_f [-] and α_u [-] are the attachment efficiencies to favorable and unfavorable attachment sites, which are assumed to equal 1.0 and 0.005, respectively (Foppen and Schijven, 2006). λ [-] is the fraction of the favorable attachment sites on the solid surface. a_{str} [-] is the colloid straining efficiency.

3.2.7 Antibiotic transport

Competitive sorption of SAs on the soil surface in the absence of manure colloids is based on the Langmuir competitive adsorption kinetics (Murali and Aylmore, 1983):

$$\frac{\partial S_i}{\partial t} = k_{ai} C_i\left(Q - \sum_j S_j\right) - k_{di} S_i \tag{3.12}$$

S_i [mol kg^{-1}] is the adsorbed antibiotic concentration on the soil, and C_i [mol L^{-1}] is the aqueous concentration. k_{ai} [L mol^{-1} s^{-1}] and k_{di} [s^{-1}] are the attachment and detachment rate coefficients for the soil. Q [mol kg^{-1}] denotes the available sorption sites on the soil. At equilibrium $\partial S_i/\partial t = 0$, it follows that $k_{ai}/k_{di} = K_i$, where K_i [L mol^{-1}] is the Langmuir-type distribution coefficient (Murali and Aylmore, 1983).

3.2.8 Colloid-facilitated transport

The transport of the three SAs in the presence of manure colloids that account for competitive sorption on the mobile and immobile colloids and competitive sorption on the soil surface are described by:

$$\frac{\partial \theta_w C_{DOM} S_i^m}{\partial t} = C_{DOM}\left[k_{ai}^m C_i\left(\frac{C_{DOM}}{\rho_{DOM}} - \sum_j S_j^m\right) - k_{di}^m S_i^m\right] + \frac{\partial}{\partial z}\left(\theta_w D \frac{\partial C_{DOM} S_i^m}{\partial z}\right) - \frac{\partial q C_{DOM} S_i^m}{\partial z} \quad (3.13)$$

$$\frac{\partial S_{DOM} S_i^{im}}{\partial t} = S_{DOM}\left[k_{ai}^{im} C_i\left(S_{DOM} - \sum_j S_j^{im}\right) - k_{di}^{im} S_i^{im}\right] \quad (3.14)$$

$$S_{DOM} = S_{DOM}^{str} + S_{DOM}^{att} \quad (3.15)$$

$$\frac{\partial S_i}{\partial t} = k_{ai} C_i\left(Q - \sum_j S_j - S_{DOM}\right) - k_{di} S_i \quad (3.16)$$

where S_i^m and S_i^{im} [mol kg^{-1}] refer to the SAs adsorbed on mobile and immobile colloids, respectively. ρ_{DOM} [kg L^{-1}] is the bulk density of DOM. k_{ai}^m [L mol^{-1} s^{-1}] and k_{di}^m [s^{-1}] are the attachment and detachment rate coefficients for the mobile colloids, while k_{ai}^{im} [L mol^{-1} s^{-1}] and k_{di}^{im} [s^{-1}] are those for immobile colloids. The ratio of the forward and backward rate constants is equal to the Langmuir distribution coefficients $k_{ai}^m/k_{di}^m = K_i^m$ [L mol^{-1}] and $k_{ai}^{im}/k_{di}^{im} = K_i^{im}$ [L mol^{-1}], for mobile and immobile colloids (Murali and Aylmore, 1983). Colloids were extracted from pig manure and thus the colloids investigated consist of a mixture of multiple colloid types. Colloids were separated into mobile and immobile colloids representing different colloid species. Separation between mobile and immobile colloid types account for different hydrophilic and hydrophobic colloid species that vary with respect to their attachment and detachment rate coefficients for colloids and sulfonamides.

Both Eq. (3.13) and (3.16) can account for colloid-facilitated solute transport. Eq. (3.13) describes 3 different sulfonamides (C_i) which compete with each other for sorption sites on mobile colloids (DOM), and thus accounts for co-transport. In Eq. (3.13), the term C_{DOM}/ρ_{DOM} represents the total sorption sites on the mobile colloids. S_i^m is the *i*th sulfonamide adsorbed on mobile colloids. $\sum_j S_j^m$ is the sum of all the three sulfonamides adsorbed on the mobile colloids. The term $C_{DOM}/\rho_{DOM} - \sum_j S_j^m$ accounts for available sorption sites that remain free on the mobile colloids. The Eq. (3.16) includes not only the competition between sulfonamides, but also the competition between sulfonamides and colloids (S_{DOM}) for the sorption sites on the soil surface. When large quantities of colloids exist and adsorb on the soil surface, they fill available sorption sites for sulfonamides blocking sulfonamide adsorption on the soil. This process also accounts for colloid-facilitated sulfonamide transport. In all there are a total of 15 equations for 15 unknown quantities providing a complete description of the problem.

3.2.9 Model calibration

Several parameters were obtained via measurements, such as soil porosity (ε), bulk density (ρ_b), volumetric water flux (q). The dispersion coefficient (D) was estimated by the inversion of the bromide BTCs using the inverse model of Hydrus-1D. Further reactive transport parameters were estimated using PEST (Doherty, 2016). To reduce the uncertainty of the parameter estimation process, the Tikhonov regularization method implemented in

PEST is used. This method stabilizes the inverse problem when many parameters are estimated (Doherty, 2003). Through this method, a parameter field of minimum error variance can be obtained when the regularization constraints are properly formulated (Doherty, 2016). Using the Tikhonov regularization method, PEST minimizes a total objective function:

$$\Phi = \Phi_m + \mu^2 \Phi_r \tag{3.17}$$

The quantity Φ is the target measurement objective function, provided by the user. The quantity Φ_m is the measurement objective function, given by the sum of squared weighted differences between field measurements and their model-generated counterparts. The quantity Φ_r is the regularization objective function which is the sum of squared weighted differences between parameters and their preferred values (equal to their initial values in this study). The factor μ is the regularization weight factor, which is calculated anew by PEST every iteration of the inversion process such that a target level of model-to-measurement fit is achieved. Based on the Marquardt-Levenberg method, PEST minimizes the regularization objective function while keeping the measurement objective function no higher than its user-supplied target measurement objective function (Doherty, 2016). The target measurement objective functions in this study were obtained from exploration of the behavior of the inversion using a range of values by achieving an acceptable fit between model outputs and field measurements (Fienen et al., 2009). In the colloid transport model, the median colloid diameter (d_p), the fraction of the favorable attachment sites (λ), colloid straining efficiency (a_{str}), detachment coefficient (k_{det}), decay rate constant (k_{dec}), and the total sorption sites (S_{max}) for each type of colloid were included in the inversion of the measured colloid BTCs. For the antibiotic transport, available sorption sites (Q), and attachment (k_{ai}) and detachment (k_{di}) coefficients for each of the three SAs were estimated by fitting the SAs BTCs.

The calibration of the colloid-facilitated transport model employs parameters that are estimated in previous runs to reduce the parameter uncertainty. Thus, the parameters d_p, λ, S_{max}, a_{str}, and k_{det} obtained from the colloid transport model and Q, k_{ai}, and k_{di} obtained from the antibiotics transport model were fixed in the colloid-facilitated transport model and not included in the parameter estimation. The total number of estimated parameter was therefore limited to five. In addition, to reduce the uncertainty of the estimated parameter, the initial values and lower and upper bounds were defined according to the literature values (λ, a_{str}, k_{det}, k_{dec}, k_{ai}^m, k_{ai}^{im}, k_{di}^m, and k_{di}^{im}) and experimental results (d_p, S_{max}, and Q). The colloid decay rate constant (k_{dec}) was recalibrated since differences in microbial biomass with different amounts of DOM influence k_{dec} (Cunha and Nunes, 2011). The attachment coefficient (k_{ai}^m and k_{ai}^{im}) and detachment coefficient (k_{di}^m and k_{di}^{im}) of each antibiotic for the sorption on mobile and immobile colloids were estimated by joint inversion of both SAs and colloid BTCs.

The composite sensitivity of each parameter was calculated by PEST using the relation (Doherty, 2016):

$$S_i = (\mathbf{J}^t\mathbf{Q}\mathbf{J})_{ii}^{1/2}/m \tag{3.18}$$

where S_i is the sensitivity for the ith parameter, **J** is the Jacobian matrix and **Q** is the cofactor matrix, and m is the number of observations with non-zero weights. The results show how much a model output (e.g. colloid or SAs breakthrough concentration) changes with respect to the perturbation of an adjustable parameter. This approach evaluates the impact (sensitivity) of parameters on the model response and reveals the dominant parameters controlling the model output.

3.2.10 Travel time analysis

The laboratory measured experimental travel time of SAs and colloids is calculated as the first normalized moment (Ptak et al., 2004):

$$t_{50} = \frac{\int_0^\infty tC(L,t)dt}{\int_0^\infty C(L,t)dt} \tag{3.19}$$

where t_{50} [h] is the mean travel time of the solute, t [h] is the time, and $C(L,t)$ [mol L^{-1}] is the solute concentration at location L and time t, L [cm] refers to the distance from the inlet of the column where the travel time is evaluated, equals to 10 cm. Comparison with the travel time of a tracer indicates the retardation of SAs or colloids in the soil.

3.3 Results and discussion

3.3.1 Variability of manure

In the manure DOM fraction, the dry matter content (DM) ranged between 0.9 to 2.4 % which is comparable to typical values given for pig slurry (<0.45 µm fraction) (Aust et al., 2009). The variations in DM are attributed to the various feeding and housing conditions of different pig life stages and storage strategies of the manure (Leenheer and Rostad, 2004). The C/N ratios of the investigated manure DOM fraction ranged from 1.6 to 5.8 and was thus lower than reported for unprocessed manures ranging from 5.7 to 10.4 (Aust et al., 2009; Zhu et al., 2014a). This difference might be due to the preconditioning of manure samples by filtration before chemical analysis eliminating organics with high molecular weight. It also indicates that the dominant N-containing compound in the manure DOM was urine (Aust et al., 2009). DOM from fattening pigs (DOM_F) contains the highest amounts of 2.39% dissolved nitrogen (DN) and the lowest C/N ratio displays its high urine content (Table 3.2). The elevated EC of DOM_F might be due to the high urine content. Pig manures are typically alkaline, a comparable pH value of 8.2 was reported for pig manure derived DOM by Businelli et al. (1999). However, a low pH value of 5.9 was found for DOM from weaners (DOM_W), which is attributed to the specific feeding during the weaning program, and the $SUVA_{280nm}$ was highest for DOM_F. These findings suggest that DOM_F has more aromatic compounds than DOM_SF and DOM_W. In general a high aromaticity suggests large amounts of hydrophobic compounds and high average molecular weights that increase the

surface binding forces of the substance (Chin et al., 1994). Besides, DOM_F also has the highest content of protein C which tends to sorb at solid interfaces (Rabe et al., 2011).

Table 3.2: Chemical properties of the manure DOM fraction.

Parameter		DM	DOC	DN	C/N ratio	pH	EC	$SUVA_{280nm}$	Protein C
Unit		%	mg kg^{-1}	mg kg^{-1}	-	-	mS cm^{-1}	L mg^{-1} m^{-1}	mg kg^{-1}
Manure type	Abbr.								
Sows + farrows	SF	0.90 (±0.02)	130.4 (±2.9)	42.3 (±3.0)	3.1	7.65	14.69	0.15	15.7 (±1.7)
Weaners	W	1.68 (±0.01)	332.3 (±4.2)	57.6 (±5.9)	5.8	5.90	16.58	0.12	23.7 (±1.9)
Fattening pigs	F	2.39 (±0.04)	154.9 (±16.7)	97.2 (±1.5)	1.6	8.61	58.40	0.35	25.3 (±5.5)

DM = dry matter

DOC = dissolved organic carbon

DN= dissolved nitrogen

EC = electrical conductivity

3.3.2 Colloid transport

The control experiment shows that the effluent concentration of colloids generated by soil decreased quickly within 72 hours which was the pre-equilibrated time before manure colloid injection (Figure 3.1). No effluent peak was observed and the final minor concentration almost had no impact on manure colloid transport. The analysis of the column experiments displays a different transport pattern for each colloid type associated with the different manure types (Figure 3.2). Compared to the mean travel time (t_{50}) of the conservative tracer bromide, all t_{50} values were longer and increased from DOM_W to DOM _SF to DOM _F. The BTCs also show an increased tailing compared to bromide, especially for DOM_SF and DOM_F. These observations suggest non-equilibrium adsorption of the colloids (Šimůnek and van Genuchten, 2008). The highest retardation was found for DOM_F, which is consistent with the high $SUVA_{280nm}$ and indicates a high adsorption of the DOM_F on the grain surfaces.

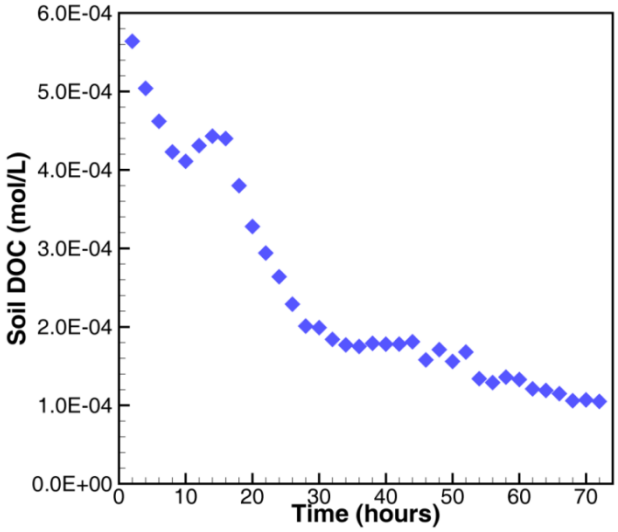

Figure 3.1: Effluent DOC concentration of soil-released colloids.

The colloid transport model fitted well the measured DOC BTCs with NRMSEs ranging from 0.01 to 0.02, indicating that colloid filtration theory is a valuable model for DOM transport (Figure 3.2). Maximum sorption sites of the soil (S_{max}) were found for DOM_W and the lowest amount for DOM_F (Table 3.3). The calculated lower S_{max} for DOM_F shows that a relatively small fraction of possible soil sorption sites are available for these colloids. This could lead to the hypothesis that DOM_F is less retarded than DOM_SF and DOM_W. However, only 24% of DOM_F was recovered compared to 81% and 67% for DOM_SF and DOM_W, calculated as the difference between the injected and the recovered amounts. This unexpected result can be explained by the small detachment rate (k_{det}) and high decay rate (k_{dec}) constants of DOM_F. The rate constant k_{det} was two and three orders of magnitude lower than for DOM_W and DOM_SF, respectively, resulting in a high immobilization and strong sorption of DOM_F on the soil surface. The high k_{dec} of DOM_F also produces a relatively low concentration in the discharge.

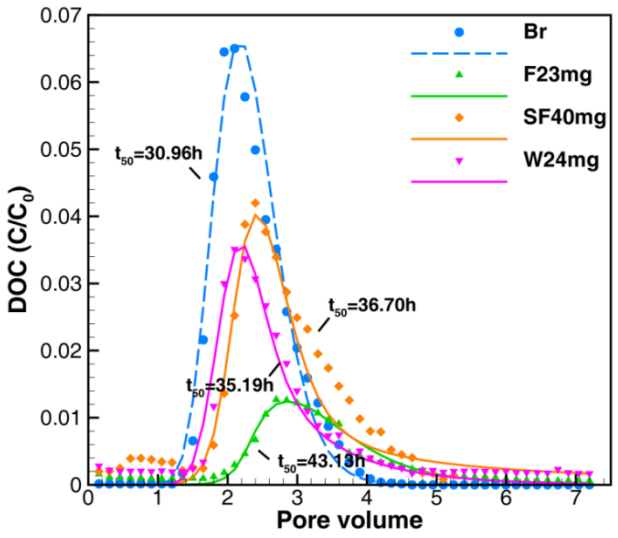

Figure 3.2: Measured (symbols) versus simulated (lines) DOM breakthrough curves (BTCs). BTCs of F23mg (green), SF40mg (orange), and W24mg (magenta) are compared with that of tracer Br (blue). t_{50} shows the central mass travel time of each compound.

It is worth mentioning that the straining effect proposed by colloid filtration theory was insignificant for all the colloid types since the calculated straining rate was rather small compared with attachment, detachment and decay rates. PEST was not able to calibrate a_{str} since it has little effect on the model results within the range between 0 and 1. The insignificance of straining can be illustrated by the ratio of the median colloid diameter to the soil median grain size (d_p/d_{50}), which were all smaller than 0.005 considered as a lower bound for significant straining (Šimůnek et al., 2006). Due to the fact that the impact of straining on the model results was negligible, correlation between straining and decay or attachment, respectively, did not affect the model results. Moreover, sensitivity runs also showed that the impact of colloid size which was involved in the straining rate calculation for each colloid remained small. However, the transport of DOM_F was very sensitive to S_{max} and k_{dec}. While for DOM_SF only S_{max} and for DOM_W k_{dec} was the most sensitive parameter, respectively. This indicates that the soil sorption sites and decay rates are the dominant parameters and processes of the colloid filtration theory to describe the migration of DOM in porous media. However, their influence varies with respect to the manure type and production history.

3.3.3 Antibiotics Transport

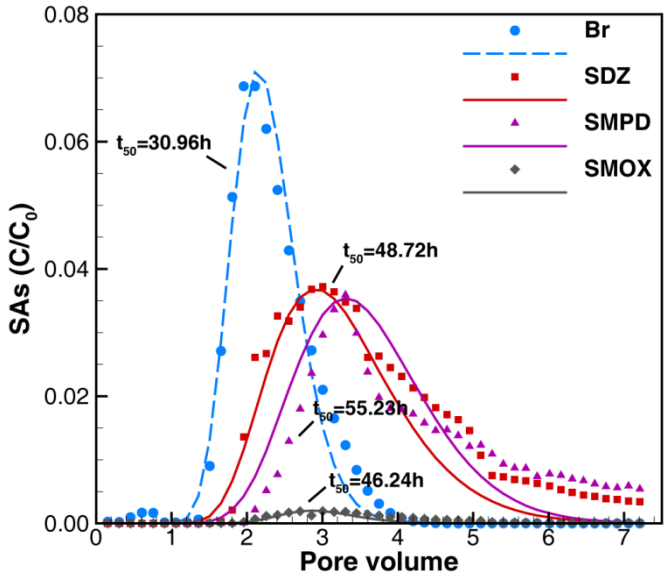

Figure 3.3: Measured (symbols) versus simulated (lines) SAs breakthrough curves (BTCs) in the absence of manure colloids. BTCs of SDZ (red), SMPD (purple), and SMOX (grey) are compared with the conservative transport of Br (blue).

The t_{50} values of all three SAs were larger than that calculated from the tracer bromide and distinct from each other (Table 3.4). This indicates different sorption affinities that are driven by the sulfonamide R-substituents. R-substituents influence the appearance of hydrophobic molecular parts, the polarity of the molecule and are responsible for the

interactions of SAs with soils (Richter et al., 2009; Thiele-Bruhn et al., 2004). For example, the high retardation of SMOX results from its unique 5-membered-ring asymmetric molecular structure that can form stable hydrogen-bonds with the soil. This phenomenon has been shown by Adsmond and Grant (2001) who observed a conformation hydrogen-bond motif for SMOX but not for other SAs. In contrast, SDZ and SMPD were less retarded by their 6-membered-ring symmetry R-substituent resulting in a more hydrophilic character than SMOX. Electrostatic forces are another driving force that controls the transport behavior of sulfonamides. During the experiment, the pH of the effluents ranged between 4.8 and 5.5. The pKa of SDZ, SMPD, and SMOX was reported as 6.48 (Sethuraman et al., 2008), 6.7 (Bustamante and Escalera, 1995), and 7.4 (Bernstein, 1982), respectively, and thus different charged species of the sulfonamides can be expected. For the prevailing low pH values the amount of negatively charged sulfonamide complexes follows the sequence of SDZ > SMPD > SMOX, as can be calculated by the Henderson–Hasselbalch equation (Po and Senozan, 2001). Recall that the soil surface was negatively charged so that the electrostatic repulsion that accelerates the transport and leaching of the negatively charged sulfonamides through the soil follows also the sequence SDZ > SMPD > SMOX.

Similar to DOM, the distinctive tailing indicates non-equilibrium adsorption mechanism also for SAs (Šimůnek and van Genuchten, 2008), thus time-dependent kinetic adsorption is the dominant process and equilibrium adsorption negligible for strong hydrophobic substances, e.g. SAs. Therefore, the Langmuir competitive kinetic sorption approach was applied in the antibiotic transport model and fitted the BTCs of SAs reasonable well with NRMSEs between 0.02 and 0.25 (Figure 3.3). Our approach couples second-order kinetic adsorption with competitive sorption assuming that there is only one type of sorption site available for all competing substances. The distribution coefficient K of SMOX between soil solution and soil surface obtained by the model was extremely high compared to SDZ and SMPD (Table 3.3).

Table 3.3: Reactive transport parameter estimated in the colloid and antibiotics transport model.

	Colloid Transport Model				Antibiotics Transport Model		
	Colloids				SAs [d]		
parameter	F23mg[a]	SF40mg[b]	W24mg[c]	parameter	SDZ	SMPD	SMOX
S_{max} [mol kg^{-1}]	2.84×10^{-3}	5.43×10^{-3}	5.26×10^{-3}	Q [mol kg^{-1}]	1.95×10^{-4}	1.95×10^{-4}	1.95×10^{-4}
λ [-]	1.70×10^{-2}	5.82×10^{-3}	4.63×10^{-3}	k_a [L mol^{-1} s^{-1}]	2.11×10^{-1}	6.15×10^{-1}	2.36×10^{-1}
k_{det} [s^{-1}]	5.96×10^{-7}	1.01×10^{-5}	3.13×10^{-5}	k_d [s^{-1}]	9.34×10^{-5}	1.95×10^{-4}	3.51×10^{-6}
k_{dec} [s^{-1}]	6.20×10^{-6}	1.22×10^{-6}	5.69×10^{-6}	K [L mol^{-1}]	2259.10	3153.85	67236.47
d_p [m]	4.99×10^{-8}	1.46×10^{-7}	3.53×10^{-7}	NRMSE	0.03	0.02	0.25
NRMSE [e]	0.02	0.02	0.01				

[a] 23mg colloid derived from fattening pig. [b] 40mg colloid derived from sows and farrows. [c] 24mg colloid derived from weaner pigs. [d] The mixture of three SAs, i.e. SDZ, SMPD, SMOX. [e] NRMSE= normalized root mean square error between measured BTCs and corresponding model results.

The sensitivity analysis showed that the model results were sensitive to the attachment coefficients of SDZ, SMPD, and SMOX and the detachment coefficients of SDZ and SMPD, but insensitive to the detachment coefficient of SMOX which might be covered up by its extremely high attachment coefficient.

3.3.4 Colloid-affected transport

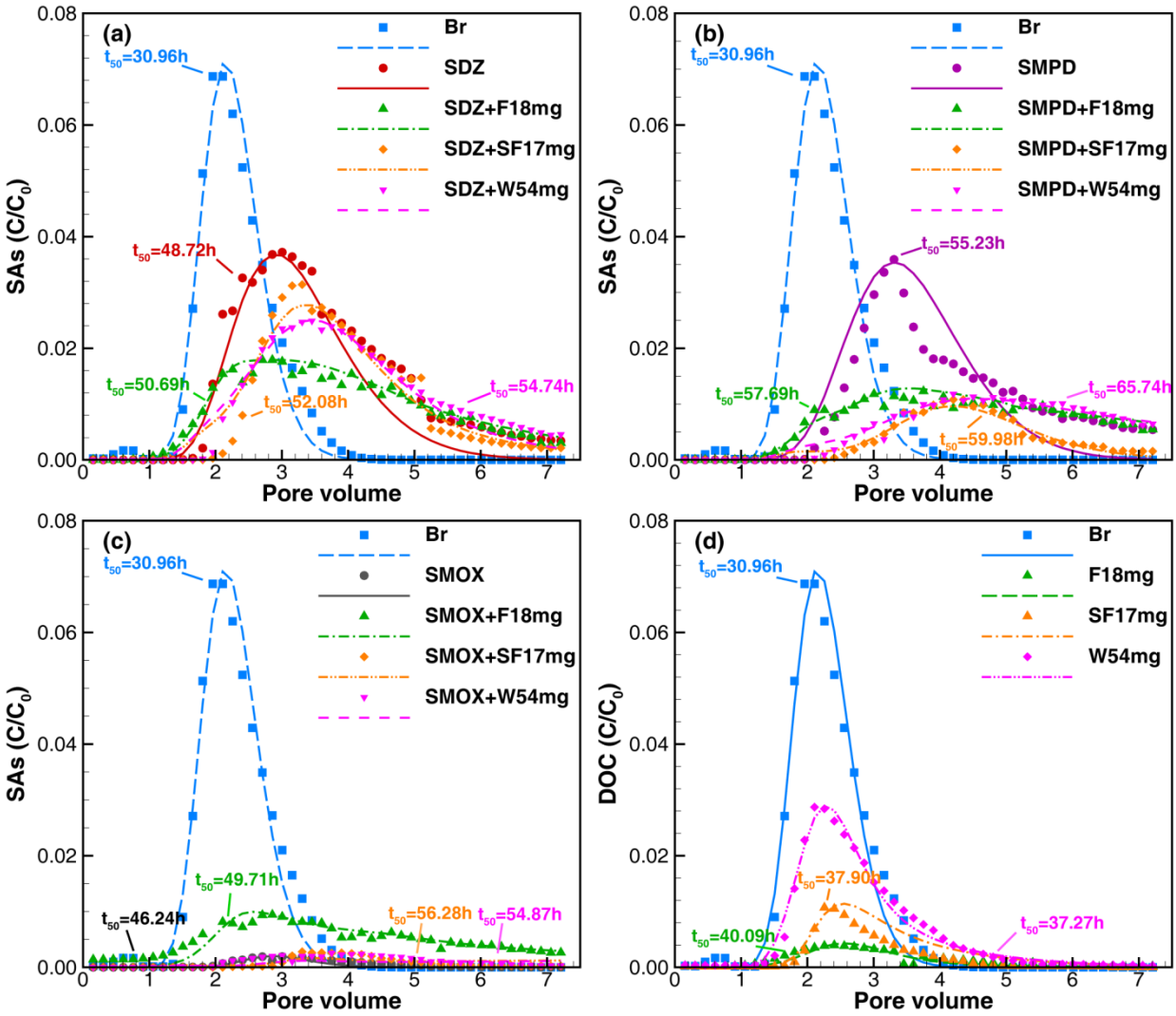

Figure 3.4: Measured (symbols) versus simulated (lines) breakthrough curves (BTCs) of SDZ (a), SMPD (b), SMOX (c), and colloids (d) in the absence and presence of colloid F18mg, SF17mg, and W54mg.

The presence of colloids either reduced or enhanced the transport of the sulfonamides (Figure 3.4). Maximum concentrations and recovery of SDZ and SMPD were lower in the presence of colloids than without, and thus DOM increased the retardation of SDZ and SMPD for all manure types (Table 3.4). This effect was most pronounced for SMPD and most likely

resulted from immobile colloids providing additional sorption sites for SDZ and especially for SMPD. In contrast, the transport of SMOX was significantly enhanced in the presence of colloids from fattening pigs due to its high amount of immobile colloids competing with SMOX for the soil sorption sites (Chefetz et al., 2008). The recovery of SMOX was distinctively larger in the presence of DOM_F than without. Thus, both processes, the adsorption of SMOX to mobile DOM_F and competitive sorption between SMOX and immobile DOM_F increased the leaching from the soil for the least hydrophilic sulfonamide SMOX.

Table 3.4: Travel time and recovery of sulfonamides in the presence and absence of colloids.

	SAs	F 10 mg + SAs	F 18 mg + SAs	F 38 mg + SAs	SF 17 mg + SAs	SF 25 mg + SAs	SF 34 mg + SAs	W 8 mg + SAs	W 54 mg + SAs	W 115 mg + SAs
SDZ										
t_{50}(h)	48.72	33.08	50.69	54.00	52.08	45.37	50.67	51.49	54.74	56.20
R1(%)[a]	128.00[b]	64.08	62.00	48.62	91.00	61.43	101.00[b]	111.42[b]	96.69	89.16
R2(%)[a]	100.00	78.58	89.42	79.73	95.11	71.71	97.52	99.36	96.55	94.78
SMPD										
t_{50}(h)	55.23	34.69	57.69	59.34	59.98	51.35	59.27	62.66	65.74	65.94
R1(%)	96.00	67.57	49.28	35.11	33.00	25.58	33.00	68.13	54.29	47.96
R2(%)	99.99	88.44	70.90	53.88	34.10	32.96	31.95	74.53	58.94	50.60
SMOX										
t_{50}(h)	46.24	34.39	49.71	52.09	56.28	45.68	50.02	50.54	54.87	54.66
R1(%)	5.00	53.67	34.88	13.63	7.00	11.40	14.00	17.98	9.38	7.28
R2(%)	9.12	80.44	48.26	26.80	8.04	7.94	8.15	7.51	7.11	6.86

[a] R1 and R2 are the cumulative recoveries at the end of the experiment in the effluents from column experiments and model results, respectively.

[b] Recovery is larger than 100% due to the experimental measurement error.

The implemented reactive transport models accounting for i) colloid filtration theory, ii) competitive kinetic sorption between the different SAs and DOM colloids, and iii) the interaction between SAs and mobile colloids, e.g., co-transport, were suitable to simulate the measured BTCs of SAs and colloids (Figure 3.4). The simulated BTCs of colloid-affected SAs transport and DOM transport were in good agreement with the measurement data as indicated by NRMSE ranging from 0.01 to 0.39. The distribution coefficients of SDZ and SMPD between the mobile colloids and soil solution, K^m, are all smaller for all manure types compared to K^{im} between the immobile colloids and soil solution, and K between soil solution and soil surfaces (Table 3.5). Thus, SDZ and SMPD have a higher affinity to sorb onto immobile colloids and soils than to mobile colloids. The recovery of SDZ and SMPD decreased with increasing colloid concentration (Table 3.4). This pattern was similar for all manure types, thus the variable pH value and C/N-ratio of different DOM types have a minor

impact on these two SAs' transport. The transport pattern of SDZ and SMPD is mostly driven by their own properties, e.g. relative low pKa.

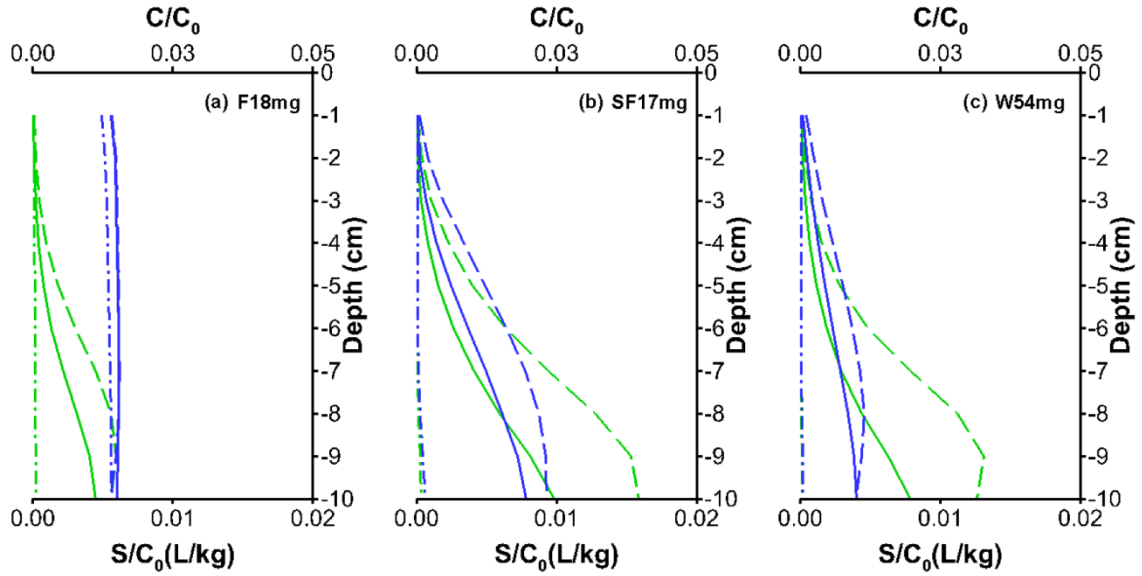

Figure 3.5: The simulated vertical profiles of mobile (green, top) and immobile (blue, bottom) colloids from (a) fattening pigs (F18mg), (b) sows and farrows (SF17mg), and (c) weaners (W54mg) in the presence of sulfonamides at t_{50} (solute central mass travel time, solid), t_{max} (time of maximum peak concentration, longdash), and t_{end} (end of the experiment, dashdot).

The distribution coefficient for SMOX, K^m, between mobile colloids and soil are all larger than the distribution coefficient, K^{im}, between immobile colloids and soil. However, the amount of mobile colloids was smaller than the amount of immobile colloids and K^m is still smaller than K, thus the maximum concentration of SMOX is still lower than those of SDZ and SMPD even if co-transport occurs. Employing competitive sorption between SMOX and colloids could reproduce the measured BTC of SMOX and colloids. Among the three kinds of colloids, SMOX shows higher recovery with DOM_F than DOM_SF and DOM_W, suggesting higher colloid-facilitated transport in the presence of manure DOM from fattening pigs. DOM_F had the highest affinity for soil. Consequently, immobile DOM_F occupied most of the available sorption sites, blocked the adsorption of SMOX on the soil, and prevented the decrease of SMOX aqueous concentration. Therefore, the dominant interaction between SMOX and DOM_F is competitive sorption on the soil surface. The presence of DOM_SF and DOM_W had little effect on SMOX transport by comparing the recovery in the absence and presence of colloids when considering experimental measurement error and model misfit (R1 and R2 in Table 3.4).

This competitive sorption effect also can be verified by simulated vertical profiles of manure colloids for different experimental times (Figure 3.5). The concentrations of all types of mobile colloids increased with increasing depth caused by advection and dispersion when the center of mass (t_{50}) and the peak concentrations (t_{max}) were reached. However, at the end of the experiment (t_{end}) mobile colloids from DOM_SF and DOM_W were reduced at all locations of the column nearly to zero due to a decreased total amount of colloids within the column. Amounts of immobile colloids from DOM_SF and DOM_W also increased along the

soil column at t_{50} and t_{max} and small concentrations can be observed at t_{end} due to their low sorption affinity on the soil surfaces (Figure 3.5b and c). However, immobile colloids from DOM_F (Figure 3.5a) decreased only slightly from t_{50} and t_{max} to t_{end} due to their high affinity to sorb onto the soil. These large amounts of immobile colloids from DOM_F that prevailed throughout the experiment and at all locations of the soil column enhanced the SMOX transport by blocking the soil sorption sites throughout the entire soil profile. However, this was not true for SDZ and SMPD as immobile colloids provide additional sorption sites and competitive sorption did not occur.

Another potential process that can facilitate the transport of SAs in the presence of colloids is pore size exclusion (Kretzschmar et al., 1999). This can be by i) blocking the small pores with the immobile colloids or ii) creating bigger stable colloid-SAs clusters. In both situations, the transport of SAs is restricted to the larger pore spaces and thus resulted in decreased travel time. This effect led to an approximate reduction in t_{50} from 46 h (SMOX) and 55h (SMPD) to 34 h (SMOX and SMPD) in the presence of colloids (Table 3.4).

The sensitivity analysis revealed the dominant process that controls the transport of SAs in the presence of colloids (Figure 3.6). For SDZ and SMPD, the model results are most sensitive to the adsorption of SAs onto immobile colloids. For SMOX, the highest and very pronounced sensitivity is found for the attachment to the mobile DOM_F ($k_{a,SMOX}^{m}$) which has a higher sensitivity than the attachment to DOM_SF and DOM_W. The decay of mobile DOM_F also shows a high sensitivity as it indirectly influences the amount of immobile colloids that compete with SMOX for the soil sorption sites.

Table 3.5: Estimated parameters in the colloid-facilitated reactive transport model.

Colloid-facilitated Model												
	F10mg + SAs				SF17mg + SAs				W8mg + SAs			
parameter	Colloid	SDZ	SMPD	SMOX	Colloid	SDZ	SMPD	SMOX	Colloid	SDZ	SMPD	SMOX
k_{dec} [s^{-1}]	6.24×10^{-7}				1.98×10^{-9}				9.05×10^{-6}			
k_a^m [L mol^{-1} s^{-1}]		1.89×10^{-3}	1.04×10^{-2}	1.93×10^{-4}		3.81×10^{-1}	7.80×10^{-3}	1.16×10^{-1}		3.92×10^{-3}	2.14×10^{-3}	2.82×10^{-1}
k_d^m [s^{-1}]		7.62×10^{-5}	3.26×10^{-4}	1.73×10^{-7}		1.35×10^{-3}	6.06×10^{-5}	7.18×10^{-4}		5.59×10^{-4}	3.41×10^{-5}	5.72×10^{-4}
K^m [L mol^{-1}]		24.80	31.90	1115.61		282.22	128.71	161.56		7.01	62.76	493.01
k_a^{im} [L mol^{-1} s^{-1}]		1.11×10^{-3}	1.38×10^{-3}	2.56×10^{-4}		1.32×10^{-3}	3.33×10^{-3}	2.11×10^{-4}		2.98×10^{-3}	6.97×10^{-3}	3.00×10^{-6}
k_d^{im} [s^{-1}]		1.18×10^{-6}	4.36×10^{-6}	4.53×10^{-4}		6.55×10^{-5}	1.56×10^{-7}	1.50×10^{-4}		2.41×10^{-5}	4.76×10^{-6}	1.56×10^{-6}
K^{im} [L mol^{-1}]		940.68	316.51	0.57		20.15	21346.15	1.41		123.65	1464.29	1.92
NRMSE	0.09	0.03	0.01	0.07	0.08	0.05	0.05	0.20	0.07	0.04	0.09	0.16
	F18mg + SAs				SF25mg + SAs				W54mg + SAs			
parameter	Colloid	SDZ	SMPD	SMOX	Colloid	SDZ	SMPD	SMOX	Colloid	SDZ	SMPD	SMOX
k_{dec} [s^{-1}]	4.20×10^{-6}				1.13×10^{-6}				5.80×10^{-6}			
k_a^m [L mol^{-1} s^{-1}]		1.79×10^{-3}	6.00×10^{-3}	1.25×10^{-3}		2.03×10^{-3}	1.33×10^{-2}	2.27×10^{-2}		2.56×10^{-3}	4.14×10^{-4}	2.54×10^{-3}

k_d^m [s^{-1}]		1.45×10^{-4}	1.16×10^{-4}	5.64×10^{-7}		1.59×10^{-4}	1.10×10^{-4}	3.41×10^{-4}		5.78×10^{-4}	1.49×10^{-5}	1.56×10^{-4}
K^m [L mol^{-1}]		12.34	51.72	2216.31		12.77	120.91	66.57		4.43	27.79	16.28
k_a^{im} [L mol^{-1} s^{-1}]		4.20×10^{-3}	5.06×10^{-3}	7.14×10^{-1}		1.63×10^{-3}	4.09×10^{-3}	3.30×10^{-7}		1.95×10^{-3}	3.28×10^{-3}	7.80×10^{-3}
k_d^{im} [s^{-1}]		2.04×10^{-5}	1.24×10^{-5}	1.99×10^{-3}		4.60×10^{-6}	2.27×10^{-7}	5.85×10^{-7}		1.87×10^{-5}	3.46×10^{-6}	1.34×10^{-4}
K^{im} [L mol^{-1}]		205.88	407.26	358.79		354.34	18017.62	0.56		104.28	947.98	58.21
NRMSE	0.07	0.02	0.01	0.04	0.09	0.05	0.05	0.39	0.02	0.02	0.03	0.23

	F38mg + SAs				SF34mg + SAs				W115mg + SAs			
parameter	Colloid	SDZ	SMPD	SMOX	Colloid	SDZ	SMPD	SMOX	Colloid	SDZ	SMPD	SMOX
k_{dec} [s^{-1}]	1.78×10^{-5}				4.73×10^{-6}				5.08×10^{-6}			
k_a^m [L mol^{-1} s^{-1}]		8.58×10^{-3}	2.25×10^{-3}	1.69×10^{-3}		3.04×10^{-3}	1.78×10^{-3}	3.45×10^{-2}		5.19×10^{-4}	2.68×10^{-3}	6.72×10^{-3}
k_d^m [s^{-1}]		4.20×10^{-4}	4.37×10^{-5}	2.01×10^{-7}		7.22×10^{-4}	3.57×10^{-5}	5.93×10^{-4}		3.30×10^{-4}	5.14×10^{-4}	1.54×10^{-4}
K^m [L mol^{-1}]		20.43	51.49	8407.96		4.21	49.86	58.18		1.57	5.21	43.63
k_a^{im} [L mol^{-1} s^{-1}]		4.91×10^{-3}	4.81×10^{-3}	2.70×10^{-2}		1.26×10^{-3}	3.43×10^{-3}	5.69×10^{-5}		2.51×10^{-3}	5.23×10^{-3}	4.36×10^{-6}
k_d^{im} [s^{-1}]		1.67×10^{-5}	6.62×10^{-6}	5.39×10^{-4}		3.08×10^{-5}	8.20×10^{-7}	6.45×10^{-6}		1.42×10^{-5}	3.52×10^{-6}	2.27×10^{-5}
K^{im} [L mol^{-1}]		294.01	726.59	50.09		40.91	4182.93	8.82		176.76	1485.80	0.19
NRMSE	0.14	0.03	0.04	0.09	0.08	0.02	0.03	0.19	0.03	0.02	0.04	0.02

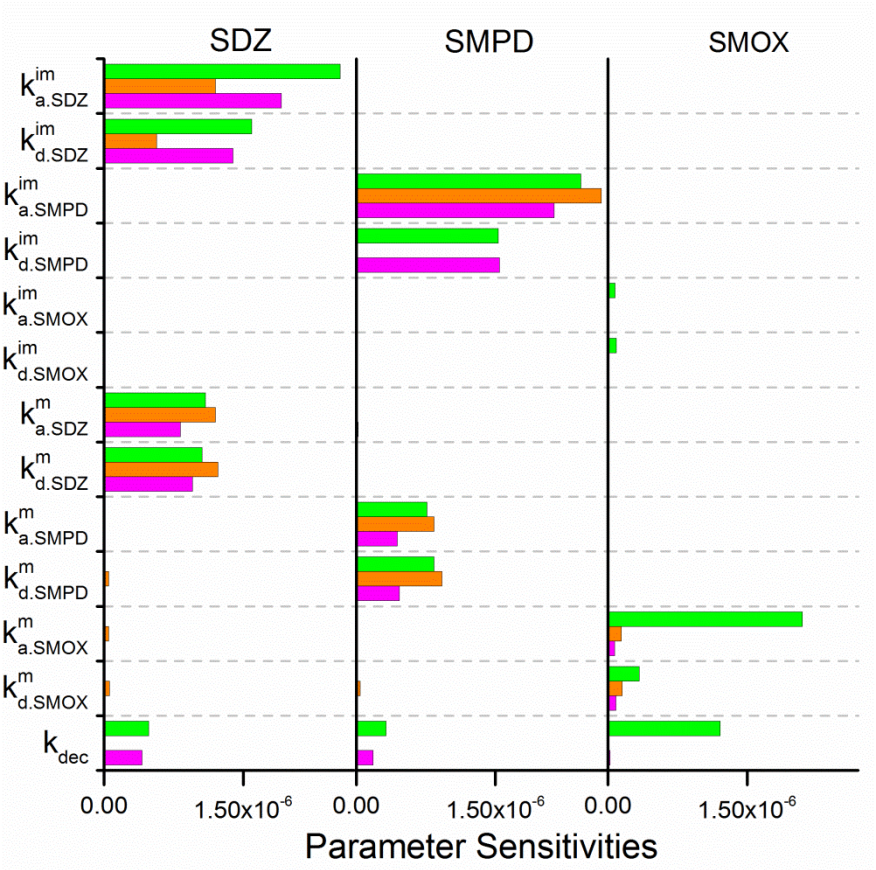

Figure 3.6: The parameter sensitivities with respect to the model results of SDZ, SMPD and SMOX from colloid-facilitated models, i.e. F18mg+AB (green), SF17mg+AB (orange), and W54mg+AB (magenta).

3.3.5 Significance of colloid quality

Colloids from different manure types differently influenced the transport of SAs. The weakly hydrophobic SAs (SDZ and SMPD) were retarded by colloids from all manure types. Yet, especially DOM_F reduced t_{50} significantly. This effect was modeled using the colloid-filtration-theory and found to be caused by pore size exclusion of the larger colloid-SAs cluster and blocking of the small pore sizes by DOM_F. For the more hydrophobic SMOX, the DOM from fattening pigs exhibited an outstanding enhancement of transport and leaching. This phenomenon suggests that manure with a high content of hydrophobic compounds, low C/N ratio, high $SUVA_{280nm}$ and protein C has a strong potential to facilitate the transport of more hydrophobic contaminants which might be expected to be stronger retarded due to their polarity characteristics. Due to the small amount of colloids added to the soil, the colloid pH did not influence the contaminant transport. However, when large amounts of colloids are discharged into the soil, the soil pH will change with respect to the colloid pH. According to the pKa of SDZ(6.48), SMPD(6.7), and SMOX(7.4), especially in the presence of DOM_F, more negatively charged SAs species will be developed and their repulsion from the negative soil surface will show an accelerated transport (Kurwadkar et al., 2007; ter Laak et al., 2006).

3.4 Conclusions

Due to the different feeding recipes and stable management, manures from different pig life stages exhibit diverse properties. A low C/N ratio, high $SUVA_{280nm}$, and protein C, which occurs mainly in manure DOM from fattening pigs and indicates a high fraction of proteins with aromatic amino acid tyrosine or tryptophan, increases the hydrophobicity of the DOM (Betts and Russell, 2003). Our experimental and numerical results demonstrate that these hydrophobic proteins might be responsible for the facilitated transport of SMOX. However, none of the investigated manure types was able to enhance the transport of SDZ and SMPD, but rather reduced their transport. This different impact of manure on the transport of sulfonamides is mainly due to the different spatial structure of R-substituents in SDZ and SMPD compared to SMOX. Thus, with respect to the impact of sulfonamides on the ecology and soils, e.g. microorganisms or plants, manure containing SDZ or SMPD has to be applied with care on farm land. On the other hand, with respect to the impact of sulfonamides on drinking water quality and water resources the usage of SMOX is most critical. However, the leaching risk of hydrophobic sulfonamides, such as SMOX, into the groundwater can be deceased by lowering the protein in the dietary. This adapted pig feeding will be able to decrease tyrosine and tryptophan-like organic compounds in manure (Portejoie et al., 2004; Zhang et al., 2012) and has a high potential to limit the leaching risk of hydrophobic sulfonamides into groundwater.

3.5 Acknowledgements

The experimental work of this research was funded by the "Fonds National de la Recherche (FNR)" from Luxembourg. We are especially grateful to our colleagues from CRTE, Luxembourg, Paul Schosseler and Tom Gallé for their cooperation. The numerical investigations were funded by the Chinese Scholarship Council (CSC). Thanks to Anne Berns for many helpful discussions. We also thank Horst Hardelauf and Jirka Šimůnek for making available a linux-cluster version of Hydrus and HP1.

3.6 References

Adsmond, D. A., Grant, D. J., 2001. Hydrogen bonding in sulfonamides. Journal of Pharmaceutical Sciences, 90(12), 2058-2077.

Aust, M. O., Thiele-Bruhn, S., Eckhardt, K. U., Leinweber, P., 2009. Composition of organic matter in particle size fractionated pig slurry. Bioresource technology, 100(23), 5736-5743.

Bernstein, L., 1982. Combination of trimethoprim with sulfonamides other than sulfamethoxazole. Review of Infectious Diseases, 4(2), 411-418.

Betts, M. J., Russell, R. B., 2003. Amino acid properties and consequences of substitutions. Bioinformatics for Geneticists, 317, 289.

Bradford, S. A., Simunek, J., Bettahar, M., van Genuchten, M. T., Yates, S. R., 2003. Modeling colloid attachment, straining, and exclusion in saturated porous media. Environmental Science & Technology, 37(10), 2242-2250.

Bradford, S. A., Torkzaban, S., Kim, H., Simunek, J., 2012. Modeling colloid and microorganism transport and release with transients in solution ionic strength. Water Resources Research, 48(9).

Brown, G. M., 1962. The biosynthesis of folic acid II. Inhibition by sulfonamides. Journal of Biological Chemistry, 237(2), 536-540.

Burkhardt, M., Stamm, C., 2007. Depth distribution of sulfonamide antibiotics in pore water of an undisturbed loamy grassland soil. Journal of Environmental Quality, 36(2), 588-596.

Businelli, M., Altieri, R., Giusquiani, P., Gigliotti, G., 1999. Complexation capacity of dissolved organic matter from pig slurry: a gel filtration and dialysis study. Water, Air, and Soil Pollution, 113(1-4), 385-394.

Bustamante, P., Escalera, B., 1995. Enthalpy and entropy contributions to the solubility of sulphamethoxypyridazine in solvent mixtures showing two solubility maxima. Journal of Pharmacy and Pharmacology, 47(7), 550-555.

Chefetz, B., Mualem, T., Ben-Ari, J., 2008. Sorption and mobility of pharmaceutical compounds in soil irrigated with reclaimed wastewater. Chemosphere, 73(8), 1335-1343.

Chen, G., Flury, M., Harsh, J. B., Lichtner, P. C., 2005. Colloid-facilitated transport of cesium in variably saturated Hanford sediments. Environmental Science & Technology, 39(10), 3435-3442.

Chin, Y. P., Aiken, G., O'Loughlin, E., 1994. Molecular weight, polydispersity, and spectroscopic properties of aquatic humic substances. Environmental Science & Technology, 28(11), 1853-1858.

Cunha, M. C., Nunes, L. M., 2011. Groundwater Characterization, Management and Monitoring. WIT Press.

de Jonge, H., Jacobsen, O. H., de Jonge, L. W., Moldrup, P., 1998. Particle-facilitated transport of prochloraz in undisturbed sandy loam soil columns. Journal of Environmental Quality, 27(6), 1495-1503.

Doherty, J., 2003. Ground water model calibration using pilot points and regularization. Groundwater, 41(2), 170-177.

Doherty, J., 2016. PEST: Model-Independent Parameter Estimation User Manual Part I: PEST, SENSAN and Global Optimisers, 6th ed, Watermark Numerical Computing, Brisbane, Australia.

Fienen, M. N., Muffels, C. T., Hunt, R. J., 2009. On constraining pilot point calibration with regularization in PEST. Groundwater, 47(6), 835-844.

Flury, M., Qiu, H., 2008. Modeling colloid-facilitated contaminant transport in the vadose zone. Vadose Zone Journal, 7(2), 682-697.

Foppen, J., Schijven, J., 2006. Evaluation of data from the literature on the transport and survival of Escherichia coli and thermotolerant coliforms in aquifers under saturated conditions. Water Research, 40(3), 401-426.

Haller, M. Y., Müller, S. R., McArdell, C. S., Alder, A. C., Suter, M. J. F., 2002. Quantification of veterinary antibiotics (sulfonamides and trimethoprim) in animal manure by liquid chromatography–mass spectrometry. Journal of Chromatography A, 952(1), 111-120.

Halling-Sørensen, B., Nielsen, S. N., Lanzky, P., Ingerslev, F., Lützhøft, H. H., Jørgensen, S., 1998. Occurrence, fate and effects of pharmaceutical substances in the environment-A review. Chemosphere, 36(2), 357-393.

Jacques, D., Šimůnek, J., Mallants, D., Van Genuchten, M. T., 2008. Modeling coupled hydrologic and chemical processes: Long-term uranium transport following phosphorus fertilization. Vadose Zone Journal, 7(2), 698-711.

Jaisi, D. P., Saleh, N. B., Blake, R. E., Elimelech, M., 2008. Transport of single-walled carbon nanotubes in porous media: filtration mechanisms and reversibility. Environmental Science & Technology, 42(22), 8317-8323.

Kemper, N., 2008. Veterinary antibiotics in the aquatic and terrestrial environment. Ecological Indicators, 8(1), 1-13.

Kretzschmar, R., Borkovec, M., Grolimund, D., Elimelech, M., 1999. Mobile subsurface colloids and their role in contaminant transport. Advances in Agronomy, 66, 121-193.

Kurwadkar, S. T., Adams, C. D., Meyer, M. T., Kolpin, D. W., 2007. Effects of sorbate speciation on sorption of selected sulfonamides in three loamy soils. Journal of Agricultural and Food Chemistry, 55(4), 1370-1376.

Leenheer, J. A., Rostad, C. E., 2004. Fractionation and characterization of organic matter in wastewater from a Swine waste-retention basin. US Department of the Interior, US Geological Survey.

Liang, Y., Bradford, S. A., Simunek, J., Heggen, M., Vereecken, H., Klumpp, E., 2013. Retention and remobilization of stabilized silver nanoparticles in an undisturbed loamy sand soil. Environmental Science & Technology, 47(21), 12229-12237.

Murali, V., Aylmore, L., 1983. Competitive adsorption during solute transport in soils: 1. Mathematical models. Soil Science, 135(3), 143-150.

Naden, P. S., Old, G. H., Eliot-Laize, C., Granger, S. J., Hawkins, J., Bol, R., Haygarth, P., 2010. Assessment of natural fluorescence as a tracer of diffuse agricultural pollution from slurry spreading on intensely-farmed grasslands. Water Research, 44(6), 1701-1712.

Parkhurst, D. L., Appelo, C., 1999. User's guide to PHREEQC (Version 2): A computer program for speciation, batch-reaction, one-dimensional transport, and inverse geochemical calculations. Water-Resour. Invest. Rep. 99-4259. USGS, Denver, CO.

Po, H. N., Senozan, N., 2001. The Henderson-Hasselbalch equation: its history and limitations. Journal of Chemical Education, 78(11), 1499.

Portejoie, S., Dourmad, J. Y., Martinez, J., Lebreton, Y., 2004. Effect of lowering dietary crude protein on nitrogen excretion, manure composition and ammonia emission from fattening pigs. Livestock Production Science, 91(1), 45-55.

Ptak, T., Piepenbrink, M., Martac, E., 2004. Tracer tests for the investigation of heterogeneous porous media and stochastic modelling of flow and transport—a review of some recent developments. Journal of Hydrology, 294(1), 122-163.

Rabe, M., Verdes, D., Seeger, S., 2011. Understanding protein adsorption phenomena at solid surfaces. Advances in Colloid and Interface Science, 162(1), 87-106.

Richter, M. K., Sander, M., Krauss, M., Christl, I., Dahinden, M. G., Schneider, M. K., Schwarzenbach, R. P., 2009. Cation binding of antimicrobial sulfathiazole to leonardite humic acid. Environmental Science & Technology, 43(17), 6632-6638.

Seetha, N., Kumar, M. M., Hassanizadeh, S. M., Raoof, A., 2014. Virus-sized colloid transport in a single pore: Model development and sensitivity analysis. Journal of Contaminant Hydrology, 164, 163-180.

Sethuraman, V. A., Lee, M. C., Bae, Y. H., 2008. A biodegradable pH-sensitive micelle system for targeting acidic solid tumors. Pharmaceutical Research, 25(3), 657-666.

Šimůnek, J., He, C., Pang, L., Bradford, S., 2006. Colloid-facilitated solute transport in variably saturated porous media: numerical model and experimental verification. Vadose Zone Journal, 5(3), 1035-1047.

Šimůnek, J., Šejna, M., van Genuchten, M. T., 2012. The C-Ride Module for HYDRUS (2D/3D) Simulating Two-Dimensional Colloid-Facilitated Solute Transport in Variably-Saturated Porous Media, Version 1.0, PC Progress, Prague, Czech Republic, pp. 45.

Šimůnek, J., van Genuchten, M. T., 2008. Modeling nonequilibrium flow and transport processes using HYDRUS. Vadose Zone Journal, 7(2), 782-797.

Šimůnek, J., van Genuchten, M. T., Šejna, M., 2008. Development and applications of the HYDRUS and STANMOD software packages and related codes. Vadose Zone Journal, 7(2), 587-600.

Sprague, L. A., Herman, J. S., Hornberger, G. M., Mills, A. L., 2000. Atrazine adsorption and colloid-facilitated transport through the unsaturated zone. Journal of Environmental Quality, 29(5), 1632-1641.

Syngouna, V. I., Chrysikopoulos, C. V., 2013. Cotransport of clay colloids and viruses in water saturated porous media. Colloids and Surfaces A: Physicochemical and Engineering Aspects, 416, 56-65.

ter Laak, T. L., Gebbink, W. A., Tolls, J., 2006. The effect of pH and ionic strength on the sorption of sulfachloropyridazine, tylosin, and oxytetracycline to soil. Environmental Toxicology and Chemistry, 25(4), 904-911.

Thiele-Bruhn, S., Seibicke, T., Schulten, H. R., Leinweber, P., 2004. Sorption of sulfonamide pharmaceutical antibiotics on whole soils and particle-size fractions. Journal of Environmental Quality, 33(4), 1331-1342.

Unold, M., Šimůnek, J., Kasteel, R., Groeneweg, J., Vereecken, H., 2009. Transport of manure-based applied sulfadiazine and its main transformation products in soil columns. Vadose Zone Journal, 8(3), 677-689.

Yao, K. M., Habibian, M. T., O'Melia, C. R., 1971. Water and waste water filtration. Concepts and applications. Environmental Science & Technology, 5(11), 1105-1112.

Zhang, F., Li, Y., Xiong, X., Yang, M., Li, W., 2012. Effect of composting on dissolved organic matter in animal manure and its binding with Cu. The Scientific World Journal, 2012.

Zhu, W., Yao, W., Zhang, Z., Wu, Y., 2014. Heavy metal behavior and dissolved organic matter (DOM) characterization of vermicomposted pig manure amended with rice straw. Environmental Science and Pollution Research, 21(22), 12684-12692.

Zhu, Y., Ma, L. Q., Dong, X., Harris, W. G., Bonzongo, J., Han, F., 2014. Ionic strength reduction and flow interruption enhanced colloid-facilitated Hg transport in contaminated soils. Journal of Hazardous Materials, 264, 286-292.

Zou, Y., Zheng, W., 2013. Modeling manure colloid-facilitated transport of the weakly hydrophobic antibiotic florfenicol in saturated soil columns. Environmental Science & Technology, 47(10), 5185-5192.

4 Numerical modeling of stream-aquifer interaction: quantifying the impact of transient streambed permeability and aquifer heterogeneity*

Authors: Dan Zhou, Ye Zhang, Guillaume Gianni, Peter Lichtner, Irina Engelhardt

Abstract **63**

4.1 Introduction **64**

4.2 Methods **66**

4.3 Results and discussions **73**

4.4 Conclusions **83**

4.5 Acknowledgements **84**

4.6 References **84**

* Submitted to Hydrological Processes as

Zhou, D., Zhang, Y., Gianni, G., Lichtner, P., Engelhardt, I., 2017. Numerical modeling of stream-aquifer interaction: quantifying the impact of transient streambed permeability and aquifer heterogeneity. Hydrological Processes (submitted).

Abstract

Stream-aquifer interaction plays a vital role in the water cycle, and a proper study of this interaction is needed for understanding groundwater recharge, contaminants migration, and for managing surface water and groundwater resources conjunctively. A model-based investigation of a field experiment in a riparian zone of the Schwarzbach river, a tributary of the Rhine River in Germany, was conducted to understand stream-aquifer interaction under alternative gaining and losing streamflow conditions. An equivalent streambed permeability, estimated by inverting aquifer responses to flood waves, show that streambed permeability increased during infiltration of stream water to aquifer and decreased during exfiltration. Aquifer permeability realizations generated by multiple-point geostatistics exhibit a high degree of heterogeneity and anisotropy. A coupled surface water groundwater flow model was developed incorporating the time-varying streambed permeability and the heterogeneous aquifer permeability. The model was able to reproduce varying pressure heads at two observation wells near the stream over a period of 55 days. Based on the aquifer realizations, a Monte Carlo analysis was carried out to simulate groundwater flow, its age distribution, and the release of a hypothetical wastewater plume into the aquifer from the stream. Results of this uncertainty analysis suggest: (1) stream-aquifer exchange flux during infiltration periods was constrained by aquifer permeability; (2) during exfiltration, this flux is constrained by the reduced streambed permeability; (3) probabilistic map of the infiltration path in the aquifer reveals that such pathways and the associated prediction of the extent of the contaminant plume are highly dependent on aquifer heterogeneity.

3.1 Introduction

Surface water-groundwater interaction has received much attention in recent decades due to its significant impact on the migration of contaminants from streams to aquifers and vice versa, thus impacting drinking water resources. Examples of studies that focus on surface water-groundwater interaction include: bioclogging effects on river infiltration (Newcomer et al., 2016), temporal variation of streambed permeability in flood seasons (Wu et al., 2015), response of surface water-groundwater exchange flux to varying streamflow (Dudley‐Southern & Binley, 2015; Fox et al., 2014), and migration of solutes including waste water related contaminants (Engelhardt et al., 2013b; Hammond & Lichtner, 2010; Lasagna et al., 2016; Xie et al., 2016). Besides topography and climate, a key factor that controls surface water-groundwater interaction is the permeability of both streambed sediments and the aquifer beneath the stream, which together control the flow pattern and commonly displays a high degree of spatial heterogeneity, spanning several orders of magnitude (Fleckenstein et al., 2006; Sophocleous, 2002; Winter et al., 1998). The permeability of streambed sediments can be affected by continuous sediment deposition, remobilization, clogging, and erosion processes, which can lead to variations of permeability in space and time (Datry et al., 2015; Geist & Auerswald, 2007; Pholkern et al., 2015). With the exception of the variability introduced from chemical reactions, crustal movements, and human activities, aquifer permeability is commonly considered to be constant in time and can also display spatial heterogeneity due to spatial variability of the hydrofacies of different geological media (Comunian et al., 2016; Fleckenstein et al., 2006; Michael et al., 2010). The variation of permeability in both space and time may have a profound influence on surface water-groundwater interaction.

Many field studies have demonstrated the existence of spatial and temporal variations of streambed permeability (Min et al., 2013; Wang et al., 2016; Wu et al., 2015). Many approaches are available to estimate streambed permeability, such as by direct measurements (e.g. pumping test, slug test, and permeameter tests) and indirect estimation (e.g. grain size analysis and seepage-meter) (Cheong et al., 2008; Kalbus et al., 2006; Pozdniakov et al., 2016). Numerous field studies have demonstrated the importance of variable streambed permeability on surface water-groundwater interaction (Newcomer et al., 2016; Pozdniakov et al., 2016; Simpson & Meixner, 2012). In most numerical investigations of surface water-groundwater interaction, streambed permeability was assumed to be temporally constant due to difficulties in detecting and measuring transient variations in permeability (e.g. Engelhardt et al., 2013b; Sun et al., 2016; Tian et al., 2015). Gianni et al. (2016) presented an analytical model to identify transient streambed permeability by inverting flood wave responses recorded in the time series of the stream stage and near-stream hydraulic head of the aquifer. The aquifer hydraulic head was simulated using a flood wave function and the streambed permeability, as a parameter of this function, is calculated via an inverse procedure. By testing using synthetic and field data, this method has been shown to be robust and reasonably accurate (Gianni et al., 2016). It further reveals the controlling effect of temporal variation of streambed permeability on surface water-groundwater interaction. However, whether the

permeability of the streambed is the single controlling factor, and under what condition the streambed controls surface water-groundwater interaction, is still unclear.

To model aquifer heterogeneities including facies, porosity, and permeability, various geostatistical tools have been developed, such as sequential indicator simulation, hierarchical sequential indicator simulation, sequential Gaussian simulation, and multiple-point geostatistics (MPS) (Guardiano & Srivastava, 1993; Strebelle, 2000; Pyrcz & Deutsch, 2014; Zappa et al., 2006; Zhou et al., 2012). These geostatistical tools characterize and quantify spatial variability using probabilistic models to generate multiple heterogeneous realizations. Multiple realizations of permeability, for example, can be used to quantify the uncertainty of this parameter and how such uncertainty can propagate into the prediction of flow and transport in aquifers. In studying surface water-groundwater interaction, geostatistical methods have been adopted to investigate the impact of aquifer facies on the spatial variability of stream seepage (Fleckenstein et al., 2006) and the spatial and temporal dynamics of stream-aquifer exchange (Frei et al., 2009). Among these methods, MPS overcome the known limitations of variograms by utilizing the spatial correlation between variables beyond two-point statistics. A training image is used by MPS to characterize the pattern of subsurface heterogeneity. With a training image, data scarcity due to limited well information from the subsurface can often be addressed satisfactorily. MPS has been developed and applied in many subsurface modeling investigations (e.g., Huysmans & Dassargues, 2009; Malone et al., 2016; Milliken et al, 2008; Zovi et al., 2017), however, few studies have adopted MPS to understand the effect of aquifer heterogeneity on surface water-groundwater interaction.

Groundwater age modeling provides a useful technique to facilitate the estimation of groundwater recharge rate and velocity, the calibration of groundwater flow models, and the assessment of the renewability of groundwater reservoirs (Kazemi et al., 2006). Particle tracking and direct simulation are the two groundwater age modeling techniques most commonly used when a groundwater flow field is known (Suckow, 2014). Compared to particle tracking, which typically considers advection and ignores the mass exchange between flow paths, direct simulation of groundwater age is more favored in that it also considers dispersion and diffusion (Suckow, 2014). Moreover, because of the uncertainty in aquifer parameters, groundwater flow fields simulated for any field-based studies will suffer uncertainty. However, most studies that applied groundwater age modeling to investigate groundwater recharge and chemistry evolution do not take such uncertainty into account (Attard et al., 2016; Lemieux & Sudicky, 2010; Yu et al., 2015). To avoid the introduction of bias into modeled groundwater age, model uncertainty cannot be neglected in groundwater age modeling.

This paper analyzes both streamflow and aquifer monitoring data collected at a riparian zone of the Schwarzbach river using computer models to (1) investigate the role of temporal variation of streambed permeability on surface water-groundwater interaction; (2) determine the impact of aquifer permeability heterogeneity, as modeled by MPS, on the prediction of groundwater flow and its uncertainty; (3) identify the most important time-variable factors controlling stream-groundwater interaction under losing and gaining streamflow conditions

utilizing uncertainty analysis of the simulated hydraulic head; (4) determine the most likely stream water infiltration paths as driven by stream-groundwater interaction using Monte-Carlo-based groundwater age modeling, which takes model uncertainty into account.

3.2 Methods

4.2.1 Study site

A riparian groundwater monitoring campaign was conducted at a field site along the Schwarzbach river, a tributary of the Rhine River, which is located southwest of Frankfurt, Germany (Figure 4.1a). During the installation of a set of monitoring wells, 44 soil samples were taken from three observation wells (GWM1, GWM2c, and S2) with a vertical sampling density of 0.2 m. Based on the grain size analysis of these samples, intrinsic permeability for each of the 0.2 m intervals was calculated using the Hazen method (Hazen, 1911). Hydraulic head, stream stage, and precipitation were measured from 15 August, 2010 to 9 October, 2010 (Engelhardt et al., 2013a). Using site data, a two-dimensional vertical transect was constructed (Figure 4.1a and b), which lies perpendicular to the main stream channel. Based on hydraulic head data collected from all the monitoring wells at this site, the general direction of the groundwater flow is from SE (southeast) to NW (northwest). The transect thus captures the general groundwater flow direction and is used for this modelling study to evaluate spatial and temporal permeability heterogeneity. A detailed description of the hydrology and hydrogeology of the field site and the installation of monitoring wells is presented in Engelhardt et al. (2013a).

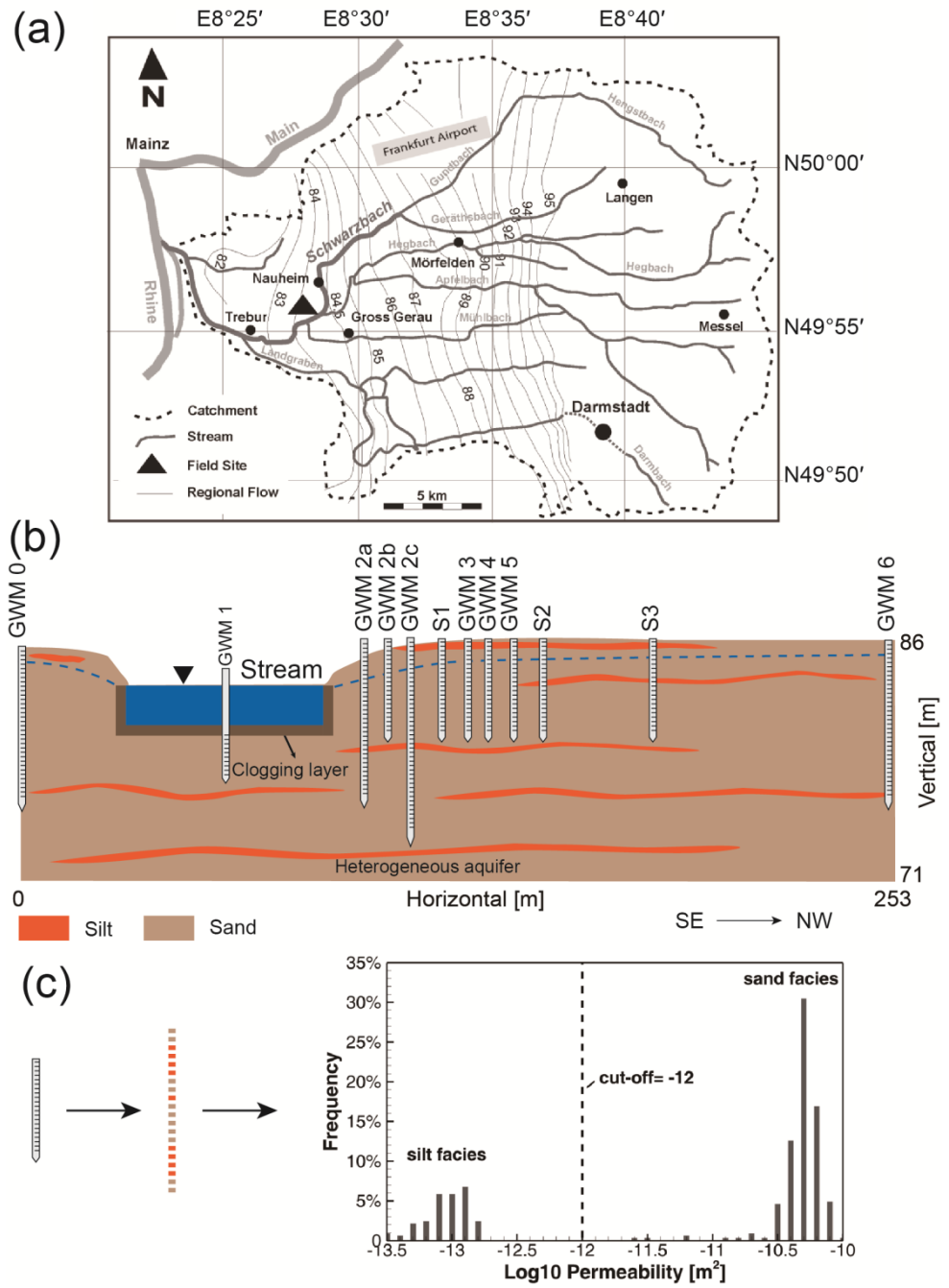

Figure 4.1: (a) Our study site at a riparian zone of the Schwarzbach river in Germany (Engelhardt et al., 2011). (b) A monitoring well network along a constructed two-dimensional vertical transect; location of the transect is shown in (a) by a triangle symbol. (c) Histogram of aquifer permeability of the collected soil samples.

4.2.2 Characterizing aquifer heterogeneity

To characterize aquifer heterogeneity, a training image was first generated to capture the facies distribution identified at the study site based on permeability histogram. Multiple realizations of facies distributions were then modeled using MPS, based on multiple point statistics derived from the training image. Permeability distribution was then simulated for each facies using sequential Gaussian simulation (SGSIM). Finally, based on the multiple

permeability fields, a set of groundwater flow simulations was conducted. Details of these procedures are described in the following.

4.2.2.1 Training image construction

The training image (TI) is a numerical representation of the perceived geological heterogeneity at a study site, which is required by most MPS algorithms. In this study, a facies categorization was first conducted according to the permeability histogram (Figure 4.1c), and the proportion of each facies type was calculated. A two-dimensional TI of sedimentary facies was generated by SGeMS (Remy et al., 2009), which reflects a representative vertical distribution of site sedimentary deposits by conditioning to the information observed in sediment core samples and a geological conceptual model (Figure 4.1b). The geological conceptual model was created based on a high-resolution seismic survey by Haimberger et al. (2005) in the northern part of the Upper Rhine Graben (URG), an area that contains our study site. That survey was carried out over a length of 80 km along the Rhine River and a length of 25 km along its tributary, the Neckar River. The borehole logs from the central URG show that these Quaternary sediments consist of fluvial and lacustrine unconsolidated calcareous sands and gravels with interbedded clay and silt layers with thickness ranging from 2-8 m (Haimberger et al., 2005). The seismically imaged facies of the Pleistocene age in the upper layers shows thick and uniform stratification with low amplitude. Combining this geometrical information with observations from boreholes, the strata at the site are interpreted to lie within a braided to low-sinuosity meandering river system. The TI domain, which represents the geological conceptual model conditioned to borehole facies data, is 150m × 15m. It is uniformly discretized with cell dimensions of 0.05m × 0.05m, so that the TI consists of 900,000 grid cells. It is twice the size of the subsequent groundwater model (75m × 15m) in the horizontal direction in order to reproduce larger scale patterns (Caers & Zhang, 2005). Two types of facies ("sand" and "silt") and their proportions were interpreted from the permeability histogram. Given the knowledge of the geological conceptual model, a sinusoid geobody type was selected in SGeMS to generate the TI.

4.2.2.2 Facies realizations

Among the available MPS algorithms for facies modeling (Mariethoz & Caers, 2014), the widely used pixel-based single normal equation simulation (SNESIM) (Strebelle, 2000) was used to generate facies realizations by conditioning to site borehole facies data while sampling the multiple point statistics from the TI. Compared with other MPS facies modeling algorithms, SNESIM was chosen due to its capacity, both in data conditioning and geological shape reproduction, and its efficient CPU performance in SGeMS. To generate each realization, SNESIM simulates the facies patterns by scanning the TI and applies the sampled statistics to simulate a facies type at each cell of the geostatistical grid. The observed facies type and location of the soil samples served as the conditioning data during the SNESIM simulation. The MPS simulation grid is 75m × 15m, with cell dimensions of 0.05m × 0.05m, and consists of 450,000 grid cells. A total of 300 facies realizations were created by SGeMS, which implements SNESIM (Remy et al., 2009).

4.2.2.3 Permeability fields

To quantify permeability spatial correlation at the study site, experimental permeability variograms in both the horizontal and vertical directions were calculated and modeled for each facies. The intrafacies permeability field within the silt and sand facies, as modeled in each SNESIM realization, was simulated using SGSIM, a conventional geostatistical method based on permeability histogram and variogram (Deutsch & Journel, 1998). A set of 300 aquifer permeability fields were modeled and then used as the input for subsequent groundwater flow and age modeling.

4.2.3 Estimating streambed permeability by analytical model inversion

Streambed permeability is one of the key factors controlling surface water-groundwater exchange (Genereux et al., 2008) and is often strongly affected by flood events in natural streams that can erode and redistribute stream sediments (Simpson & Meixner, 2012). In this study, three flood events with different peak magnitudes were recorded between 9-18th, 29-33rd, and 45-49th days since August, 2010. At a given location, the streambed permeability can be expected to be highly transient between alternative losing and gaining conditions when there are significant deposition and remobilization of sediment particles (Simpson & Meixner, 2012). To estimate the temporal variation of streambed permeability and reduce model uncertainty, a technique developed by Gianni et al. (2016) was adopted to rapidly calculate a transient streambed permeability and to identify its impact on the location and timing of water fluxes at the sediment water interface. This technique represents a heterogeneous streambed with homogeneous properties (i.e., an equivalent permeability), which was proven feasible if both the calibration and prediction are made for a connected flow regime (Irvine et al., 2012). Because the average stream width and thickness at our study site are on the scale of a few meters and groundwater flow and age distribution are modelled at the full field scale, the extent of the streambed in the coupled surface water-groundwater modelling is represented by only 20 grid cells. Clearly, a homogeneous representation of the streambed is considered suitable for the scale of investigation, and sub-grid streambed heterogeneity is assumed to be accounted for by an estimated equivalent permeability of the streambed, as explained below.

The transient streambed permeability is estimated from recorded pressure heads within the aquifer and the stream stage through the inversion of a numerical convolution between discretized stream stage and aquifer response using the analytical model of Gianni et al. (2016). This model describes the aquifer response in the presence of a clogging layer (i.e. a streambed layer with permeability less than that of the surrounding aquifer) to a unit step variation of the stream stage (Hall & Moench, 1972):

$$h(x,t) = \mathrm{erfc}\left(\frac{x}{2\sqrt{\alpha t}}\right) - \exp\left(\frac{x}{r} + \frac{\alpha t}{r^2}\right)\mathrm{erfc}\left(\frac{x}{2\sqrt{\alpha t}} + \frac{\sqrt{\alpha t}}{r}\right) \quad (4.1)$$

where $h(x,t)$ [m] is the hydraulic head at distance x perpendicular to the stream edge and at a time t after the beginning of the unit step variation of the stream stage; $erfc$ and exp are the complementary error function and the exponential function, respectively. α [m^2 s^{-1}] is aquifer hydraulic diffusivity, $\alpha = K_a \rho g d_a / \mu S$, where K_a [m^2] is aquifer permeability, ρ [kg m^{-3}] is fluid density, g [m s^{-2}] is gravity acceleration, μ [kg m^{-1} s^{-1}] is fluid dynamic viscosity, d_a [m] is thickness of the aquifer, and S is storativity [-]. S is estimated to be 6.75×10^{-4} from a

previous field investigation (Engelhardt et al., 2013a). The retardation coefficient r [m] represents the required thickness of aquifer to cause the same head loss as the streambed. $r = dK_a/K$, d [m] is streambed thickness, and K [m^2] is streambed permeability.

When both d and K_a are known, then r can be used as a surrogate for the estimation of the streambed permeability. By the convolution of stream stage variations with equation (4.1), water table variation was computed at the observation well GWM2a over time. Parameter r is then estimated by minimizing the sum of squared error between the observed and modeled pressure heads at GWM2a. The approach is implemented using the mathematical software MATLAB. Due to the high heterogeneity of the aquifer, it is not suitable to calculate the average aquifer diffusivity for the whole transect. Thus, three aquifer diffusivities (0.1, 1 and 10 m^2/s) were tested in the analytical inversion. The time series of observed groundwater table at GWM2a are segmented in partially overlapping time intervals, referred to as parameter optimization window (POW), which is comprised of two parameters, the size (time interval width) and the shift (POW moving length). Based on the segmentation of the time series, a set of varying streambed permeability over time was calculated.

4.2.4 Stream-groundwater flow model

A previous study by Engelhardt et al. (2013a) used the same monitoring campaign data to set up a groundwater flow model with MODFLOW. In that model, the aquifer permeability was assigned layer-by-layer in a deterministic sense, and the streambed permeability was assumed temporally and spatially homogenous. Uncertainty in flow and transport simulations due to aquifer spatial variation and streambed temporal variation of permeability was not considered. This research builds upon the previous work and the site streambed and aquifer permeability variation were modeled using analytical inversion of aquifer response and geostatistical MPS simulations conditioned to lithofacies observations at well locations, respectively. Because our lithofacies observations exhibit high vertical resolution at the scale of 0.05 m, the 300 permeability models created by MPS simulations exhibit high spatial resolution at the scale of 0.05 m by 0.05 m. This approach thus avoids upscaling the lithofacies model, which can lead to lost resolution in representing the site geology. As a result, a large suite of high resolution permeability MPS realizations were created as input for Monte Carlo flow simulation, thus computational requirement is much larger and a high performance groundwater flow code is needed. This research conducts stream-groundwater flow simulation using PFLOTRAN (Hammond & Lichtner, 2010; Hammond et al., 2014), an open source, massively parallel, subsurface flow and reactive transport simulator with parallelization through the PETSc library (Balay et al., 1997). In solving subsurface flow and transport problems ranging from single to two-phase flow, as well as reactive species transport, it has exhibited excellent scaling performance (Zhang et al., 2017).

Numerical model set-up. A two-dimensional saturated flow model was set up for a transect length of 75 m and an aquifer depth of 15 m (refer to the transect in Figure 4.1b). The model

is discretized into 450,000 grid cells with a cell resolution of 0.05m × 0.05m, which corresponds to the scale of the MPS simulation model. Given the observed highly transient stream stage and groundwater flow due to summer precipitation and flood events, this high resolution horizontal and vertical cell size was chosen across the model domain to guarantee numerical stability under variably saturated conditions. The stream is surrounded by a 1 m thick streambed which is assumed to be highly controlled by the surface water-groundwater exchange. The simulation period continues over 55 days, i.e., from 15 August, 2010 to 9 October, 2010.

Flow equation. The governing mass conservation equation for the variably saturated flow is given by (Bear, 1979):

$$\frac{\partial}{\partial t}(\rho n s) = \nabla \cdot \left[\frac{\rho k k_r}{\mu}(\nabla \mathrm{P} - \rho g \nabla z)\right] + q \tag{4.2}$$

where ρ [kg L^{-1}] is water density, n [-] is porosity, s [-] is saturation, k [m^2] is permeability, k_r [-] is relative permeability, P [Pa] is pressure, g [m s^{-2}] is gravitational acceleration, z [m] is elevation above the sea level (head datum), q [kg L^{-1} s^{-1}] are sources and sinks. The van Genuchten-Mualem (VGM) model was used to relate fluid pressure, saturation, and k_r (van Genuchten, 1980; Mualem, 1976):

$$s = [1 + |\alpha h|^n]^{-m} \tag{4.3}$$

$$k_r = \sqrt{s}\left[1 - \left(1 - s^{1/m}\right)^m\right]^2 \tag{4.4}$$

where h [m] is matric potential. α, m, and n are empirical parameters and cited from Carsel & Parrish (1988), $m = 1 - 1/n$. Due to the thin unsaturated zone compared to the model vertical dimension, the model uncertainty from these empirical parameters would be minor.

Initial and boundary conditions. The initial and boundary conditions were set in a similar manner to the MODFLOW/MT3DMS model by Engelhardt et al. (2013a). The initial hydraulic heads across the model domain were defined from the head gradient measured between the observation well GWM0 and GWM6. The SE (southeast) boundary was defined by the prescribed hydraulic head using the observed hydraulic head at GWM0. The NW (northwest) boundary was defined by the hydraulic head that was derived from the interpolation between S3 and GWM6. The groundwater recharge was assigned to the model top layer with a recharge rate of 15% of the precipitation that infiltrated into the groundwater (Berthold & Hergesell, 2005). The model bottom layer was defined as a no flow boundary, corresponding to low permeable silty clay layer. The observed time variable stream stage was assigned to the model cells that represent the stream bottom with a time variable head boundary. The porosity for the streambed was 0.12 with homogeneous distribution (Engelhardt, 2013a). The porosity for silt and sand facies were 0.35 and 0.39 throughout the aquifer domain, respectively, which were derived from the mean porosity of each facies. The porosity of streambed and aquifer were assumed to be homogeneous and constant. The time-varying streambed permeability was assumed to be spatially homogeneous and assigned to the

cells of the streambed. The permeability fields of the aquifer were assigned to the aquifer cells according to the geostatistical realizations.

Uncertainty analysis. The multiple realization mode of PFLOTRAN was used to conduct the Monte Carlo simulations of variably saturated flow in streambed and in the connected aquifer using each of the 300 aquifer permeability realizations as input. Simultaneously, 300 Monte Carlo simulations ran on 3 processor groups with each group consisting of 100 simulations that ran one after another. A total of 96 processor cores were utilized. The computed pressure heads, a total of 300 sets, were obtained to define the influence of permeability uncertainty on the simulated heads. Based on the simulated and measured hydraulic heads at observation wells GWM2a and S3, a mean absolute error (MAE) of each realization was calculated:

$$\mathrm{MAE} = \frac{1}{n}\sum_{i=1}^{n}|h_{mi} - h_{si}| \tag{4.5}$$

n [-] is the number of the measured hydraulic head, h_{mi} [m] and h_{si} [m] are the measured and simulated hydraulic head, respectively. It provides a criterion that a realization is acceptable to represent the site geology if its MAE is below a user-defined value (Anderson et al, 2015). A cumulative mean absolute error (CMAE) was further calculated versus the number of realizations to estimate how many realizations are sufficient for convergence:

$$\mathrm{CMAE} = \frac{1}{j}\sum_{i=1}^{j}\mathrm{MAE}_i \tag{4.6}$$

j is the number of realizations and MAE_i is the mean absolute error of the i-th realization. The maximum, minimum, and arithmetic mean simulated heads were calculated based on the acceptable realizations. Standard deviations of the simulated heads were calculated for the acceptable realizations to represent the uncertainty.

4.2.5 Groundwater age simulation

The groundwater age is calculated by the advection-dispersion equation for nonreactive tracer transport that is implemented in PFLOTRAN following the method described in Goode (1996):

$$\frac{\partial A}{\partial t} = \nabla \cdot \boldsymbol{D} \cdot \nabla \mathrm{A} - \nabla \cdot A\frac{\mathbf{q}}{\theta} + 1 \tag{4.7}$$

$$A = \frac{\int_0^\infty tC\ \mathrm{d}t}{\int_0^\infty C\ \mathrm{d}t} \tag{4.8}$$

where A [d] is the tracer mean age with concentration C [mol L^{-1}], θ [L L^{-1}] is the porosity, $\mathbf{q}$ is the specific-discharge vector, $\mathbf{D}$ is the dispersion tensor. The right side term "+1" denotes each molecule getting one day older every day. Building upon the flow model, the initial age of 1×10^{-8} d and concentration of 1×10^{-16} mol L^{-1} of a dummy tracer was defined across the model domain. A zero gradient boundary condition was defined at the SE, NW, top, and bottom boundary, respectively.

Because the site saturated permeability was explicitly modeled at high resolution, the longitudinal and transverse dispersivity were all set to zero (assuming sub-grid dispersion is negligible), thus the computed age reflects a purely advective travel time distribution along the groundwater streamlines. The resultant groundwater age only refers to the time from the start of the simulation. It reveals the infiltration paths from surface water into groundwater and can help to visualize zones that received surface water fluxes with younger ages. The groundwater age simulation was conducted for each acceptable flow model. A probabilistic infiltration path was then delineated based on the ensemble of simulated infiltration paths, thus taking into account the geological uncertainty. The area with high or close to 100% probability indicates the highest confidence in the predicted infiltration paths.

4.3 Results and discussions

4.3.1 Facies category

Grain size analysis of the soil samples shows that the aquifer beneath and in close proximity to the stream is highly heterogeneous and is composed of interbedded silt, clay, and sand layers (including fine, median and coarse sand layers). Permeability is calculated with the Hazen method (Hazen, 1911), using the d_{50} values from the grain size curve, that vary from 2.61×10^{-14} to 9.74×10^{-11} m^2 (Figure 4.1c). The distribution of permeability indicates the existence of two hydrofacies populations, one representing a silt-rich facies and the other a sand-rich facies (referred to herein as the silt and sand facies). A cut-off value separating the two populations was identified at 1×10^{-12} m^2. The bimodal permeability distribution in the histogram shows the primary control of facies on permeability, thus facies modelling is necessary to capture the permeability variation and to honour the observed spatial transition. Variogram analysis of the permeability data shows that the horizontal/vertical anisotropy ratio is 5:1, both for silt and sand facies. The uncertainty of the Hazen method and insufficient horizontal data are the main reason for lack of agreement between the experimental and the modeled variograms in the horizontal direction, both in silt and sand facies. Moreover, to capture within-facies variability, a subsequent permeability simulation was conducted within each facies using sequential Gaussian simulation (SGSIM), which used the histogram and variogram models of permeability developed for each facies (Figures 4.1c and 4.2, Table 4.1). The approach adopted thus captures both large-scale facies transitions and small-scale within-facies permeability variation.

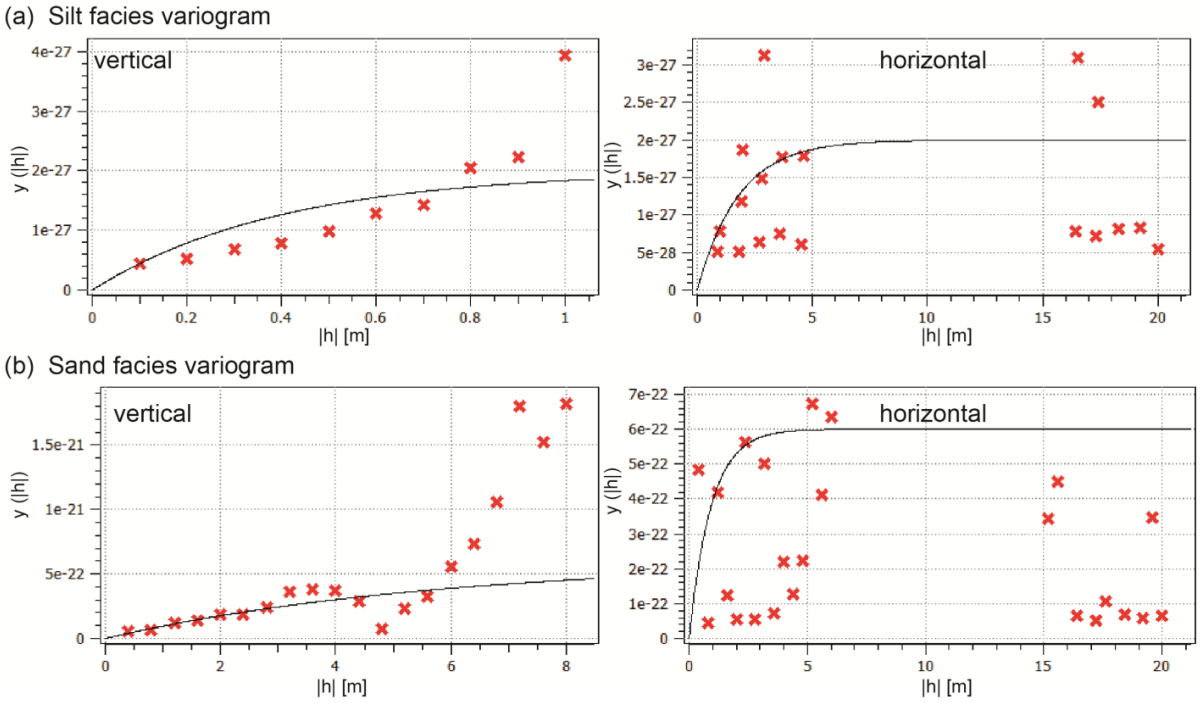

Figure 4.2: Horizontal and vertical experimental (dots) and modeled (curves) permeability variograms for silt and sand facies, respectively.

Table 1. Variogram parameters of permeability for the silt and sand facies.

Facies	Variogram type	Nugget $(m^2)^2$	Ranges (m)			Angles			Sill $(m^2)^2$
			Max	Med	Min	azimuth	dip	rake	
Silt	Exponential	0	17	3.4	0	90	0	0	6×10^{-22}
Sand	Exponential	0	5	1	0	90	0	0	2×10^{-27}

4.3.2 Aquifer heterogeneity

A stationary training image (Figure 4.3a) was constructed based on geological information from well data (Figure 4.3b) and the geological transect (Figure 4.1b). In the TI, the red region corresponds to the silt facies with low permeability materials such as silt and clay, while the background, or blue region, corresponds to the sand facies with high permeability materials such as sand and gravel. A total of 300 facies realizations (Figure 4.3c) were generated with SNESIM by (1) sampling the local conditional probabilities from the training image using a MPS template, and (2) constraining the realizations by observed facies identified in soil samples. The optimal reproduction was determined by visual inspection

using a 60-node search template with a dimension of 100 m × 100 m, 6 multi-grid, and a 0.5 servosystem factor to approach the target facies proportion (0.3 : 0.7). The template dimension and the number of multi-grids are the most influential parameters for the pattern reproduction. The SNESIM realizations preserve the heterogeneous facies structure that is consistent with the geological conceptual model. They show a mean proportion and standard deviation of 0.347 and 0.011 for silt facies, and 0.653 and 0.011 for sand facies, respectively. Next, the permeability filed was simulated within silt and sand facies using SGSIM in each facies realization. The assembled 300 permeability fields then served as input for the subsequent groundwater flow model (Figure 4.3d).

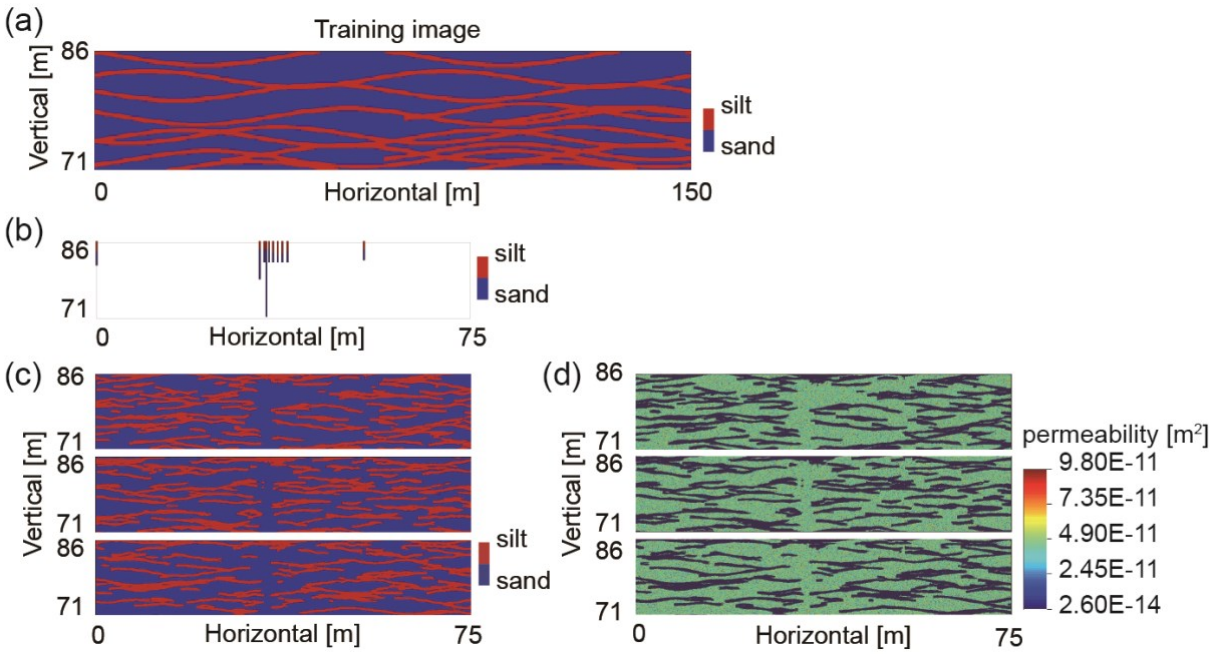

Figure 4.3: (a) The training image (TI) and (b) well identified facies that were used for constraining the MPS simulations of facies; (c) Examples of SNESIM facies realizations; (d) Assembled permeability fields.

4.3.3 Streambed permeability

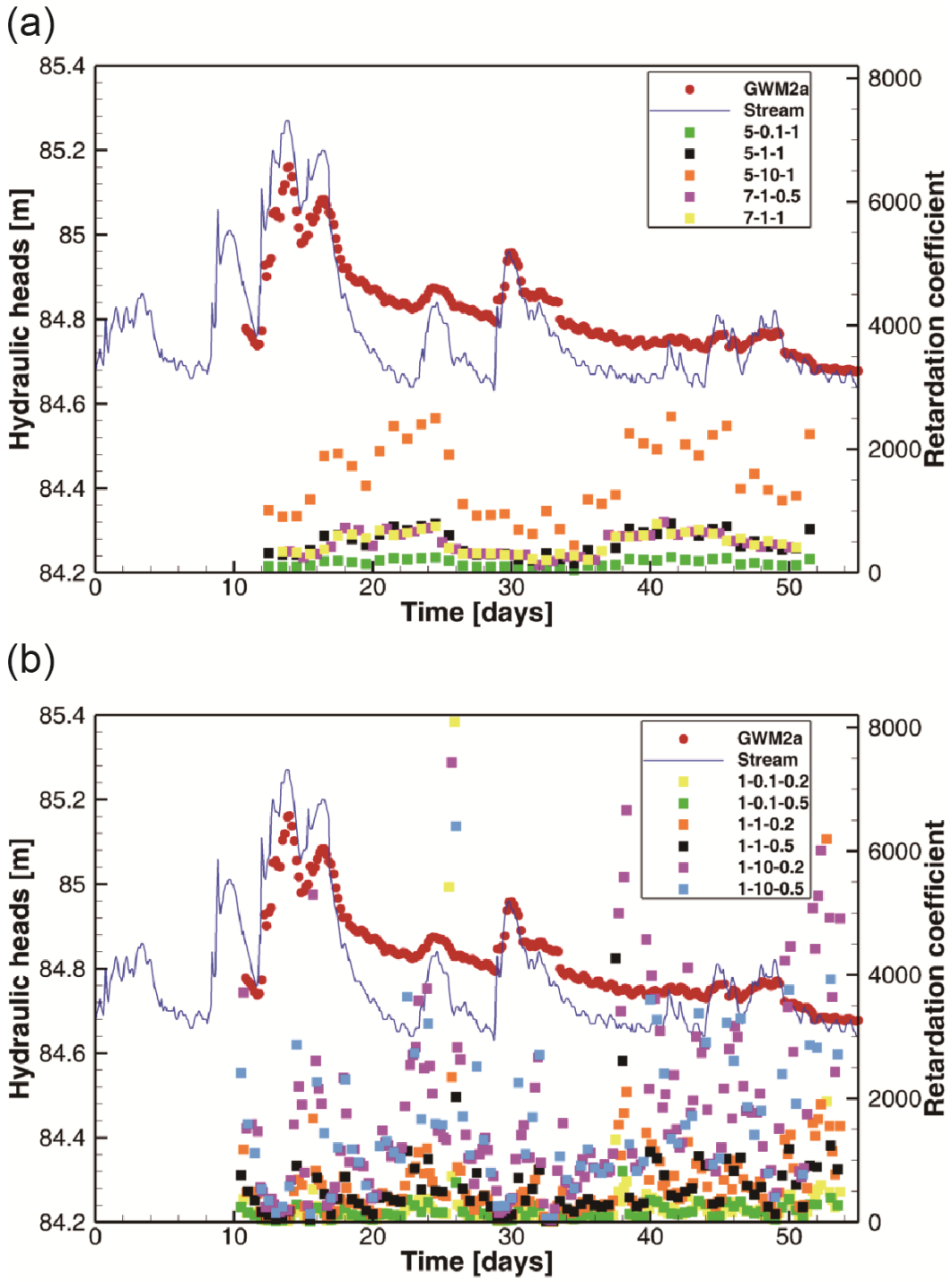

Figure 4.4: The estimated retardation coefficients (square symbols) versus stream stage (lines) and observed hydraulic heads (cycle symbols) at GWM2a. The 11 sets of retardation coefficients indicated with different colors correspond to different parameter combinations of POW size, aquifer diffusivity, and POW shift, respectively.

The retardation coefficients (r) were calculated for different POW size, shift, and aquifer diffusivities to evaluate the input parameter sensitivity (Figure 4.4). The retardation coefficients were calculated from the 10^{th} day until the end of the simulation period. The aquifer response to the stream stage variation is represented by the measured hydraulic head at GWM2a. Three sets of aquifer diffusivity (0.1 m^2/s, 1 m^2/s, and 10 m^2/s) were tested to

represent the whole transect from the range of minimum values of 0.01m^2/s to maximum values of 19.28m^2/s calculated from the measured soil sample permeability (Figure 4.1) and storativity. Under the same POW size (5 days) and shift (1 day), an increase of aquifer diffusivity from 0.1 m^2/s to 1 m^2/s to 10 m^2/s resulted in a 3-fold increase in the retardation coefficient. Given that retardation coefficient represents the effective thickness of aquifer that is required to cause the same head loss as the streambed layer (Hantush, 1965), the increase of retardation coefficient indicates more thickness of aquifer is needed to cause the observed head loss due to the streambed. If the head drop and flux are known, according to Darcy's law (Whitaker, 1986), the increase of the diffusivity (or permeability) will also result in an increase of aquifer thickness, since the aquifer permeability is proportional to diffusivity. By comparing different POW sizes (1, 5, and 7 days), it can be shown that the model using a larger POW size was able to capture more head observations and reproduce the general trend, but the transient head fluctuation at small time interval was not well captured. Models with a lower POW size with 0.5 day with aquifer diffusivities of 0.1, 1, and 10 m^2/s, and shifts of 0.2 and 0.5 day per time step were also tested, but no signals were observed due to the limited observations that this POW can capture. Although smaller POW size and shift can capture transient head fluctuation, the decrease of the POW size and shift can produce a number of outliers due to the decrease of the signal (observations) to noise ratio (Figure 4.4b). Thus, the estimation of the retardation coefficient depends highly on the choice of the POW size and shift, and the accurate estimation of the effective aquifer diffusivity. Each set of retardation coefficients estimated under different scenarios (POW size and shift, aquifer diffusivity) were converted into permeability datasets and transferred to the groundwater flow model. The optimal set of streambed permeability values that can reproduce the historical hydraulic head records was the combination of POW, with 1 day size and 0.2 day shift, and 10 m^2/s aquifer diffusivity. Given the quick response of the pressure head at GWM2a to the stream stage, the small window size and shift is reasonably expected.

4.3.4 Model uncertainty

First, the cumulative mean absolute error (CMAE) in hydraulic heads for the stochastic forward runs using 300 aquifer permeability fields was calculated. Figure 4.5a shows that the CMAE stabilized after approximately 50 realizations at 0.09 m, indicating that 50 runs would have been sufficient for model convergence (Anderson et al., 2015). If the MAE in hydraulic head is then calculated for each stochastic forward run, the question of whether or not the realization still stays within the acceptable calibration range can be determined (Figure 4.5b). An optimal cut-off value of 0.06 m was chosen by testing the MAE value from 0.04 to 0.1 m to judge the obtained results. Those realizations with a MAE of more than 0.06 m did not yield an acceptable model and were removed, leaving 33 conditioned realizations for the uncertainty analysis. Results from the 33 forward runs were summarized by plotting the maximum, mean, minimum, and standard deviations of the simulated hydraulic heads, versus the measured hydraulic heads (Figure 4.6). Figure 4.6 shows that most of the observed hydraulic heads at GWM2a and S3 lie in the range between the maximum and minimum simulated hydraulic heads, except that the hydraulic heads around 14th day at GWM2a were underestimated, which might be due to the underestimation of the streambed permeability during the heavy flood event. The hypothesis of spatial homogeneity for streambed might be

the main assumption that led to the non-representation of preferential flow from stream into groundwater.

The stochastic forward modeling was conducted again using the suite of aquifer permeability realizations, but the streambed layer was removed. Figure 4.5c shows that CMAE was stabilized at a higher value of 0.115 m than that of 0.09 m in Figure 4.5a. All of the MAEs were higher than the cutoff value, which means none of these simulations yielded an acceptable model (Figure 4.5d). By comparing the simulations to those of Figure 4.5a and b, which include the streambed layer with temporally transient permeability, the essential role of streambed in the stream-groundwater interaction processes is elucidated.

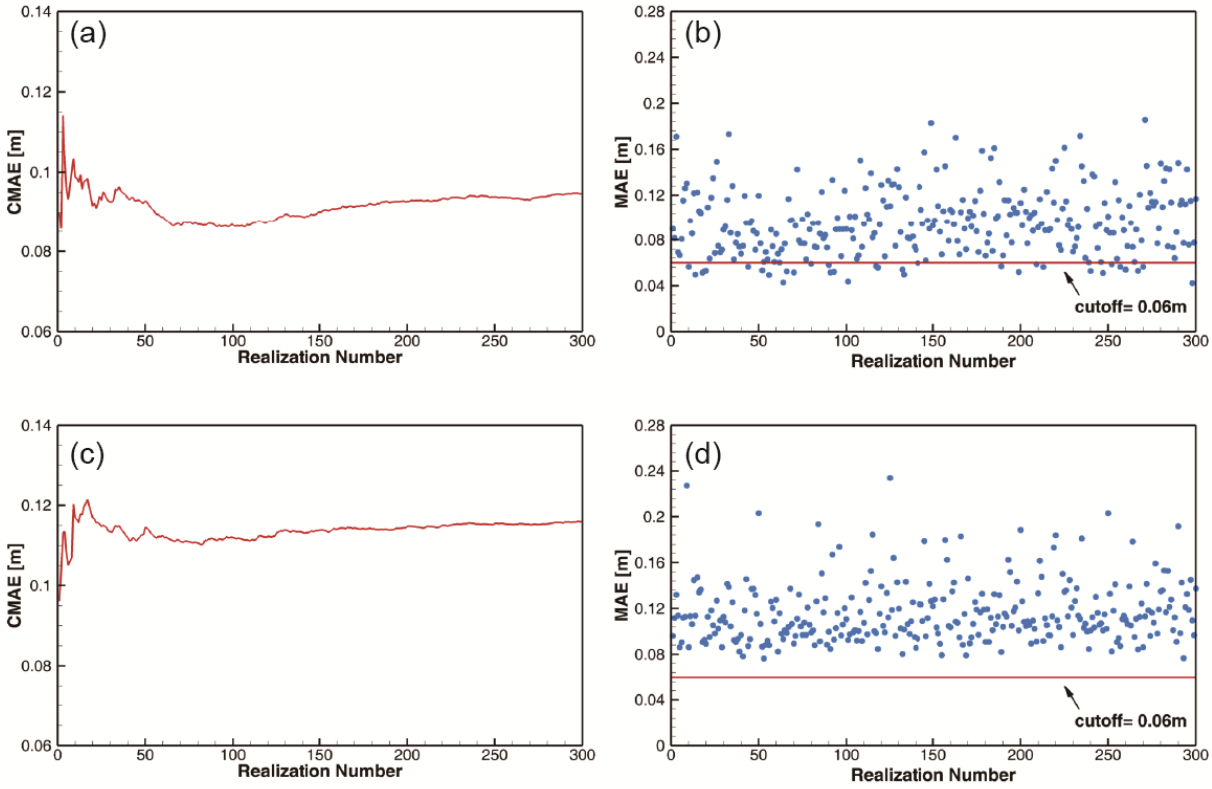

Figure 4.5: Cumulative mean absolute error (CMAE) and mean absolute error (MAE) of the Monte Carlo simulations with 300 aquifer permeability fields and with the optimal transient streambed permeability (a and b), and without the streambed layer (c and d). (a) The relatively stable CMAE after 50 realizations indicates convergence of the Monte Carlo process. (b) The acceptable simulations were conditioned by removing the runs with MAE greater than 0.06 m. (c) A higher set of CMAE was observed compared with (a) due to the large deviation of simulated hydraulic head from measured data when streambed was not incorporated. (d) All the MAEs were above the cutoff line, indicating that the outliers do not yield an acceptable model.

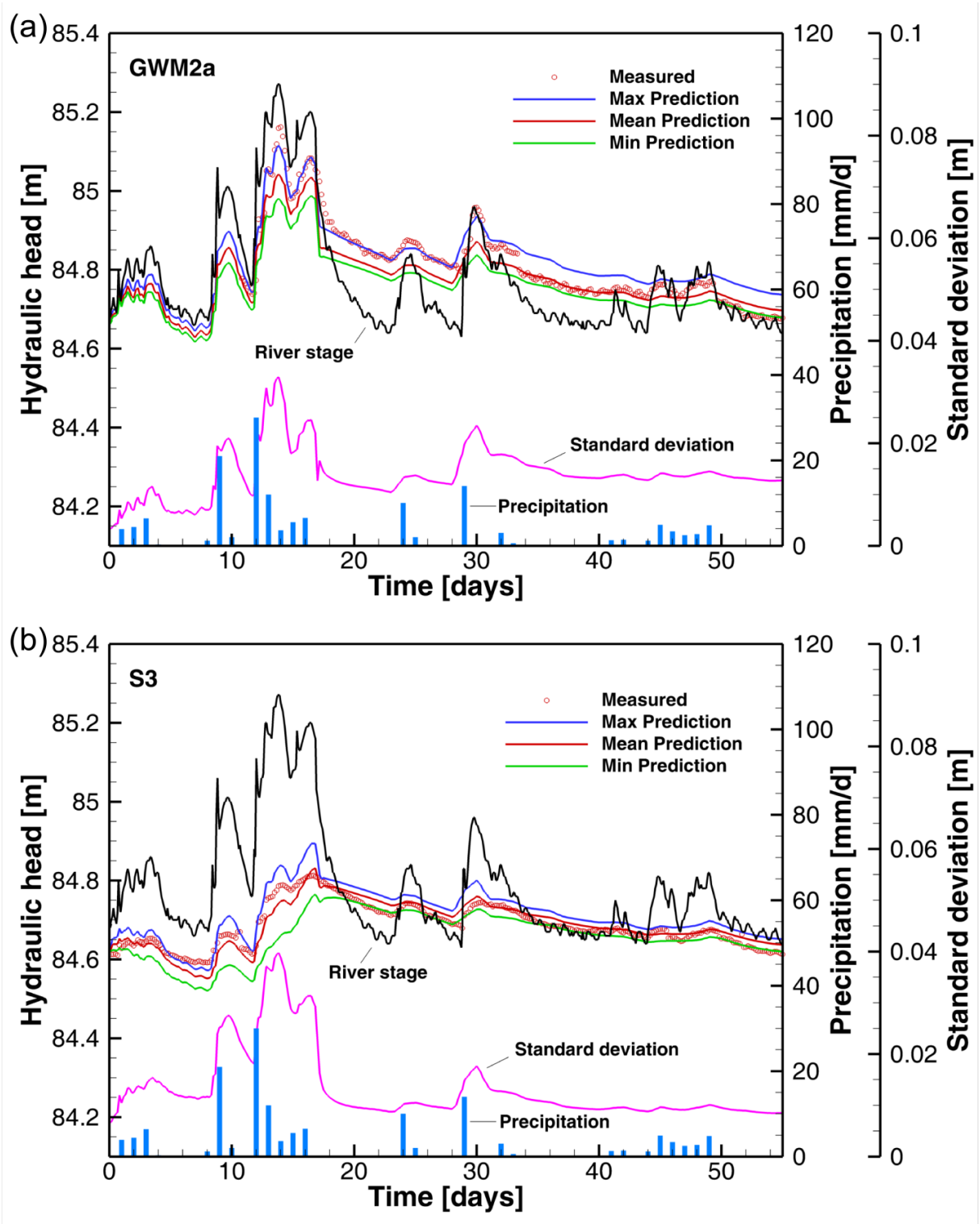

Figure 4.6: Results of conditioned stochastic forward runs at the observation wells (a) GWM2a and (b) S3, respectively. The maximum, mean, and minimum values of the simulated hydraulic heads are compared with the measured data. Standard deviation shows that the uncertainty of simulated hydraulic heads varies with precipitation and flood periods.

The simulated hydraulic heads from the conditioned stochastic runs match well with the observed values at the observation well GWM2a and S3 (Figure 4.6a and b). For GWM2a, the maximum uncertainty of 0.033 m occurred at 14th day during the first flood period (9-18th days), followed by a relatively smaller uncertainty of 0.024 m at the 30th day during the

second flood period (29-33th days). The greater distance between the stream and the observation well S3 decreased the response of hydraulic head at S3 to the variation of stream stage, even during the flood periods and heavy precipitation events. However, the model uncertainty reached a maximum value of 0.04 m at the 14th day during the first flood period. Another peak value of 0.017 m is observed for the second flood period. In summary, high uncertainties were following the two heavy precipitation events (9-18th and 29-33th days). Given that the transient streambed permeability was identical in each model run, the high uncertainties are attributed to the aquifer permeability fields that vary between each stochastic simulation. In contrast to infiltration periods, during the exfiltration periods the uncertainties were distinctively lower. The higher uncertainties during the infiltration periods can be explained by the decreased control of streambed on the exchange fluxes during infiltration periods.

The streambed permeability has been proven by several authors, e.g. Hatch et al., 2010; Kurtz et al., 2012; Taylor et al., 2013; Zhang et al., 2011, to be a highly dynamic parameter due to clogging, sedimentation, and remobilization of the sediments (Emmett & Leopold, 1963). Smaller particles have a greater tendency to be mobilized, which in turn will increase the entire streambed permeability during the floods due to the increased porosity caused by larger particles, while the clogging and deposition of transported sediments during dry seasons will decrease streambed permeability. Thus, during dry seasons, the streambed limits the surface water-groundwater exchange, while it promotes the exchange during floods. This is coincident with the simulated water flux at the stream-aquifer interface (Figure 4.7). During the infiltration periods, the reduced streambed permeability due to sediment remobilization resulted in predicted water fluxes with a large standard deviation, while the increased streambed permeability by sediment clogging and deposition limited the exchange flux during the exfiltration periods. The high flux standard deviation during infiltration periods originated from the variation of aquifer permeability fields, which then decreased during exfiltration periods due to the increased control of the streambed on the exchange flux.

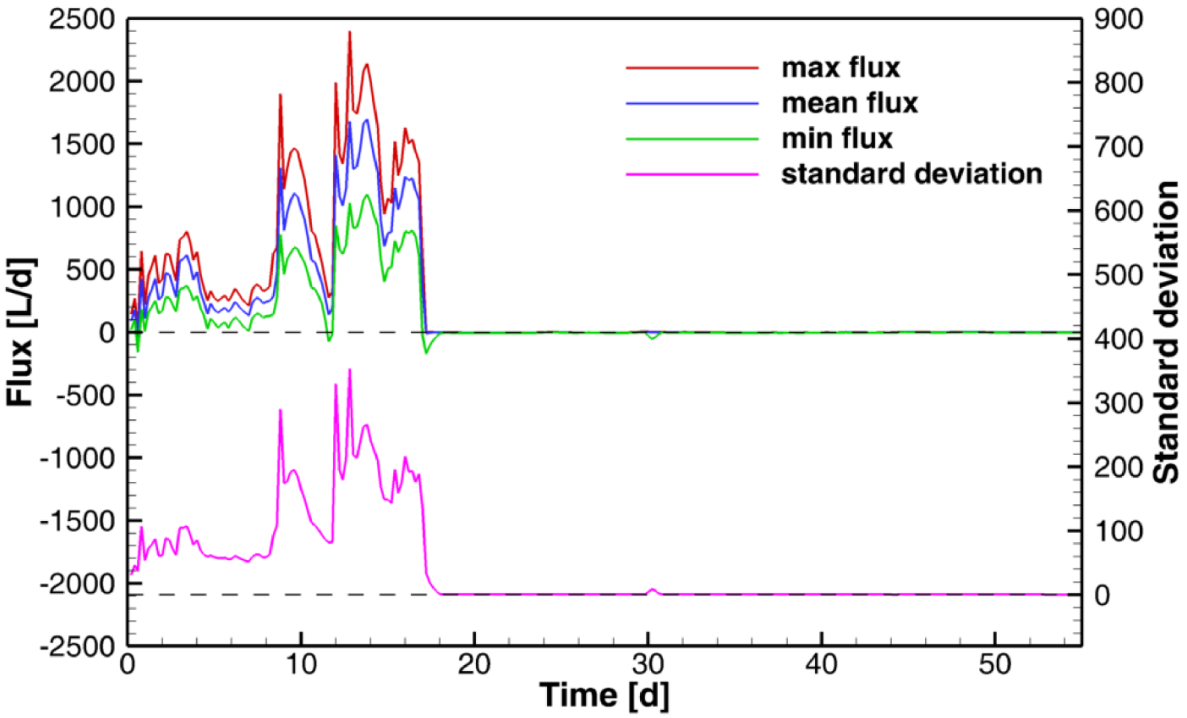

Figure 4.7: The simulated water flux at the stream-aquifer interface. The maximum, mean, and minimum values of the water flux are summarized from 33 realizations. Positive and negative values indicate water infiltration from the stream into the aquifer and exfiltration from the aquifer to the stream, respectively.

4.3.5 Surface water infiltration path

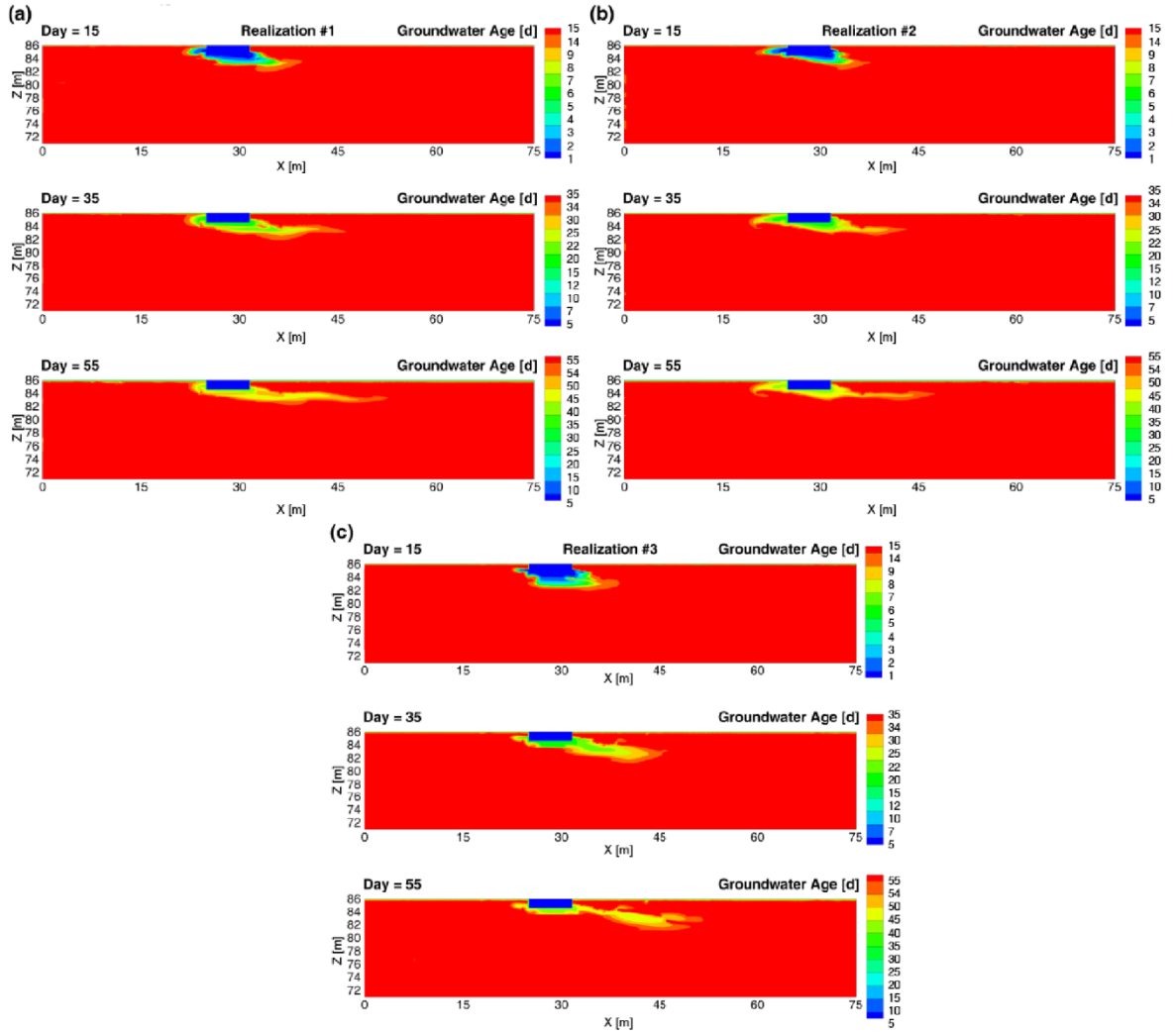

Figure 4.8: Simulated groundwater age of (a) realization #1, (b) realization #2, and (c) realization #3 at days 15, 35, and 55. Day 15 corresponds to the infiltration period, while days 35 and 55 correspond to the exfiltration periods.

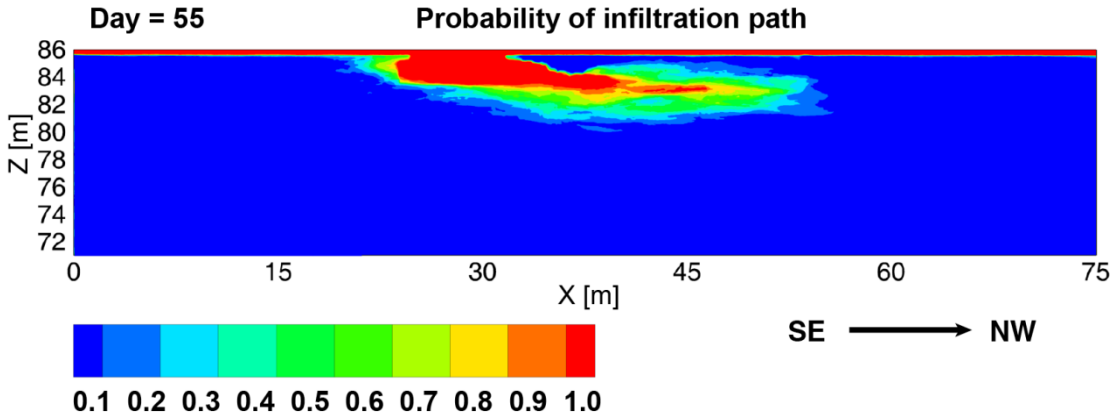

Figure 4.9: Probabilistic area of contribution with low (blue) to high (red) for surface water infiltration path based on the 33 groundwater age realizations.

The groundwater age distribution was calculated for each of 33 realizations (Figure 4.8). Younger groundwater was observed during the infiltration period (day 15) than the

exfiltration periods (days 35 and 55). The different aquifer permeability field used in each realization resulted in a highly different age distribution and thus the implicit differences in the flow path. Due to the heterogeneous and anisotropic permeability distribution, longer preferential flow paths were observed in the model domain down hydraulic gradient. The distinctive flow paths shown by each realization indicate the dominant control of aquifer heterogeneity on stream water infiltration.

Figure 4.9 provides the probabilistic map of the surface water infiltration path after 55 days simulation time. The map summarizes how many times a cell contributed to the path divided by the total number of realizations. The area with a probability of 1.0 represents the case where a cell contributed to the path in all 33 runs. The surface water derived from rainfall penetrated to a depth of 0.5 m from the top layer in 100% probability. The stream water infiltrated into the aquifer with a horizontal length ranging from 8.4 m (100% probability) to 24.2 m (10% probability) in a NW direction from the right stream bank, and with a depth ranging from 1.6 m (100% probability) to 4.6 m (10% probability) from the stream bottom. The water infiltrated from the stream flowed primarily towards the NW direction as it integrated with the regional groundwater flow system. This method provides a probabilistic estimation of the surface water infiltration path based on the Monte Carlo concept. Although it only considers advective flow without dispersion, sorption, or geochemical reactions, tracking water particle paths in terms of probability can still be used to evaluate a hypothetical wastewater plume in a qualitative sense. For example, areas with extreme probability (0% or 100%) are expected to be less sensitive to particle numbers and discretization levels than those with uncertain probability (around 50%) (Juckem et al., 2014). The probability map also provides a reference for the optimization of monitoring wells and solute sampling depths.

4.4 Conclusions

The estimated streambed permeability from the inversion of flood wave responses shows a transient pattern of the streambed permeability, which decreased during infiltration periods and increased during exfiltration periods. The estimation of streambed permeability depends strongly on the selection of the POW size, shift, and aquifer diffusivity. It is worth mentioning that the aquifer anisotropy, especially in the vertical direction, might impose a significant impact on the estimation of the retardation coefficient, as layers with lower or higher permeability could be activated alternatively by the varying height of the groundwater table. The aquifer permeability simulated using multiple-point geostatistics with multiple realizations are highly heterogeneous and anisotropic. Each realization captures both facies and sub-facies scale variability. By incorporating the transient streambed permeability and heterogeneous aquifer permeability, the newly developed groundwater flow model was able to reproduce the recorded fluctuation of hydraulic head at two observation wells. Our numerical results demonstrate that the exchange flux of the stream-groundwater interaction during infiltration periods was mainly reduced by the aquifer, while the streambed shows dominant limitation on the exchange flux during exfiltration periods with its reduced permeability. Therefore it is essential to consider the influence of transient streambed permeability when studying stream-groundwater interaction under variable stream stage and discharge situations.

Groundwater age simulation using multiple permeability realizations quantifies the uncertainty in the stream water infiltration path with a probabilistic map. Stream water infiltrated into the aquifer to a depth of 1.6 m (100% probability) to 4.6 m (10% probability) below the stream. Laterally, stream water infiltrated towards the northwest direction up to 8.4 m (100% probability) to 24.2 m (10% probability) from the stream. Based on the computed probabilities, the region from the stream bottom to a depth of 1.6 m and from the stream right bank to a lateral distance of 8.4 m has experienced stream-aquifer interaction with the highest confidence. The large variation in path probability, however, shows the significant control of aquifer heterogeneity on groundwater flow. The probability map also provides a forecast envelope for a hypothetical wastewater plume that is released from the streambed.

In the future, we will install additional stream and aquifer piezometers at the site along with seepage meters. The new monitoring data will verify the results of this study and can be used to refine the model and its parametrization, thus reducing uncertainty in the simulated groundwater age and flow paths.

4.5 Acknowledgements

The authors gratefully acknowledge the computing time granted by the supercomputer HLRN of North German Supercomputing Alliance and the HPC-Cluster of TU Freiberg. The first author also acknowledges generous financial support from the China Scholarship Council (CSC).

4.6 References

Anderson, M. P., Woessner, W. W., Hunt, R. J., 2015. Applied groundwater modeling: simulation of flow and advective transport. San Diego: Academic press.

Attard, G., Rossier, Y., Eisenlohr, L., 2016. Urban groundwater age modeling under unconfined condition–Impact of underground structures on groundwater age: Evidence of a piston effect. Journal of Hydrology, 535, 652-661.

Balay, S., Gropp, W. D., McInnes, L. C., Smith, B. F., 1997. Efficient management of parallelism in object-oriented numerical software libraries. In: Arge E., Bruaset A.M., Langtangen H.P. (eds) Modern Software Tools for Scientific Computing. Birkhäuser, Boston, MA.

Bear, J., 1979. Hydraulics of Groundwater. New York: McGraw-Hill.

Carsel, R. F., Parrish, R. S., 1988. Developing joint probability distributions of soil water retention characteristics. Water Resources Research, 24(5), 755-769.

Caers, J., Zhang, T., 2005. Multiple-point geostatistics: a quantitative vehicle for integrating geologic analogs into multiple reservoir models. AAPG Memoir, 383–394.

Cheong, J. Y., Hamm, S. Y., Kim, H. S., Ko, E. J., Yang, K., Lee, J. H., 2008. Estimating hydraulic conductivity using grain-size analyses, aquifer tests, and numerical modeling in a riverside alluvial system in South Korea. Hydrogeology Journal, 16(6), 1129-1143.

Comunian, A., De Micheli, L., Lazzati, C., Felletti, F., Giacobbo, F., Giudici, M., Bersezio, R., 2016. Hierarchical simulation of aquifer heterogeneity: implications of different simulation settings on solute-transport modeling. Hydrogeology Journal, 24(2), 319-334.

Datry, T., Lamouroux, N., Thivin, G., Descloux, S., Baudoin, J. M., 2015. Estimation of sediment hydraulic conductivity in river reaches and its potential use to evaluate streambed clogging. River Research and Applications, 31(7), 880-891.

Deutsch, C. V., Journel, A. G., 1998. Geostatistical software library and user's guide. New York: Oxford University Press.

Dudley-Southern, M., Binley, A., 2015. Temporal responses of groundwater-surface water exchange to successive storm events. Water Resources Research, 51(2), 1112-1126.

Emmett, W. W., Leopold, L. B., 1963. Downstream pattern of riverbed scour and fill (pp. 399-409). In Proceedings of the Federal Interagency Sedimentation Conference.

Engelhardt, I., Piepenbrink, M., Trauth, N., Stadler, S., Kludt, C., Schulz, M., Schüth, C., Ternes, T. A., 2011. Comparison of tracer methods to quantify hydrodynamic exchange within the hyporheic zone. Journal of Hydrology, 400(1), 255-266.

Engelhardt, I., Prommer, H., Moore, C., Schulz, M., Schüth, C., Ternes, T. A., 2013a. Suitability of temperature, hydraulic heads, and acesulfame to quantify wastewater-related fluxes in the hyporheic and riparian zone. Water Resources Research, 49(1), 426-440.

Engelhardt, I., Prommer, H., Schulz, M., Vanderborght, J., Schüth, C., Ternes, T. A., 2013b. Reactive transport of iomeprol during stream-groundwater interactions. Environmental Science & Technology, 48(1), 199-207.

Fleckenstein, J. H., Niswonger, R. G., Fogg, G. E., 2006. River-aquifer interactions, geologic heterogeneity, and low-flow management. Groundwater, 44(6), 837-852.

Fox, A., Boano, F., Arnon, S., 2014. Water Resources Research, 50(3), 1895-1907.

Frei, S., Fleckenstein, J. H., Kollet, S. J., Maxwell, R. M., 2009. Patterns and dynamics of river–aquifer exchange with variably-saturated flow using a fully-coupled model. Journal of Hydrology, 375(3), 383-393.

Geist, J., Auerswald, K., 2007. Physicochemical stream bed characteristics and recruitment of the freshwater pearl mussel (Margaritifera margaritifera). Freshwater Biology, 52(12), 2299-2316.

Genereux, D. P., Leahy, S., Mitasova, H., Kennedy, C. D., Corbett, D. R., 2008. Spatial and temporal variability of streambed hydraulic conductivity in West Bear Creek, North Carolina, USA. Journal of Hydrology, 358(3), 332-353.

Gianni, G., Richon, J., Perrochet, P., Vogel, A., Brunner, P., 2016. Rapid identification of transience in streambed conductance by inversion of a floodwave response. Water Resources Research, 52, 2647–2658.

Goode, D. J., 1996. Direct simulation of groundwater age. Water Resources Research, 32(2), 289-296.

Guardiano, F. B., Srivastava, R. M., 1993. Multivariate Geostatistics: Beyond Bivariate Moments. In: Soares A. (eds) Geostatistics Tróia '92. Quantitative Geology and Geostatistics, vol 5. Dordrecht: Springer.

Hall, F. R., Moench, A. F., 1972. Application of the convolution equation to stream-aquifer relationships. Water Resources Research, 8(2), 487-493.

Haimberger, R., Hoppe, A., Schäfer, A., 2005. High-resolution seismic survey on the Rhine River in the northern Upper Rhine Graben. International Journal of Earth Sciences, 94(4), 657-668.

Hammond, G. E., Lichtner, P. C., 2010. Field-scale model for the natural attenuation of uranium at the Hanford 300 Area using high-performance computing, Water Resources Research, 46(9).

Hammond, G. E., Lichtner, P. C., Mills, R. T., 2014. Evaluating the performance of parallel subsurface simulators: An illustrative example with PFLOTRAN. Water Resources Research, 50(1), 208-228.

Hantush, M. S., 1965. Wells near streams with semipervious beds. Journal of Geophysical Research, 70(12), 2829-2838.

Hatch, C. E., Fisher, A. T., Ruehl, C. R., Stemler, G., 2010. Spatial and temporal variations in streambed hydraulic conductivity quantified with time-series thermal methods. Journal of Hydrology, 389(3), 276-288.

Hazen, A., 1911. Discussion: Dams on sand foundations. Transactions, American Society of Civil Engineers, 73, 199.

Huysmans, M., Dassargues, A., 2009. Application of multiple-point geostatistics on modelling groundwater flow and transport in a cross-bedded aquifer (Belgium). Hydrogeology Journal, 17(8), 1901.

Irvine, D. J., Brunner, P., Franssen, H. J. H., Simmons, C. T., 2012. Heterogeneous or homogeneous? Implications of simplifying heterogeneous streambeds in models of losing streams. Journal of Hydrology, 424, 16-23.

Juckem, P. F., Fienen, M. N., Hunt, R. J., 2014. Simulation of groundwater flow and interaction of groundwater and surface water on the Lac du Flambeau Reservation, Wisconsin (No. 2014-5020). Reston, VA, USA: US Geological Survey.

Kalbus, E., Reinstorf, F., Schirmer, M., 2006. Measuring methods for groundwater-surface water interactions: a review. Hydrology and Earth System Sciences Discussions, 10(6), 873-887.

Kazemi, G.A., Lehr, J.H., Perrochet, P., 2006. Groundwater Age. New Jersey: John Wiley & Sons.

Kurtz, W., Hendricks Franssen, H. J., Vereecken, H., 2012. Identification of time-variant river bed properties with the ensemble Kalman filter. Water Resources Research, 48(10).

Lasagna, M., De Luca, D. A., Franchino, E., 2016. Nitrate contamination of groundwater in the western Po Plain (Italy): the effects of groundwater and surface water interactions. Environmental Earth Sciences, 75(3), 1.

Lemieux, J. M., Sudicky, E. A., 2010. Simulation of groundwater age evolution during the Wisconsinian glaciation over the Canadian landscape. Environmental Fluid Mechanics, 10(1-2), 91-102.

Malone, B. P., Jha, S. K., Minasny, B., McBratney, A. B., 2016. Comparing regression-based digital soil mapping and multiple-point geostatistics for the spatial extrapolation of soil data. Geoderma, 262, 243-253.

Mariethoz, G., Caers, J., 2014. Multiple-point geostatistics: stochastic modeling with training images. Hoboken, New Jersey, USA: John Wiley & Sons.

Michael, H. A., Li, H., Boucher, A., Sun, T., Caers, J., Gorelick, S. M., 2010. Combining geologic-process models and geostatistics for conditional simulation of 3-D subsurface heterogeneity. Water Resources Research, 46(5).

Milliken, W. J., Levy, M., Strebelle, S. B., Zhang, Y., 2008. The Effect of Geologic Parameters and Uncertainties on Subsurface Flow: Deepwater Depositional Systems. Society of Petroleum Engineers, SPE Paper 114099, 1–16.

Min, L., Yu, J., Liu, C., Zhu, J., Wang, P., 2013. The spatial variability of streambed vertical hydraulic conductivity in an intermittent river, northwestern China. Environmental Earth Sciences, 69(3), 873-883.

Mualem, Y., 1976. A new model for predicting the hydraulic conductivity of unsaturated porous media. Water Resources Research, 12(3), 513-522.

Newcomer, M. E., Hubbard, S. S., Fleckenstein, J. H., Maier, U., Schmidt, C., Thullner, M., Ulrich, C., Flipo, N., Rubin, Y., 2016. Simulating bioclogging effects on dynamic riverbed permeability and infiltration, Water Resources Research, 52(4), 2883-2900.

Pholkern, K., Srisuk, K., Grischek, T., Soares, M., Schäfer, S., Archwichai, L., Saraphirom, P., Pavelic, P., Wirojanagud, W., 2015. Riverbed clogging experiments at potential river bank filtration sites along the Ping River, Chiang Mai, Thailand. Environmental Earth Sciences, 73(12), 7699-7709.

Pozdniakov, S. P., Wang, P., Lekhov, M. V., 2016. A semi-analytical generalized Hvorslev formula for estimating riverbed hydraulic conductivity with an open-ended standpipe permeameter. Journal of Hydrology, 540, 736-743.

Pyrcz, M. J., Deutsch, C. V., 2014. Geostatistical reservoir modeling. New York: Oxford university press.

Remy, N., Boucher, A., Wu, J., 2009. Applied geostatistics with SGeMS: a user's guide. New York: Cambridge University Press.

Simpson, S. C., Meixner, T., 2012. Modeling effects of floods on streambed hydraulic conductivity and groundwater-surface water interactions. Water Resources Research, 48(2).

Sophocleous, M., 2002. Interactions between groundwater and surface water: the state of the science, Hydrogeology Journal, 10(1), 52–67.

Strebelle, S., 2000. Sequential Simulation Drawing Structures from Training Images. PhD thesis, Stanford University, Stanford, CA.

Suckow, A., 2014. The age of groundwater–definitions, models and why we do not need this term. Applied Geochemistry, 50, 222-230.

Sun, X., Bernard-Jannin, L., Garneau, C., Volk, M., Arnold, J. G., Srinivasan, R., Sauvage, S., Sánchez-Pérez, J. M., 2016. Improved simulation of river water and groundwater

exchange in an alluvial plain using the SWAT model. Hydrological Processes, 30(2), 187-202.

Taylor, A. R., Lamontagne, S., Crosbie, R. S., 2013. Measurements of riverbed hydraulic conductivity in a semi-arid lowland river system (Murray–Darling Basin, Australia). Soil Research, 51(5), 363-371.

Tian, Y., Zheng, Y., Wu, B., Wu, X., Liu, J., Zheng, C., 2015. Modeling surface water-groundwater interaction in arid and semi-arid regions with intensive agriculture. Environmental Modelling & Software, 63, 170-184.

Van Genuchten, M. T., 1980. A closed-form equation for predicting the hydraulic conductivity of unsaturated soils. Soil Science Society of America Journal, 44(5), 892-898.

Wang, L., Song, J., Zhang, B., Guo, H., Jiang, W., Wen, M., Zhang, G., 2016. Spatial and temporal variations of streambed vertical hydraulic conductivity in the Weihe River, China. Water, 8(3), 70.

Whitaker, S., 1986. Flow in porous media I: A theoretical derivation of Darcy's law. Transport in Porous Media, 1(1), 3-25.

Winter, T. C., Harvey, J. W., Franke, O. L., Alley, W. M., 1998. Ground water and surface water – a single resource. US Geological Survey Circular 1139.

Wu, G., Shu, L., Lu, C., Chen, X., Zhang, X., Appiah-Adjei, E. K., Zhu, J., 2015. Variations of streambed vertical hydraulic conductivity before and after a flood season. Hydrogeology Journal, 23(7), 1603-1615.

Xie, Y., Cook, P. G., Simmons, C. T., 2016. Solute transport processes in flow-event-driven stream–aquifer interaction. Journal of Hydrology, 538, 363-373.

Yu, C., Yao, Y., Cao, G., Zheng, C., 2015. A field demonstration of groundwater vulnerability assessment using transport modeling and groundwater age modeling, Beijing Plain, China. Environmental Earth Sciences, 73(9), 5245-5253.

Zappa, G., Bersezio, R., Felletti, F., Giudici, M., 2006. Modeling heterogeneity of gravel-sand, braided stream, alluvial aquifers at the facies scale. Journal of Hydrology, 325(1), 134-153.

Zhang, M., Zhang, Y., Lichtner, P., 2017. Evaluating model complexity in simulating supercritical CO2 dissolution, leakage, footprint, and reservoir pressure for three-dimensional hierarchical aquifer. International Journal of Greenhouse Gas Control, 64, 284-299.

Zhang, Y., Hubbard, S., Finsterle, S., 2011. Factors governing sustainable groundwater pumping near a river. Groundwater, 49(3), 432-444.

Zhou, H., Gómez-Hernández, J. J., Li, L., 2012. A pattern-search-based inverse method. Water Resources Research, 48(3).

Zovi, F., Camporese, M., Franssen, H. J. H., Huisman, J. A., Salandin, P., 2017. Identification of high-permeability subsurface structures with multiple point geostatistics and normal score ensemble Kalman filter. Journal of Hydrology, 548, 208-224.

5 Synthesis and Outlook

5.1 Summary of results **90**
5.2 Limitations **94**
5.3 Outlook **95**

5.1 Summary of results

5.1.1 Experimental and numerical investigations of silver nanoparticle transport under variable flow and ionic strength in soil

Under continuous flow condition, the transport of AgNP was retarded through the unsaturated soil columns compared to tracer. A high AgNP mobility was observed at the initial first pore volume followed by a quickly decreased mobility. This can be explained by the size or charge exclusion and the time-dependent filling of retention sites, which increasingly retarded AgNP transport with time. The presence of Ca^{2+} in the effluent that was released from soil might also contribute to AgNP retention by promoting the bridging complexation between soil grains and the functionalized nanoparticles. The numerical results reveals that the key process that affects AgNP transport under unsaturated and continuous flow conditions is the kinetic attachment both at the soil-water-interface (SWI) and air-water-interface (AWI). It also indicates that SWI has limited influence for colloid retention even under favorable chemical conditions because of its limited retention sites. Although the attachment coefficient at AWI was much smaller than that at SWI, the irreversible attachment at AWI made a comparable contribution to AgNP retention compared to the reversible attachment at SWI. Thus, the attachment at both SWI and AWI play a dominant role in AgNP transport.

Under flow interruption condition, the flow interruption leads to a dramatically reduced AgNP transport and a strong AgNP retention in the soil. Water loss and increased electrical conductivity were observed due to the evaporation during flow interruption. These physicochemical changes could lead to transformation processes such as homo- and heteroaggregation and thus may influence the transport and retention of AgNP. The effluent AgNP concentration after flow interruption dramatically decreased compared to continuous flow condition. The numerical analysis indicates that during flow interruption the attachment at SWI decreased with the increase of the attachment at AWI. Zones at AWI with low or stagnant flow velocity derived by water loss, grain−grain contacts or developed at the solid−water−air interface might provide a perfect sticking location for AgNP. Thus, the attachment to the AWI occurring during flow interruption is the key process for AgNP retention. After flow restarted, only very few AgNP were released due to the irreversible attachment at AWI and the reversible attachment at SWI but with less detachment.

The reduction of ionic strength (IS) was observed to promote AgNP transport. The effluent soil colloids may act as mobile carriers for AgNP facilitated transport when IS reduced. The DLVO calculation indicates that the reduction of IS increased the maximum energy barrier and secondary minimum depth between AgNP and soil surface, which decreased the deposition probability of AgNP on soil surface at SWI. However, the irreversible attachment at AWI counteracted the release of AgNP at SWI which had small AgNP detachment rate. Thus, only a few of AgNP was remobilized.

The numerical model with CFT-DLVO-CRM theory reproduced well of the measured AgNP BTCs under either constant or transient hydrological and hydrogeochemical conditions. Flow interruption in an unsaturated system increases AgNP retention with a decreased flow rate and water content loss. The decrease of IS can promote AgNP transport by increasing the electrical double layer of AgNP, soil colloids, and soil grains. The release of AgNP into aqueous phase by decreased IS can pose significant threat to groundwater contamination. The transient hydrology and hydrochemistry prevail in the subsurface due to the transient hydraulic gradient by precipitation, evaporation, or river infiltration, which influence AgNP mobility all the time. Thus, a comprehensive consideration of these transient conditions is necessary to evaluate and predict the groundwater contamination by AgNP.

5.1.2 Impact of manure-related DOM on sulfonamide transport in arable soils

The manure composition was first analyzed. Dry matter contents measured in different pig manure samples show large variation, which are attributed to the various feeding and housing conditions for different pig life stages and the different manure storage strategies. The measured C/N ratios of the filtered manure DOM fraction was found to be lower than that of the reported unprocessed manure due to the preconditioning of manure samples by filtration before chemical analysis eliminating organics with high molecular weight. The low C/N ratios also indicate that the dominant composition was N-containing compound which was urine by reference to the literature. A highest amount of dissolved nitrogen (DN) and the lowest C/N ratio were found in DOM from fattening pigs (DOM_F), which displays higher urine content than that from weaners (DOM_W) and sows and farrows (DOM_SF). The highest content of $SUVA_{280nm}$ and protein C were also found for DOM_F, suggesting that DOM_F contained more aromatic compounds than DOM_SF and DOM_W.

Travel time analysis reveals the different transport patterns of manure-derived colloids in soil. The mean travel time increased from DOM_W to DOM _SF to DOM _F. A non-equilibrium adsorption pattern of the colloids for soil is suggested by their increased breakthrough curves (BTCs) tailing compared to that of tracer bromide. The highest retardation was found for DOM_F, which is consistent with its high $SUVA_{280nm}$ and indicates a high adsorption of DOM_F on soil grain surfaces. The colloid transport model results show that the highest retardation of DOM_F was attributed to its small detachment rate and high decay rate. The straining effect that is proposed by colloid filtration theory was not significant for all the DOM type due to the straining rate was rather small compared to the colloid attachment, detachment, and decay rates. Sensitivity analysis indicates that sorption sites on soil surface and colloid decay rate are the dominant parameters and processes of the colloid filtration theory to describe the migration of DOM in porous media.

Each of the three sulfonamides (SDZ, SMPD, and SMOX) shows different transport patterns in soil. Travel time analysis and recovery rates reveal their different sorption affinities for soil surface as SMOX > SMPD > SDZ. The antibiotic transport model shows an

extremely high distribution coefficient of SMOX between soil solution and soil surface than that of SDZ and SMPD, indicating a high affinity of SMOX to soil. The different molecular structure of R-substituent which can influence their hydrophobicity and polarity might be responsible for their different affinities with soil. The highest retardation was observed for SMOX due to its unique 5-membered-ring asymmetric R-substituent that can form stable hydrogen-bonds with the soil. On the contrary, SDZ and SMPD were less retarded by their 6-membered-ring symmetric R-substituent resulting in a more hydrophilic character than SMOX. By considering the negatively charged soil surface and the antibiotic pKa values, electrostatic force becomes another driving force that can accelerate the transport of antibiotic through the soil as SDZ > SMPD > SMOX. However, compared with the affinity with soil surface, the electrostatic force played a minor role for SMOX.

Distinctive sulfonamides transport patterns were observed in the presence of manure colloid. Experimental results show that none of the investigated manure derived colloid types was able to enhance the transport of SDZ and SMPD, but rather reduce their transport. The colloid-facilitated antibiotic transport model reveals that the immobile colloids absorbed on the soil surface provided additional sorption sites for SDZ and SMPD. Meanwhile, SDZ and SMPD have higher affinities to sorb onto immobile colloids and soils than to mobile colloids. These two processes promoted the reduced transport of SDZ and SMPD by manure colloids. On the contrary, the transport of SMOX was enhanced in the presence of DOM_F, while DOM_SF and DOM_W had little effect on SMOX transport. The model results suggest that the large amount of immobile DOM_F competing with SMOX for the soil sorption sites and the adsorption of SMOX to mobile DOM_F were the main two reasons for the facilitated transport. The composition of DOM_F, low C/N ratio, high SUVA280 nm, and protein C, indicates a high proportion of proteins with aromatic amino acid tyrosine or tryptophan, which can increase the DOM_F hydrophobicity. These hydrophobic proteins are the key component driving the facilitated transport of SMOX. In contrast, DOM_SF and DOM_W with low content of hydrophobic proteins had little impact on SMOX. Moreover, with the presence of hydrophobic proteins in DOM_F only reduced transport of SDZ and SMPD were observed, which were fully attributed to the different spatial structure of R-substituents compared with SMOX.

Thus, manure composition indeed influences the mobility of sulfonamides but depends on the manure composition and the antibiotic type. Manures with high contents of hydrophobic compounds, such as tyrosine or tryptophan, are likely to facilitate the transport of hydrophobic sulfonamide such as SMOX. Weakly hydrophobic sulfonamides, such as SDZ and SMPD, have less affinity for soil, thus the role of their potential facilitated transport is minor even some colloids act as carriers. This study suggests that adjusting pig feeding program to reduce the intake amount of tyrosine and tryptophan would be helpful to reduce the leaching risk of hydrophobic sulfonamide, such as SMOX, into groundwater. For SDZ and SMPD, no additional concern is needed since the presence of manure colloid can reduce their transport in soils.

5.1.3 Numerical modeling of stream-aquifer interaction: quantifying the impact of transient streambed permeability and aquifer heterogeneity

The permeability of the soil samples shows a large variation. The corresponding permeability histogram exhibit a bimodal permeability distribution, which indicates two facies populations, silt-rich facies and sand-rich facies, and shows the primary control of facies on permeability distribution. The permeability variogram analysis shows that the horizontal/vertical anisotropy ratio is 5:1 both for silt and sand facies. The constructed training image well reflects the sedimentary deposits based on information from sediment samples and the geological conceptual model. The 300 single normal equation simulation (SNESIM) realizations using the training image as the prior geological knowledge preserve the heterogeneous spatial structure and are consistent with the geological conceptual model. The subsequential 300 permeability realizations implemented by sequential Gaussian simulation (SGS) exhibit a high degree of heterogeneity.

The streambed permeability calculated by the inversion of flood wave responses show a temporally transient pattern which increased during infiltration periods while decreased during exfiltration periods. The increase of streambed permeability is probably due to the remobilization of the streambed particles during flood events, and the decrease of streambed permeability may be due to the precipitation of transported particle and streambed bioclogging during the dry period. The estimation of streambed permeability highly depends on the selection of the POW size, shift, and aquifer diffusivity. A large POW size is able to capture the variation trend of stream stage but is less able to present the transient pattern of head fluctuation. The optimal set of streambed permeability that can reproduce the historical stream stage records was the combination of POW with 1 day size and 0.2 day shift and 10 m^2/s aquifer diffusivity.

The surface water-groundwater flow model well reproduced the varying pressure heads measured at two observation wells near the stream by incorporating the temporally variable streambed permeability and the spatially heterogeneous aquifer permeability. The mean absolute error (MAE) of each realization shows that 33 of 300 realizations were acceptable compared to the observation data, while none of those 300 realizations yielded an acceptable model if removing streambed data since all of the MAEs were out of the cut-off value. This reveals the fundamental role of streambed in stream-aquifer interaction. The high model uncertainty during the infiltration periods are attributed to the aquifer permeability fields that vary between each stochastic simulation, while uncertainty decreased during the exfiltration periods due to the decreased streambed permeability. The simulated exchange flux at the stream-aquifer interface shows that high exchange flux was observed during infiltration period when streambed permeability increased, while limited exchange flux occurred during exfiltration period when streambed permeability decreased. The numerical modeling of exchange flux demonstrate that the exchange flux of the stream-groundwater interaction during infiltration periods was mainly reduced by the aquifer, while the streambed shows

dominant limitation on the exchange flux during exfiltration periods with its reduced permeability.

The estimated 33 surface water infiltration paths implemented by the groundwater age simulation in the sense of Monte Carlo show a high degree of variation. Longer preferential flow paths were observed in the model domain down hydraulic gradient, due to the permeability anisotropy. The probabilistic infiltration map demonstrates that the stream water infiltrated into the aquifer with a depth of 1.6 m (100% probability) to 4.6 m (10% probability) below the stream and 8.4 m (100% probability) to 24.2 m (10% probability) long toward NW direction. The large variation of probability indicates that the aquifer heterogeneity of permeability imposes a significant control on the groundwater flow. The proposed probabilistic infiltration paths provide decision makers a valuable reference to optimize the monitoring campaign.

5.1.4 Synthesis

The key processes that influence the transport of urban-related contaminant (AgNP) and agricultural related contaminants (SDZ, SMPD, and SMOX) in natural soils, and the factors that control the stream-aquifer interaction were identified in this thesis. Flow interruption and increase of IS can decrease AgNP mobility in unsaturated condition. The presence of manure colloid can reduce the transport of SDZ and SMPD by providing additional sorption sites, but increase SMOX mobility by the co-transport process especially in the presence of tyrosine and tryptophan-like organic compounds. Exchange flux during stream-aquifer interaction was mainly reduced by the aquifer during infiltration periods, and reduced by the streambed during exfiltration period. The results of this thesis show that the pathway of contaminants from city and agriculture to subsurface water cycle highlights the significant impacts of hydrological and geochemical conditions on contaminant transport. The heterogeneous geological features, insufficient site characterization, and variable hydrological and hydrochemical patterns promote the decisions to be made on groundwater exploitation and remediation under the consideration of uncertainty. The investigated contaminant pathways from this thesis provide researchers, practitioners, and decision makers a valuable reference for groundwater resource management.

5.2 Limitations

Chapter 2 Experimental and numerical investigations of silver nanoparticle transport under variable flow and ionic strength in soil

(a) Three column experiment scenarios only have one replicate for each. The insufficient column replicates may introduce large bias and uncertainty in statistics.

(b) Due to the lack of experimental retention profiles of AgNP, the model simulated retention profile is not able to be verified.

(c) The numerical model is based on CFT-DLVO-CRM theory, the parameter in CRM, f which refers to the fraction of retained colloids that is not released by the flow rate or chemical alteration, can only be obtained by the inverse of the numerical model under a given experimental condition (e.g. flow rate and ionic strength). Thus, it limits the forecast simulation for a different experimental condition.

Chapter 3 Impact of manure-related DOM on sulfonamide transport in arable soils

(a) Colloid solutions with different concentrations were applied due to the extremely heterogeneous distribution of DOM in solution made it impossible to acquire a desired DOC-concentration by dilution. Thus, the influence of colloid concentration on sulfonamide transport is assumed to be minor in advance.

(b) Due to the lack of comprehensive chemical measurement for manure composition, it is still uncertain which specific components constitute the DOM hydrophobicity that facilitates the transport of SMOX and their specific concentrations.

(c) The influence of different manure pH was ignored since the limited injection of colloids into the soil. However, when large amount of manure colloids discharge into the subsurface, the impact of pH on facilitated transport is unknown.

Chapter 4 Numerical modeling of stream-aquifer interaction: quantifying the impact of transient streambed permeability and aquifer heterogeneity

(a) The aquifer permeability was estimated by Hazen method from soil grain size analysis. The resultant lack of agreement between the experimental and modeled permeability variograms due to the limited well data and Hazen method will inevitably introduce uncertainty into the calculated permeability spatial correlation, and thus the simulated permeability fields.

(b) The estimation of streambed permeability was based on the assumption of a homogeneous streambed. However, in real situation, a heterogeneous pattern is more common. Thus, the influence of streambed preferential flow on stream-aquifer interaction was ignored.

5.3 Outlook

Chapter 2 Experimental and numerical investigations of silver nanoparticle transport under variable flow and ionic strength in soil

This chapter investigated the transport behaviors of AgNP under variable flow and ionic strength followed by the numerical model analysis for the implicit mechanisms. As highlighted in the limitation section, few column replicates in each scenario may introduce bias and uncertainty. A set of three column replicates for each scenario is recommended for

future research which, one the contrary, will tremendously increase the burden for chemical analysis and the soil packing in each column while guaranteeing the identical physical conditions, such as porosity, hydraulic conductivity, and bulk density. In order to verify the validation of model simulated retention profile, the experimental retention profile is also needed in future research. With regard to the model application limits, for example the estimation of fraction of retained colloids that is not released by the flow rate or chemical alteration, current colloid release theory is based on analytical analysis by lumping the impact of flow rate or chemical alteration into one parameter f which is only obtained by model inverse. A new theory is needed to describe colloid release in the numerical sense while separate the dynamic impact of varying flow rate or chemical alteration on colloid release.

To comprehensively understand the fate and transport of AgNP, the impact of other factors in the environment are nonnegligible. For example, the influence of different soil types with respect to the variation of soil composition on AgNP transport. It is unclear which soil composition is mainly responsible for AgNP retention. Moreover, the mobile colloid in the solution from soil or other sources such as bacteria, may form clusters with AgNP either facilitate the transport of AgNP by acting as carrier or retard the transport due to the size exclusion. The coating of AgNP by organic matter, chlorine, or sulphur species may insulate AgNP from soil surface and enhance their mobility and persistence in soil. Further, the aging, transformation, dissolution, and bioaccumulation in aquatic organisms are all potentially influence the transport of AgNP.

Chapter 3 Impact of manure-related DOM on sulfonamide transport in arable soils

This chapter investigated the influence of different manure colloids on three sulfonamides transport in soils. As highlighted in the limitation section, the different colloid concentrations applied for each scenario were due to the solution heterogeneity. The optimal approach currently is to agitate the solution sufficiently before dilution. However, a solute with concentration deviation is inevitable. The effective manure composition that can facilitate the transport of SMOX was speculated to be tyrosine or tryptophan, but a further exhausted measurement for the manure composition is lack to verify this speculation. Thus, with the results from this chapter, further research on manure colloid facilitated contaminant transport is recommended to analyze the manure composition by emphasizing on the hydrophobic proteins, such as tyrosine or tryptophan.

There are many other factors that may influence the colloid facilitated transport in nature environment and need to be taken into consideration. For example, the variation of pH in soil may pose significant impacts on colloid and colloid facilitated sulfonamide transport by changing their charged state. The variable saturation condition derived soil-water-interface and air-water-interface may influence the retention of colloid, sulfonamide, and colloid-sulfonamide cluster in soil. The varying ionic strength due to groundwater recharge or evaporation may have the potential to change the affinity of sulfonamide with colloid to form the cluster and sulfonamide and colloid with soil surface, thus influence the facilitated

transport. More factors, such as the aging and transformation of colloid and sulfonamide, preferential flow, and variable flow rate, may all retard or facilitate their transport.

Chapter 4 Numerical modeling of stream-aquifer interaction: quantifying the impact of transient streambed permeability and aquifer heterogeneity

This chapter discussed the influence of transient streambed permeability and aquifer heterogeneity on stream-aquifer interaction. The estimation of aquifer permeability using Hazen method would generate larger uncertainty compared to the direct measurement using permeameter, and thus the simulated multiple permeability fields and the simulated pressure heads. Therefore, the model uncertainty that originates from permeability estimation should be taken into account. Due to the simplification of a heterogeneous streambed pattern to a homogenous pattern, the influence of preferential flow on stream-aquifer interaction was ignored. However, the characterization of the heterogeneous streambed is a laborious work, because it needs multiple sampling wells and a continuous sediment grain size analysis, due to the alternative sedimentation and remobilization processes, to calculate the spatial correlation. The simplification of streambed into a homogenous pattern is acceptable as long as the streambed extent is thin enough compared to vertical extent of the aquifer.

Groundwater age simulation based on Monte Carlo provides a probabilistic manner to visualize the surface water infiltration path and a hypothetical wastewater plume. In this study, only advection was considered for the simulation. Dispersion and diffusion were ignored. Thus, the resultant groundwater age distribution was underestimated. To properly estimate the groundwater age, diffusion and spatial variation of dispersion in heterogeneous aquifer need to be considered prior to groundwater age modeling. Moreover, to reduce uncertainty in simulated groundwater age, temperature and conservative solute tracer transport experiments and models are recommended to conduct and compare the groundwater age distribution by different approaches, thus to refine the model and model parameterization.

Statement of contributions

Chapter 2: Experimental and numerical investigations of silver nanoparticle transport under variable flow and ionic strength in soil

Status: published in Environmental Science & Technology, 51(4), 2096-2104, 8 February 2017. This is the postprint version of the article in this dissertation.

J. Makselon and E. Klumpp designed lab column experiments. J. Makselon conducted the lab column experiments and analyzed the results. D. Zhou and I. Engelhardt designed the numerical modeling experiments. D. Zhou developed the numerical model followed by performing simulation and analyzing the model results. J. Makselon wrote the manuscript with text and figure contributions of numerical modeling from D. Zhou. D. Jacques provided the important basic model code. All authors made contributions to improve the manuscript.

Chapter 3: Impact of manure-related DOM on sulfonamide transport in arable soils

Status: published in Journal of Contaminant Hydrology, 192, 118-128, 16 July 2016. This is the postprint version of the article in this dissertation.

D. Zhou and I. Engelhardt designed the numerical modeling experiments. D. Zhou developed the numerical model, conducted the simulations, and analyzed the model results. S. Thiele-Bruhn and M. G. Arenz-Leufen designed the lab column experiments. M. G. Arenz-Leufen conducted lab column experiments and analyzed the results. D. Jacques provided the important basic model code. P. Lichtner provided important suggestions to improve the model. All authors made contributions to improve the manuscript.

Chapter 4: Numerical modeling of stream-aquifer interaction: quantifying the impact of transient streambed permeability and aquifer heterogeneity

Status: submitted to Hydrological Processes on 02 November 2017. This is the preprint version of the article in this dissertation.

D. Zhou and I. Engelhardt designed the numerical modeling experiments. D. Zhou is responsible for developing the numerical model, conducting the simulations, and analyzing the model results. G. Gianni calculated the datasets of transient streambed permeability. Y. Zhang and P. Lichtner supported the implementation of multiple-point geostatistics and PFLOTRAN. All authors made contributions to improve the manuscript.

Bibliography

Ala-aho, P., Rossi, P. M., Isokangas, E., Kløve, B., 2015. Fully integrated surface-subsurface flow modelling of groundwater–lake interaction in an esker aquifer: Model verification with stable isotopes and airborne thermal imaging. Journal of Hydrology, 522, 391-406.

Barceló, D., Petrovic, M., 2007. Pharmaceuticals and personal care products (PPCPs) in the environment. Analytical and Bioanalytical Chemistry, 387(4), 1141-1142.

Bayer, P., Huggenberger, P., Renard, P., Comunian, A., 2011. Three-dimensional high resolution fluvio-glacial aquifer analog: Part 1: Field study. Journal of Hydrology, 405(1), 1-9.

Benn, T., Benn, T., Cavanagh, B., Hristovski, K., Posner, J. D., Westerhoff, P., 2010. The release of Nanosilver from Consumer Products Used in the Home. Journal of Environmental Quality, 39(6), 1875-1882.

Benn, T. M., Westerhoff, P., 2008. Nanoparticle silver released into water from commercially available sock fabrics. Environmental Science & Technology, 42(11), 4133-4139.

Berg, J. C., 2010. An introduction to interfaces & colloids: the bridge to nanoscience. World Scientific.

Bertrand, G., Siergieiev, D., Ala-Aho, P., Rossi, P. M., 2014. Environmental tracers and indicators bringing together groundwater, surface water and groundwater-dependent ecosystems: importance of scale in choosing relevant tools. Environmental Earth Sciences, 72(3), 813-827.

Blackwell, P. A., Kay, P., Boxall, A. B., 2007. The dissipation and transport of veterinary antibiotics in a sandy loam soil. Chemosphere, 67(2), 292-299.

Boulton, A. J., Datry, T., Kasahara, T., Mutz, M., Stanford, J. A., 2010. Ecology and management of the hyporheic zone: stream–groundwater interactions of running waters and their floodplains. Journal of the North American Benthological Society, 29(1), 26-40.

Bound, J. P., Voulvoulis, N., 2004. Pharmaceuticals in the aquatic environment—a comparison of risk assessment strategies. Chemosphere, 56(11), 1143-1155.

Bradford, S. A., Torkzaban, S., Kim, H., Simunek, J., 2012. Modeling colloid and microorganism transport and release with transients in solution ionic strength. Water Resources Research, 48(9).

Brayner, R., Dahoumane, S. A., Yéprémian, C., Djediat, C., Meyer, M., Couté, A., Fiévet, F., 2010. ZnO nanoparticles: synthesis, characterization, and ecotoxicological studies. Langmuir, 26(9), 6522-6528.

Brunner, P., Therrien, R., Renard, P., Simmons, C. T., Hendricks Franssen, H. J., 2017. Advances in understanding river-groundwater interactions. Reviews of Geophysics, 55.

Burkhardt, M., Stamm, C., 2007. Depth distribution of sulfonamide antibiotics in pore water of an undisturbed loamy grassland soil. Journal of Environmental Quality, 36(2), 588-596.

Burkhardt, M., Stamm, C., Waul, C., Singer, H., Müller, S., 2005. Surface runoff and transport of sulfonamide antibiotics and tracers on manured grassland. Journal of Environmental Quality, 34(4), 1363-1371.

Burkholder, J., Libra, B., Weyer, P., Heathcote, S., Kolpin, D., Thorne, P. S., Wichman, M., 2007. Impacts of waste from concentrated animal feeding operations on water quality. Environmental Health Perspectives, 115(2), 308.

Castellano, J. J., Shafii, S. M., Ko, F., Donate, G., Wright, T. E., Mannari, R. J., Payne, W. G., Smith, D. J., Robson, M. C., 2007. Comparative evaluation of silver-containing antimicrobial dressings and drugs. International Wound Journal, 4(2), 114-122.

Chen, G., Flury, M., Harsh, J. B., Lichtner, P. C., 2005. Colloid-facilitated transport of cesium in variably saturated Hanford sediments. Environmental Science & Technology, 39(10), 3435-3442.

Cohen, S. Z., Creeger, S. M., Carsel, R. F., Enfield, C. G., 1984. Potential pesticide contamination of groundwater from agricultural uses. Treatment and Disposal of Pesticide Wastes, pp297-325.

Colman, B. P., Espinasse, B., Richardson, C. J., Matson, C. W., Lowry, G. V., Hunt, D. E., Wiesner, M. R., Bernhardt, E. S., 2014. Emerging contaminant or an old toxin in disguise? Silver nanoparticle impacts on ecosystems. Environmental Science & Technology, 48(9), 5229-5236.

Comunian, A., De Micheli, L., Lazzati, C., Felletti, F., Giacobbo, F., Giudici, M., Bersezio, R., 2016. Hierarchical simulation of aquifer heterogeneity: implications of different simulation settings on solute-transport modeling. Hydrogeology Journal, 24(2), 319-334.

de Jonge, H., Jacobsen, O. H., de Jonge, L. W., Moldrup, P., 1998. Particle-facilitated transport of prochloraz in undisturbed sandy loam soil columns. Journal of Environmental Quality, 27(6), 1495-1503.

de Jonge, L. W., Moldrup, P., Rubæk, G. H., Schelde, K., Djurhuus, J., 2004. Particle leaching and particle-facilitated transport of phosphorus at field scale. Vadose Zone Journal, 3(2), 462-470.

Derjaguin, B. V., Landau, L., 1993. Theory of the stability of strongly charged lyophobic sols and of the adhesion of strongly charged particles in solutions of electrolytes. Progress in Surface Science, 43(1-4), 30-59.

Daniluk, T. L., Lautz, L. K., Gordon, R. P., Endreny, T. A., 2013. Surface water–groundwater interaction at restored streams and associated reference reaches. Hydrological Processes, 27(25), 3730-3746.

El Badawy, A. M., Aly Hassan, A., Scheckel, K. G., Suidan, M. T., Tolaymat, T. M., 2013. Key factors controlling the transport of silver nanoparticles in porous media. Environmental Science & Technology, 47(9), 4039-4045.

Elimelech, M., O'Melia, C. R., 1990. Kinetics of deposition of colloidal particles in porous media. Environmental Science & Technology, 24(10), 1528-1536.

Emery, X., Parra, J., 2013. Integration of crosswell seismic data for simulating porosity in a heterogeneous carbonate aquifer. Journal of Applied Geophysics, 98, 254-264.

Engelhardt, I., Prommer, H., Schulz, M., Vanderborght, J., Schüth, C., Ternes, T. A., 2013. Reactive transport of iomeprol during stream-groundwater interactions. Environmental Science & Technology, 48(1), 199-207.

Esplugas, S., Bila, D. M., Krause, L. G. T., Dezotti, M., 2007. Ozonation and advanced oxidation technologies to remove endocrine disrupting chemicals (EDCs) and pharmaceuticals and personal care products (PPCPs) in water effluents. Journal of Hazardous Materials, 149(3), 631-642.

Evans, E., Wilcox, A. C., 2014. Fine sediment infiltration dynamics in a gravel-bed river following a sediment pulse. River Research and Applications, 30(3), 372-384.

Fitch, P. J., Lovell, M. A., Davies, S. J., Pritchard, T., Harvey, P. K., 2015. An integrated and quantitative approach to petrophysical heterogeneity. Marine and Petroleum Geology, 63, 82-96.

Fleckenstein, J. H., Niswonger, R. G., Fogg, G. E., 2006. River-aquifer interactions, geologic heterogeneity, and low-flow management. Groundwater, 44(6), 837-852.

Frei, S., Fleckenstein, J. H., Kollet, S. J., Maxwell, R. M., 2009. Patterns and dynamics of river-aquifer exchange with variably-saturated flow using a fully-coupled model. Journal of Hydrology, 375(3), 383-393.

Flury, M., Qiu, H., 2008. Modeling colloid-facilitated contaminant transport in the vadose zone. Vadose Zone Journal, 7(2), 682-697.

Gargiulo, G., Bradford, S. A., Simunek, J., Ustohal, P., Vereecken, H., Klumpp, E., 2008. Bacteria transport and deposition under unsaturated flow conditions: The role of water content and bacteria surface hydrophobicity. Vadose Zone Journal, 7(2), 406-419.

Gianni, G., Richon, J., Perrochet, P., Vogel, A., Brunner, P., 2016. Rapid identification of transience in streambed conductance by inversion of floodwave responses. Water Resources Research, 52(4), 2647-2658.

Grabowski, R. C., Surian, N., Gurnell, A. M., 2014. Characterizing geomorphological change to support sustainable river restoration and management. Wiley Interdisciplinary Reviews: Water, 1(5), 483-512.

Gregory, J., 1981. Approximate expressions for retarded van der Waals interaction. Journal of Colloid and Interface Science, 83(1), 138-145.

Gu, C., Hornberger, G. M., Mills, A. L., Herman, J. S., Flewelling, S. A., 2007. Nitrate reduction in streambed sediments: Effects of flow and biogeochemical kinetics. Water Resources Research, 43(12).

Guardiano, F. B., Srivastava, R. M., 1993. Multivariate Geostatistics: Beyond Bivariate Moments. In: Soares A. (eds) Geostatistics Tróia '92. Quantitative Geology and Geostatistics, vol 5. Springer, Dordrecht.

Halbus, A. F., Horozov, T. S., Paunov, V. N., 2017. Colloid particle formulations for antimicrobial applications. Advances in Colloid and Interface Science.

He, X. L., Sonnenborg, T. O., Jørgensen, F., Jensen, K. H., 2014. The effect of training image and secondary data integration with multiple-point geostatistics in groundwater modelling. Hydrology and Earth System Sciences, 18(8), 2943-2954.

Heberer, T., 2002. Occurrence, fate, and removal of pharmaceutical residues in the aquatic environment: a review of recent research data. Toxicology Letters, 131(1), 5-17.

Hogg, R., Healy, T. W., Fuersten, D. W., 1966. Mutual coagulation of colloidal dispersions. Transactions of the Faraday Society, 62, 1638-1651.

Honeyman, B. D., 1999. Geochemistry: Colloidal culprits in contamination. Nature, 397(6714), 23-24.

Hu, L. Y., Chugunova, T., 2008. Multiple-point geostatistics for modeling subsurface heterogeneity: A comprehensive review. Water Resources Research, 44(11).

Huysmans, M., Dassargues, A., 2009. Application of multiple-point geostatistics on modelling groundwater flow and transport in a cross-bedded aquifer (Belgium). Hydrogeology Journal, 17(8), 1901-1911.

Hydutsky, B. W., Mack, E. J., Beckerman, B. B., Skluzacek, J. M., Mallouk, T. E., 2007. Optimization of nano-and microiron transport through sand columns using polyelectrolyte mixtures. Environmental Science & Technology, 41(18), 6418-6424.

Jirgensons, B., Straumanis, M. E., 2013. A short textbook of colloid chemistry. Elsevier.

Kemper, N., 2008. Veterinary antibiotics in the aquatic and terrestrial environment. Ecological Indicators, 8(1), 1-13.

Kersting, A. B., Efurd, D. W., Finnegan, D. L., Rokop, D. J., 1999. Migration of plutonium in ground water at the Nevada Test Site. Nature, 397(6714), 56.

Knapp, C. W., Zhang, W., Sturm, B. S., Graham, D. W., 2010. Differential fate of erythromycin and beta-lactam resistance genes from swine lagoon waste under different aquatic conditions. Environmental Pollution, 158(5), 1506-1512.

Kretzschmar, R., Borkovec, M., Grolimund, D., Elimelech, M., 1999. Mobile subsurface colloids and their role in contaminant transport. Advances in Agronomy, 66, 121-193.

Kvesitadze, G., Khatisashvili, G., Sadunishvili, T., Ramsden, J. J., 2006. Contaminants in the environment. Biochemical Mechanisms of Detoxification in Higher Plants: Basis of Phytoremediation, 1-53.

Langhoff, J. H., Rasmussen, K. R., Christensen, S., 2006. Quantification and regionalization of groundwater–surface water interaction along an alluvial stream. Journal of Hydrology, 320(3), 342-358.

Lansdown, A. B., 2002. Silver. I: Its antibacterial properties and mechanism of action. Journal of Wound Care, 11(4), 125-130.

Lasagna, M., De Luca, D. A., Franchino, E., 2016. Nitrate contamination of groundwater in the western Po Plain (Italy): the effects of groundwater and surface water interactions. Environmental Earth Sciences, 75(3), 240.

Li, Z., Zhou, L., 2010. Cadmium transport mediated by soil colloid and dissolved organic matter: a field study. Journal of Environmental Sciences, 22(1), 106-115.

Liang, Y., Bradford, S. A., Simunek, J., Heggen, M., Vereecken, H., Klumpp, E., 2013a. Retention and remobilization of stabilized silver nanoparticles in an undisturbed loamy sand soil. Environmental Science & Technology, 47(21), 12229-12237.

Liang, Y., Bradford, S. A., Simunek, J., Vereecken, H., Klumpp, E., 2013b. Sensitivity of the transport and retention of stabilized silver nanoparticles to physicochemical factors. Water Research, 47(7), 2572-2582.

Liggett, J. E., Werner, A. D., Smerdon, B. D., Partington, D., Simmons, C. T., 2014. Fully integrated modeling of surface-subsurface solute transport and the effect of dispersion in tracer hydrograph separation. Water Resources Research, 50(10), 7750-7765.

Lin, S., Cheng, Y., Bobcombe, Y., L. Jones, K., Liu, J., Wiesner, M. R., 2011. Deposition of silver nanoparticles in geochemically heterogeneous porous media: predicting affinity from surface composition analysis. Environmental Science & Technology, 45(12), 5209-5215.

Lin, S., Cheng, Y., Liu, J., Wiesner, M. R., 2012. Polymeric coatings on silver nanoparticles hinder autoaggregation but enhance attachment to uncoated surfaces. Langmuir, 28(9), 4178-4186.

Lin, E., Page, D., Pavelic, P., 2008. A new method to evaluate polydisperse kaolinite clay particle removal in roughing filtration using colloid filtration theory. Water Research, 42(3), 669-676.

Liu, J., Aruguete, D. M., Murayama, M., Hochella Jr, M. F., 2009. Influence of size and aggregation on the reactivity of an environmentally and industrially relevant nanomaterial (PbS). Environmental Science & Technology, 43(21), 8178-8183.

McClellan, K., Halden, R. U., 2010. Pharmaceuticals and personal care products in archived US biosolids from the 2001 EPA national sewage sludge survey. Water Research, 44(2), 658-668.

Michael, H. A., Li, H., Boucher, A., Sun, T., Caers, J., Gorelick, S. M., 2010. Combining geologic-process models and geostatistics for conditional simulation of 3-D subsurface heterogeneity. Water Resources Research, 46(5).

Morales, V. L., Zhang, W., Gao, B., Lion, L. W., Bisogni, J. J., McDonough, B. A., Steenhuis, T. S., 2011. Impact of dissolved organic matter on colloid transport in the vadose zone: Deterministic approximation of transport deposition coefficients from polymeric coating characteristics. Water Research, 45(4), 1691-1701.

Morones, J. R., Elechiguerra, J. L., Camacho, A., Holt, K., Kouri, J. B., Ramírez, J. T., Yacaman, M. J., 2005. The bactericidal effect of silver nanoparticles. Nanotechnology, 16(10), 2346.

Mueller, M., Pander, J., Wild, R., Lueders, T., Geist, J., 2013. The effects of stream substratum texture on interstitial conditions and bacterial biofilms: methodological strategies. Limnologica-Ecology and Management of Inland Waters, 43(2), 106-113.

Mustafa, S., Bahar, A., Aziz, Z. A., Suratman, S., 2016. Modelling contaminant transport for pumping wells in riverbank filtration systems. Journal of Environmental Management, 165, 159-166.

Neumann, N. N., Curtis, P. J., 2016. River-groundwater interactions in salmon spawning habitat: riverbed flow dynamics and non-stationarity in an end member mixing model. Ecohydrology, 9(7), 1410-1423.

Newcomer, M. E., Hubbard, S. S., Fleckenstein, J. H., Maier, U., Schmidt, C., Thullner, M., Ulrich, C., Flipo, N., Rubin, Y., 2016. Simulating bioclogging effects on dynamic riverbed permeability and infiltration. Water Resources Research, 52(4), 2883-2900.

Pal, S., Tak, Y. K., Song, J. M., 2007. Does the antibacterial activity of silver nanoparticles depend on the shape of the nanoparticle? A study of the gram-negative bacterium Escherichia coli. Applied and Environmental Microbiology, 73(6), 1712-1720.

Paniconi, C., Putti, M., 2015. Physically based modeling in catchment hydrology at 50: Survey and outlook. Water Resources Research, 51(9), 7090-7129.

Partington, D., Therrien, R., Simmons, C. T., Brunner, P., 2017. Blueprint for a coupled model of sedimentology, hydrology, and hydrogeology in streambeds. Reviews of Geophysics.

Pozdniakov, S. P., Wang, P., Lekhov, M. V., 2016. A semi-analytical generalized Hvorslev formula for estimating riverbed hydraulic conductivity with an open-ended standpipe permeameter. Journal of Hydrology, 540, 736-743.

Pruden, A., Pei, R., Storteboom, H., Carlson, K. H., 2006. Antibiotic resistance genes as emerging contaminants: studies in northern Colorado. Environmental Science & Technology, 40(23), 7445-7450.

Pyrcz, M. J., Deutsch, C. V., 2014. Geostatistical reservoir modeling. Oxford university press.

Rai, M., Yadav, A., Gade, A., 2009. Silver nanoparticles as a new generation of antimicrobials. Biotechnology Advances, 27(1), 76-83.

Rajagopalan, R., Tien, C., 1976. Trajectory analysis of deep-bed filtration with the sphere-in-cell porous media model. AIChE Journal, 22(3), 523-533.

Rassam, D. W., Pagendam, D. E., Hunter, H. M., 2008. Conceptualisation and application of models for groundwater–surface water interactions and nitrate attenuation potential in riparian zones. Environmental Modelling & Software, 23(7), 859-875.

Rollet, A. J., Piégay, H., Dufour, S., Bornette, G., Persat, H., 2014. Assessment of consequences of sediment deficit on a gravel river bed downstream of dams in restoration perspectives: application of a multicriteria, hierarchical and spatially explicit diagnosis. River Research and Applications, 30(8), 939-953.

Rosenberry, D. O., Pitlick, J., 2009. Local-scale variability of seepage and hydraulic conductivity in a shallow gravel-bed river. Hydrological Processes, 23(23), 3306-3318.

Sagee, O., Dror, I., Berkowitz, B., 2012. Transport of silver nanoparticles (AgNPs) in soil. Chemosphere, 88(5), 670-675.

Schlüter, S., Vogel, H. J., 2011. On the reconstruction of structural and functional properties in random heterogeneous media. Advances in Water Resources, 34(2), 314-325.

Simpson, S. C., Meixner, T., 2012. Modeling effects of floods on streambed hydraulic conductivity and groundwater-surface water interactions. Water Resources Research, 48(2).

Šimůnek, J., He, C., Pang, L., Bradford, S. A., 2006. Colloid-facilitated solute transport in variably saturated porous media. Vadose Zone Journal, 5(3), 1035-1047.

Song, J. E., Phenrat, T., Marinakos, S., Xiao, Y., Liu, J., Wiesner, M. R., Tilton, R. D., Lowry, G. V., 2011. Hydrophobic interactions increase attachment of gum arabic-and PVP-coated Ag nanoparticles to hydrophobic surfaces. Environmental Science & Technology, 45(14), 5988-5995.

Sophocleous, M., 2002. Interactions between groundwater and surface water: the state of the science. Hydrogeology Journal, 10(1), 52-67.

Sprague, L.A., Herman, J.S., Hornberger, G.M., Mills, A.L., 2000. Atrazine adsorption and colloid-facilitated transport through the unsaturated zone. Journal of Environmental Quality, 29 (5), 1632–1641.

Stoob, K., Singer, H. P., Mueller, S. R., Schwarzenbach, R. P., Stamm, C. H., 2007. Dissipation and transport of veterinary sulfonamide antibiotics after manure application to grassland in a small catchment. Environmental Science & Technology, 41(21), 7349-7355.

ter Laak, T. L., Gebbink, W. A., Tolls, J., 2006. The effect of pH and ionic strength on the sorption of sulfachloropyridazine, tylosin, and oxytetracycline to soil. Environmental Toxicology and Chemistry, 25(4), 904-911.

Topp, E., Monteiro, S. C., Beck, A., Coelho, B. B., Boxall, A. B., Duenk, P. W., Kleywegt, S., Lapen, D. R., Payne, M., Sabourin, Li, H., 2008. Runoff of pharmaceuticals and personal care products following application of biosolids to an agricultural field. Science of the Total Environment, 396(1), 52-59.

Torkzaban, S., Bradford, S. A., van Genuchten, M. T., Walker, S. L., 2008. Colloid transport in unsaturated porous media: The role of water content and ionic strength on particle straining. Journal of Contaminant Hydrology, 96(1), 113-127.

Torkzaban, S., Bradford, S. A., Vanderzalm, J. L., Patterson, B. M., Harris, B., Prommer, H., 2015. Colloid release and clogging in porous media: effects of solution ionic strength and flow velocity. Journal of Contaminant Hydrology, 181, 161-171.

Thio, B. J. R., Montes, M. O., Mahmoud, M. A., Lee, D. W., Zhou, D., Keller, A. A., 2011. Mobility of capped silver nanoparticles under environmentally relevant conditions. Environmental Science & Technology, 46(13), 6985-6991.

Unold, M., Šimůnek, J., Kasteel, R., Groeneweg, J., Vereecken, H., 2009. Transport of manure-based applied sulfadiazine and its main transformation products in soil columns. Vadose Zone Journal, 8(3), 677-689.

Wang, D., Jaisi, D. P., Yan, J., Jin, Y., Zhou, D., 2015. Transport and retention of polyvinylpyrrolidone-coated silver nanoparticles in natural soils. Vadose Zone Journal, 14(7).

Wang, Q., Kim, D., Dionysiou, D. D., Sorial, G. A., Timberlake, D., 2004. Sources and remediation for mercury contamination in aquatic systems—a literature review. Environmental Pollution, 131(2), pp.323-336.

Wang, Y., Li, Y., Fortner, J. D., Hughes, J. B., Abriola, L. M., Pennell, K. D., 2008. Transport and retention of nanoscale C60 aggregates in water-saturated porous media. Environmental Science & Technology, 42(10), 3588-3594.

Winter, T. C., 1998. Ground water and surface water – a single resource: US Geological Survey Circular 1139. US Geological Survey, Denver, CO.

Yao, K. M., Habibian, M. T., O'Melia, C.R., 1971. Water and waste water filtration. Concepts and applications. Environmental Science & Technology, 5 (11), 1105–1112.

Zappa, G., Bersezio, R., Felletti, F., Giudici, M., 2006. Modeling heterogeneity of gravel-sand, braided stream, alluvial aquifers at the facies scale. Journal of Hydrology, 325(1), 134-153.

Zhang, H., Chen, B., Banfield, J. F., 2010. Particle size and pH effects on nanoparticle dissolution. The Journal of Physical Chemistry C, 114(35), 14876-14884.

Zhao, L., Dong, Y. H., Wang, H., 2010. Residues of veterinary antibiotics in manures from feedlot livestock in eight provinces of China. Science of the Total Environment, 408(5), 1069-1075.

Zhu, Y., Ma, L. Q., Dong, X., Harris, W. G., Bonzongo, J. C., Han, F., 2014. Ionic strength reduction and flow interruption enhanced colloid-facilitated Hg transport in contaminated soils. Journal of Hazardous Materials, 264, 286-292.

Zhou, H., Gómez-Hernández, J. J., Li, L., 2012. A pattern-search-based inverse method. Water Resources Research, 48(3).

Zhou, P., Su, C., Li, B., Qian, Y., 2006. Treatment of high-strength pharmaceutical wastewater and removal of antibiotics in anaerobic and aerobic biological treatment processes. Journal of Environmental Engineering, 132(1), 129-136.

Zou, Y., Zheng, W., 2013. Modeling manure colloid-facilitated transport of the weakly hydrophobic antibiotic florfenicol in saturated soil columns. Environmental Science & Technology, 47(10), 5185-5192.